VYSOKÉ UČENÍ TECHNICKÉ V BRNĚ
BRNO UNIVERSITY OF TECHNOLOGY

FAKULTA CHEMICKÁ
ÚSTAV CHEMIE MATERIÁLŮ

FACULTY OF CHEMISTRY
INSTITUTE OF MATERIALS SCIENCE

THE CRYSTALLIZATION KINETICS IN SEMICRYSTALLINE NANOCOMPOSITES

KINETIKA KRYSTALIZACE V SEMIKRYSTALICKÝCH NANOKOMPOZITECH

DIZERTAČNÍ PRÁCE
DOCTORAL THESIS

AUTOR PRÁCE — Ing. KATEŘINA HYNŠTOVÁ
AUTHOR

VEDOUCÍ PRÁCE — prof. RNDr. JOSEF JANČÁŘ,CSc.
SUPERVISOR

BRNO 2010

HYNŠTOVÁ, K. *Kinetika krystalizace v semikrystalických nanokompozitech.* Brno: Vysoké učení technické v Brně, Fakulta chemická, 2010. 86 s. Vedoucí dizertační práce prof. RNDr. Josef Jančář, CSc.

Prohlášení

Prohlašuji, že jsem disertační práci vypracovala samostatně a že všechny použité zdroje jsem správně a úplně citovala. Disertační práce je z hlediska obsahu majetkem Fakulty Chemické Vysokého Učení Technického v Brně a může být použita ke komerčním účelům jen se souhlasem vedoucího disertační práce a děkana FCH-VUT.

Podpis

Declaration

I declare that this Ph.D. thesis has been worked out independently and that all used references have been cited correctly and fully. No part of this publication may be reproduced, stored in a retrieval system, or transmitted in any form, or any means, electronic, mechanical, photocopying, recording or otherwise without the prior written permission of the supervisor of this work and the dean of Brno University of Technology.

Signature

ABSTRACT

The crystal growth greatly affects morphology and, thus, physical properties of semicrystalline polymers. In this PhD work, the effect of adding high specific surface area silica nano-filler on the crystallization kinetics of linear polyethylene was investigated. In polymers, adding high specific surface area filler is able to alter the chain dynamics even at very low filler loadings. It is suggested that in the vicinity of the filler surface, polymer chains exhibit retarded reptation motion due to the chain immobilization caused by either the filler-polymer interaction or by chain constraints between closely packed nanoparticles.

The polarized optical microscope equipped with a hot stage was employed to measure the spherulites growth rates in the medium crystallization regime II. It was shown that even weak interaction between PE chains and silica nano-filler above glass transition temperature leads to substantial decrease of the spherulite growth rate. The measured data were correlated with predictions based on the theoretical models and molecular simulations of molecular dynamics of the crystallizing polymer.

The observed decrease of spherulite growth rate, G, in dependence on both the silica nano-filler content and polyethylene molecular weight was interpreted utilizing the chain immobilization hypothesis, where the dynamics adsorption and desorption of the chain at the filler interface results in the slowing down of the reptation motion.

Keywords: polyethylene, nanocomposite, crystallization kinetics, reduced reptation

ABSTRAKT

Růst krystalů zásadně ovlivňuje morfologii a tím také fyzikální vlastnosti semikrystalických polymerů. Tato PhD práce přináší alternativní pohled na popis kinetiky krystalizace v polyolefinech plněných slabě interagujícími částicemi. V nanokompozitních materiálech vysoký specifický povrch plniva i při nízkých plněních zásadně ovlivňuje dynamiku řetězců. V blízkosti povrchu plniva začíná hrát významnou roli zpomalená reptace způsobená jak vzájemnými interakcemi plnivo-polymer tak prostorovým omezením mezi nanočásticemi.

Růst krystalů byl zkoumán pomocí polarizovaného optického mikroskopu vybaveného horkým stolkem. Výsledky byly korelovány s teoretickými modely a rozsáhlými počítačovými simulacemi na molekulární úrovni.

Pozorovaný pokles rychlosti růstu sférolitů v závislosti na obsahu plniva a molekulové hmotnosti matrice je interpretován na základě imobilizační hypotézy.

Klíčová slova: Polyetylen, nanokompozit, kinetika krystalizace, zpomalená reptace

ACKNOWLEDGEMENTS

This work has been supported by Czech ministry of Education, Sports and Youth project MSM 0021630501 and Czech Grant Agency project P205/10/2259.

TABLE OF CONTENTS

1 INTRODUCTION

Many useful materials in the future are expected to be created with various self-organizing molecules. Crystallization is a typical case of polymer self-organization, which has long been investigated since the discovery of chain-folding as the principal mode of crystallization. The chain-folded lamellae are main building blocks of polymeric materials and their spatial distribution dominates all physicochemical properties of the materials. Crystal structures and crystallization mechanisms are therefore central subjects in science and technology of polymers.

Also in most processing technologies, crystallization process can affect physical properties of final articles made of semicrystalline polymers, substantially. The kinetics of polymer crystallization is controlled by the diffusion of chains to the phase transition zone. Changes in morphology brought about by a change in temperature or by the external factors will cause changes in physical properties and in the response to an applied stress. Thus, due to the close relation between the properties and morphology, the nature and consequences of the changes connected with the nanoparticles addition must be fully understood.

The nature of the polymer nanocomposites research is shifting the main emphasis on the research of fundamental aspects of physics of long chain molecules in both non-Newtonian liquids and disordered and ordered solids. New phenomena now observed on the micro-scale are being discovered with huge potential application benefits. Despite its importance, no generally acceptable explanation of the peculiarities of the development of the crystalline structure observed in nanocomposites with semicrystalline matrices has been published in the scientific literature so far.

2 POLYMER CRYSTALLIZATION

Crystallization of flexible polymers with a large number of internal degrees of freedom involves very complicated molecular motions of various space and time scales, ranging from large scale transport of whole chains to atomistic scale rearrangement of crystalline stems in perfecting crystalline order. In contrast to the global chain dynamics in the melt, the molecular motions during crystallization can be very sensitive to the chemical structure just like the crystal structure being specific to the structure of constituent molecules.

Many stereo-regular polymers, whether synthetic or biological, form partially crystalline solids, which consist of crystalline lamellae and intervening amorphous layers [1]. The crystalline polymers are known to show characteristic multi-scale structures ranging from local crystalline structure to macroscopic structure of spherulites (Fig. 1). Since the morphology is closely related to the properties, it is in the focus of the scientific interest continuously [2-4]. The crystal structure of polymer is almost uniquely determined as the lowest free-energy state, and the energy analyses by computer modeling have contributed much to the structure determinations [5-7]. On the other hand, the large-scale structure, the way of lamellar stacking or branching for example, may be determined by the balance of equilibrium and kinetic processes of crystallization. They show a great deal of varieties depending on the crystallization conditions such as temperature, pressure, solvent as well as on molecular structure itself [1, 8-10].

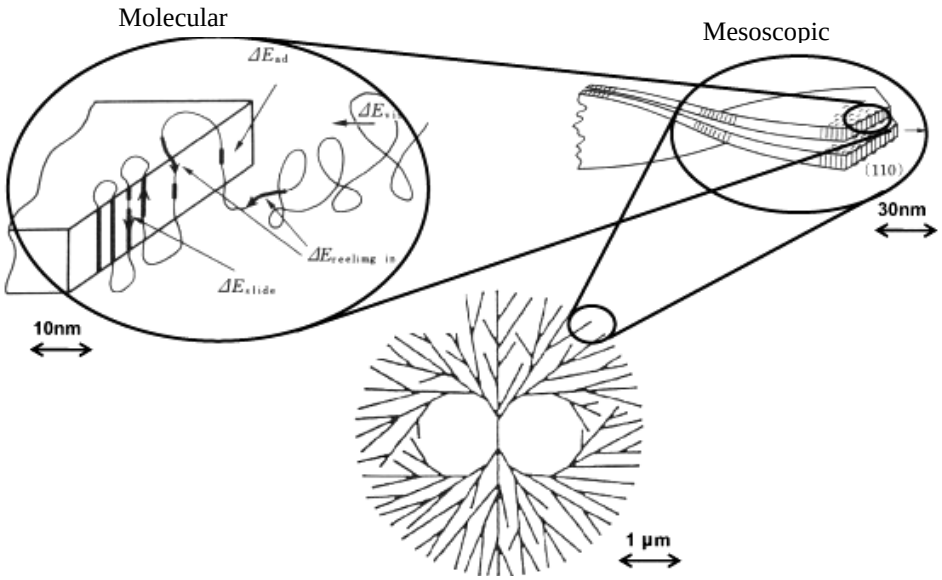

Figure 1: Multi-scale structures of crystalline polymers, from molecular-level structure of the lamella crystal growing by reeling in random coiled chains in the melt, to mesoscopic level structure of growing lamellae showing cooperative layering and twisting, and to final macroscopic spherulitic aggregate of the lamella [11].

On the basis of the secondary nucleation mechanism, a framework of the molecular scenario was first proposed by Lauritzen and Hoffman (LH) soon after the discovery of chain-folded crystallization [12-15]. Due to the great success of the LH-theory especially in predicting characteristic changes in lamellar thickness and crystal growth rate with crystallization temperature T_c, most of the discussions thereafter have been concentrated on understanding various experiments in terms of the LH-theory.

As for the very beginning of crystallization in isotropic melt, the presence of unknown impurities in polymer samples has long obscured the primary nucleation mechanism, and we could find only limited number of reports. Recent surge of investigations on the very early stages of crystallization will have an origin in the proposal of peculiar instability in undercooled melt before the onset of crystallization, a spinodal-decomposition (SD) or phase-separation assisted nucleation scenario [16].

Emerging also is the new enthusiasm about novel crystallization in strongly confined systems; very thin film [17] polymers in a cylindrical cavities or nanorods [18] or nanodomains in phase separated block-copolymers [19] and [20].The presence of surface or interface will cause strong constraints on polymer conformations and enforce peculiar chain trajectories during crystallization.

The polymer crystallization thus involves quite new topics as well as historical unsolved problems. Long flexible polymers are considered to show chain-folded crystallization from highly entangled states by reeling in their chain tails. The experimental knowledge available is mostly macroscopic, and detailed molecular processes of polymer crystallization are not readily accessible. It is the fundamental task to find out possible molecular pathways from mechanical and statistical–mechanical points of view.

In the presence of nanofillers who are of the similar dimensions as the polymer chain, one more variable is introduced into the polymer when investigating the kinetics of the crystallization process.

In the following sections, the simulations of crystallization in simple polymers under quiescent condition with direct relevance to our studied system will be reviewed firstly followed by the brief survey on the crystallization in nanocomposites.

2.1 Crystallization under quiescent conditions

Crystallization in polymers is usually divided into two separate processes, the emergence of small crystalline domains called primary nuclei, and their subsequent growth. The primary nucleus is a nanometer-sized structure which shape may be treated by equilibrium thermodynamics, while the growing crystals have very thin platelet shape which must be kinetically controlled.

From a thermodynamic point of view, the system can be considered an open system that is allowed to exchange energy with the surrounding. All events in nature are trying to reach the minimum free Gibbs energy. When the difference of the initial and final states ΔG is negative the events are spontaneous. This can be described as

$$\Delta G = \Delta H - T\Delta S, \tag{1}$$

where the change in the free energy which consists of the change in enthalpy ΔH and the change in the entropy ΔS multiplied by the temperature T and for the spontaneously occurring events is always negative in value [21]. The crystal growth depends largely on the diffusion of chains to the crystal surface and is kinetically controlled. The maximum overall growth rate is observed at the temperature between glass transition temperature T_g and melting temperature T_m as a result of the balance between the nucleation and crystal surface growth rate. Also, it was revealed that with increasing molecular weight the growth rates are decreased for the same degrees of undercooling [22] (Figure 2).

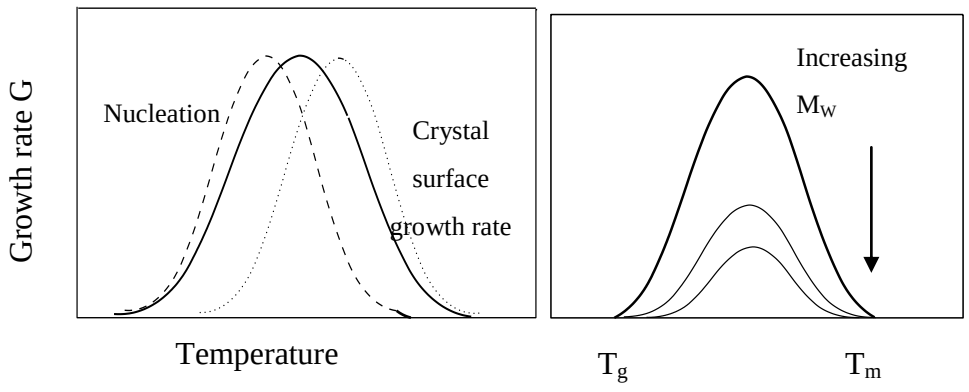

Figure 2: Observed trends in polymer crystal growth: Dependence of growth rates on temperature found in polymer processing. With increasing molecular weight the growth rate is lower and the maximum is slightly shifted to higher temperatures.

2.1.1 Emergence of the crystalline order

The primary nucleus occurs as a result of density fluctuations. After it exceeds a critical size the crystal starts to grow. The emergence of the embryo nuclei has been observed by AFM and also in practice not all of the nuclei developed into the beginning of the lamellae, some of them disappeared or disintegrated [23].

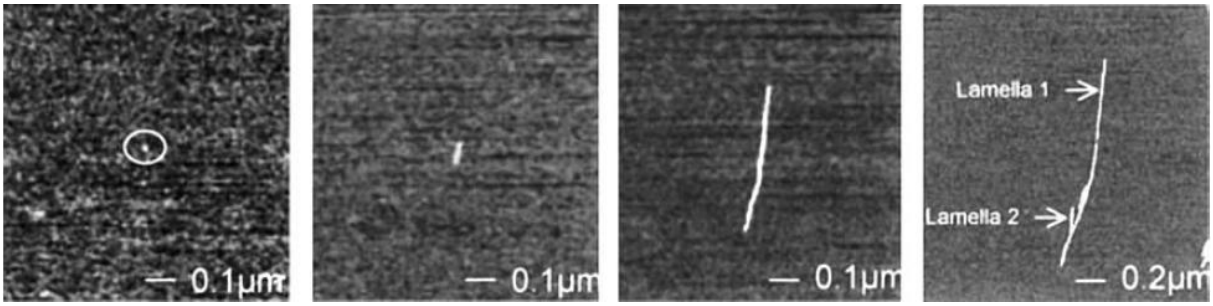

Figure 3: AFM images of the embryo, one growing lamella and the later development of the branches [23].

The early stages of the nuclei development take place on a nano-scale and into their behavior the statistics must be included, thus, the theoretical dealing with the nucleation processes is quite difficult. The significant progress in this area has arrived with the development of computer simulations.

Early, innumerable simulation studies on polymer solution and melt have been reported. The first report on crystallization of chain molecules was for short *n*-alkanes by Roe et al. in 1988 [24]. They observed fast crystallization of alkane molecules into platelets. A limited number of studies have since followed, on crystallization and melting in alkanes of various chain lengths [25], on transient pre-crystalline state in undercooled melt [26] on steady-state growth of lamella [27] on crystallization in ultra-thin films [28] and [29], etc. The primary nucleation in polymers did not attract much attention at first probably because of ubiquitous heterogeneous nucleation due to impurities. Conceptually the primary nuclei are imagined as either neat chain-folded crystallites or fringed micellar clusters depending on the way how the constituent chains participate in the nuclei formation [1] But the direct approach to the problem by started with the simulation for polymer nucleation, that was given by Kavassalis and Sundararajan, who first demonstrated a clear transition in polyethylene (PE) from a globular state to a chain-folded crystallite, where the driving force for crystallization was dominantly van der Waals attraction between constituent atoms (Fig. 4) [30]. There followed many studies, by adopting similar models and methods, on detailed pathways of PE crystallization [31] and crystallization in PE of various topologies [32], [33] and [34].

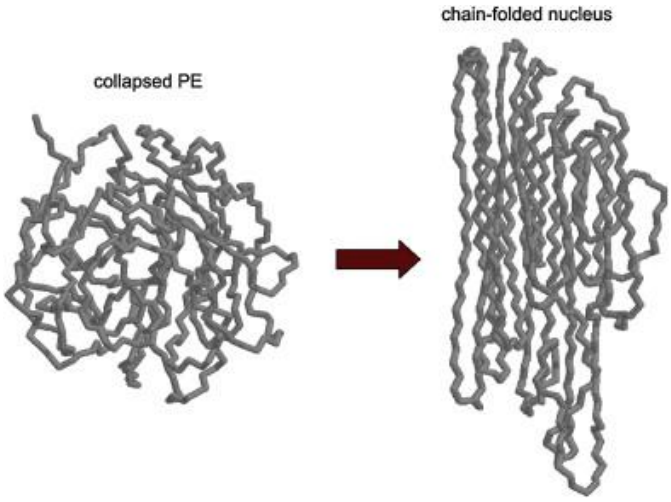

Figure 4: Formation of a crystal nucleus of a single PE chain in a vacuum. The chain conformation changes from a spherical globule to a stretched rod [30].

With ever increasing computer performance, simulations in much larger systems have become feasible. From a series of work on the development of coarse-grained models for polymers, Mayer and Muller-Plathe have build up a model of poly(vinyl alcohol) (PVA) for studying early stage of crystallization. They investigated the emergence of crystalline order from the isotropic melt by rapid quenching [35] and [36]. They could reproduce many elementary processes of homogenous nucleation that showed good correspondence with experiments and other simulations, in temperature dependence of lamella thickness, structure of fold surface, etc. In their work, they neglected long-range force (van der Waals attraction) to accelerate computation. Their model has the energy contribution due to intrachain interactions only and the dominant driving force for crystallization is entropic, which seems to ignore dominant driving force for polymer crystallization in conventional sense. However, their work is reminiscent of the classical solid–liquid transition in systems of repulsive spherical atoms [37] and poses an intriguing problem as to the intrinsic driving force for polymer crystallization.

Usual image of initial crystallization in the melt is a primary nucleation. The structure of the primary nuclei in the melt should be compared with those in solution described before. In the case of melt crystallization two distinct images of the primary nucleus, chain-folded nucleus and fringed micelle nucleus have long been conceived. Molecular simulations must give definitive answer to this question. They have adopted a PE-like molecular model and investigated homogeneous nucleation from highly supercooled melt [38]. By first identifying the primary nuclei and thereby examining individual conformation of the chains forming the nuclei they found that the primary nucleus in the melt has similar elongated rod-like structures as those observed in vacuum or in solution. The overall shapes of the nuclei in the melt are,

however, highly perturbed, and the interfaces between the nuclei and the surrounding melt are not so definite [38].

Rigorous MD approaches to the structure of highly undercooled melt were attempted by Gee et al. using rather realistic models of PE and poly(vinylidene fluoride) (PVDF), though the molecular models were again slightly modified to facilitate crystallization [39] and [40]. Systems of millions of atoms were considered to investigate meso-scale density fluctuation proposed in the SD scenario. From these simulations, they obtained affirmative results showing peculiar density anomaly at the very early stage of crystallization, and they concluded that this is really an indication of the SD mechanism. However, real space image of the simulated density fluctuation and its molecular origin are not well documented. As to the density anomaly in the supercooled melt, Meyer et al. made contrary observation that there is no density fluctuation having specific wave length [36] Muthukumar et al. [41] also made a critical discussion on the basis of their LD simulation for a single chain and dynamical structure factor $S(q,t)$ which has shown apparent resemblance to that considered as the evidence of SD mechanism [16] They argued that the characteristic SAXS peak may not be an indication of the SD mechanism but simply due to the interference between baby nuclei of small crystalline clusters [41]. Emergence of local crystalline order in highly-quenched melt, whether it is due to usual primary nucleation or phase separations, may depend sensitively on molecular properties such as chain rigidity or chain length. Further investigations are obviously needed to clarify the confusion.

Above discussed nucleation has been of homogeneous nature. However, with the presence of impurities or fillers with a similar crystallographic structure as the matrix, the heterogeneous nucleation may occur and the nucleation mechanisms are changed. These two types can be distinguished also visually. In case of homogeneous nucleation first branches develop when the lamella reaches a size of the order of 1μm. If the branching is repeated for all the later starting lamellae, whenever they reach a length of the order of 1μm, the embryo gradually develops into an object as it is shown in Figure 5. Finally, it will become a spherulite with a characteristic feature, a pair of "eyes", at its center.

Figure 5: In situ AFM recording of a homogeneous nucleation [42].

If spherulites start from heterogeneity by heterogeneous nucleation, a different growth pattern is observed, as is depicted in Figure 6. In this case, several lamellae develop simultaneously, emanating from the surface of heterogeneity. As a consequence, the growing object shows quasi spherical symmetry from the very beginning. This differs from the initial anisotropy associated with a homogeneous nucleation which is retained up to the end in the form and direction of the two eyes.

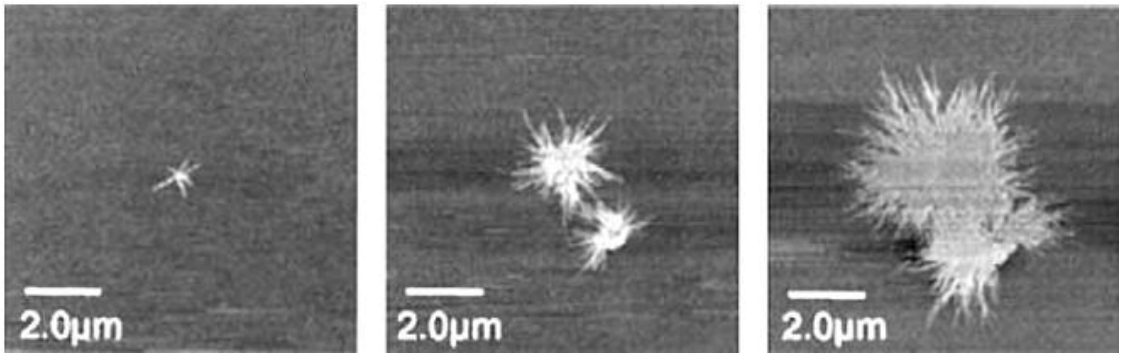

Figure 6: In situ AFM recording of a heterogeneous nucleation [42]. The spherulite grows into all dimensions from the very beginning.

In this PhD thesis, the subsequent linear growth rate is investigated. However, the nuclei formation is very important parameter, that, when changed in the presence of used fillers, would interfere with the interpretation of the obtained results.

2.1.2 Growth of the chain-folded lamellae

Polymer lamellae show steady growth through chain-folded to form various higher order structures. The crystal growth has been the central issue in the study of polymer crystallization, since the final morphology of polymer solid is dominated by the growth process of lamellae. Contrary to the homogenous nucleation discussed previously, basic molecular processes of the crystal growth are those that take place at crystal–solution or crystal–melt interface, the crystal growth front, on which the molecules diffuse, adsorb, and crystallize (Fig. 7).

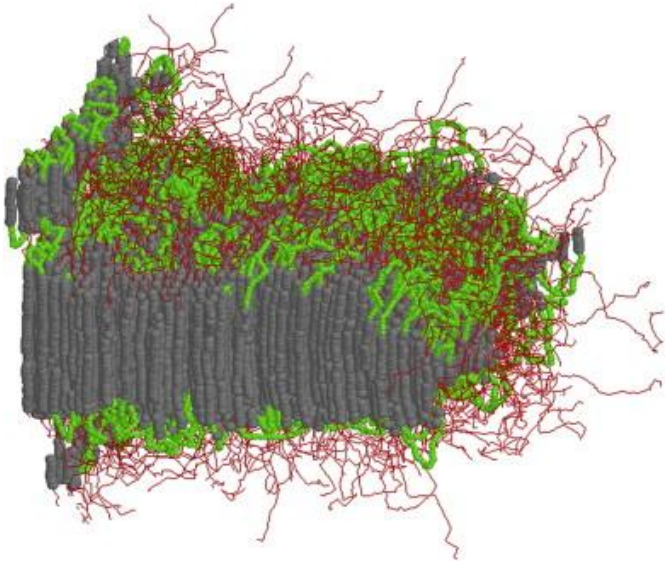

Figure 7: Chain-folded lamella growing in the melt from the left crystal substrate; the figure was generated by our MD simulation for 1280 chains of PE-like molecules [38]. Segments are depicted according to their types, crystalline stems in dark gray, folds in green, and cilia in red.

In the early work on the preparations of single lamellas of unfractioned polyethylene, crystallization from dilute xylene solution was carried out by slow cooling a heated solution or by isothermal crystalization [43]. In the later work both optical microscopy with polarized light and transmission electron microscopy were used. Later on, the lamellar crystals of polyethylene were obtained by crystallization from dilute solution and the folded chain hypothesis was advanced [44]. A schematic representation is shown in Figure 8. In this drawing, each straight line represents a section of a polymer chain incorporated in the crystal lattice and contains a number of repeat units – unit cells; the loops shown depict the folds.

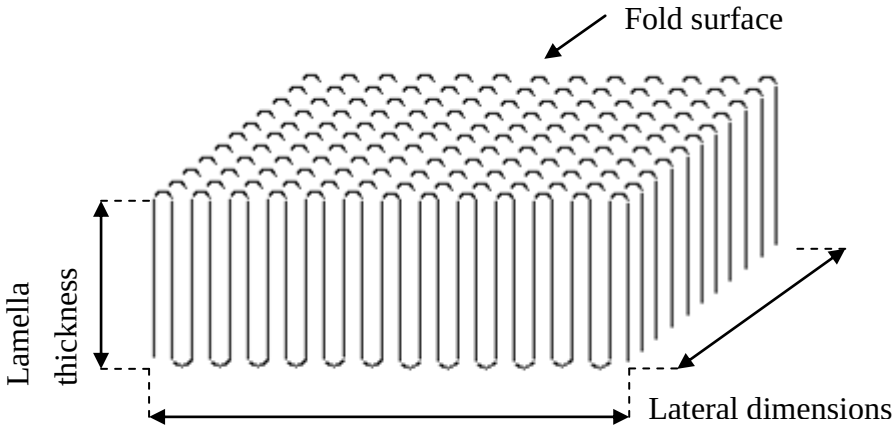

Figure 8: Stack of polymer chains folded back on themselves – schematic representations of lamella

The folds in the lamella can be tight adjacent re-entrant, loose adjacent re-entrant, nonadjacent re-entrant or short protruding chain ends. The originally proposed regularly folded adjacent re-entry model was questioned by Flory [45], who advocated a switchboard model, with predominant non-adjacent re-entry of the chains. Neutron scattering experiments and related calculations favored the non-adjacent re-entry model.

Considering the molecular dynamics processes, the standard LH-theory of polymer crystal growth has succeeded in explaining various observations theory and its conclusions is one of the most studied and discussed theories to capture the crystal growth rate in molecular detail and serve to establish the general framework for explaining several important observations regarding the crystallization behavior of flexible polymers [12-15]. Hoffman assumed that chain folding and lamellar formation are kinetically controlled, the resulting crystals being metastable. It was showed that close to T_m the value of the linear growth rate slope K_g changes, indicating a change in nucleation mechanisms (Fig. 9). Based on these results three nucleation regimes have been proposed and for each one mechanism of crystal growth suggested [13].

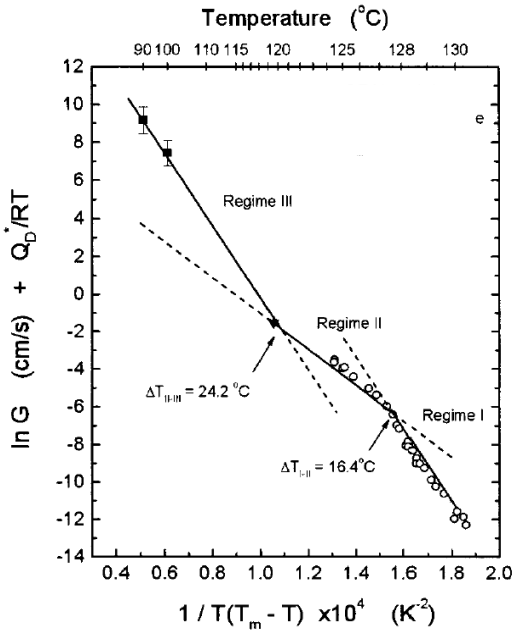

Figure 9: Plot showing three crystallization regimes in PE [13].

Regime I corresponds to a low undercooling where the diffusion is not restricted and deposition is occurring within a single layer completion. Crystallization process is limited by the attachment of the first fully extended stem to a smooth surface of crystal. In Regime II, where the reptation motion is the most pronounced, the nucleation event occurs simultaneously within one single layer (Fig. 10). Regime III crystallize within multiple layers and is mainly observed in the industry during processing, being present at the high

undercoolings[13]. This theory was broadened by Miller to comprehend the reptation of the chain to the crystal surface [12].

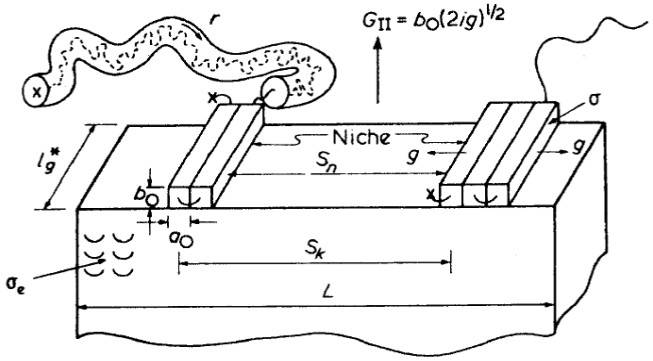

Figure 10: Model for regime II growth showing multiple nucleation [13]. The quantity S_k represents the mean separation between the primary nuclei and S_n denotes the mean distance between the associated niches. The primary nucleation rate is I, and the substrate completion rate is g. The overall observable rate is G. Reptation tube contains molecule being reeled in a rate r onto substrate [46].

Since the theory is phenomenological one based on many assumptions on the molecular pathway and the microscopic structure of growth surface, many independent molecular scenarios have been put forward, such as modified surface nucleation models by Point [47] Keller [48], Hikosaka [49] rough surface growth model by Sadler [50] molecular nucleation theory by Wunderlich [1], bundle nucleation model by Allegra [51]. In the studies by Point and by Sadler and Gilmer the crystallizing surface might sample several conformations before finding one which is stable and contributes to growth [47, 50]. The theory developed by Sadler and Gilmer incorporates the entropic barrier. It is based on the interpretation of the kinetic Monte Carlo simulations, where individual motions of molecules are governed randomly in accordance with the given conditions such as excluded volume, bonding energies and repulsive forces. An important point of the theory is both the addition and removal of the mers during crystallization and thus more accurate description of the reality in polymers.

Recently, mesophase-domain mediated growth by Strobl [52] has introduced a model where a layer of granular crystals, which develop from a mesomorphic layer of highly ordered melt, precedes the formation of the final lamella [53]. Very interestingly, this hypothesis mimics the VLF dependence. Both nucleation and growth rate are considered. This hypothesis is based primarily on the investigation of differences between melting and crystallization mechanisms. It was pointed out, that crystal formation is not direct process and, thus, above

mentioned “multistage model” has been formulated. The spherulite growth rate u is described by equation [53]

$$u = u_0 \exp\left(-\frac{T_A}{T-T_V}\right) \cdot exp\left(-\frac{T_G}{T_{zg}-T}\right) \quad (2)$$

T_V, the Vogel temperature, is located 30-70°C below the glass transition temperature T_G and T_A is an activation temperature. T_{zg} is the zero growth temperature, where u goes to zero. The T_G and T_{zg} were shown to be dominant in the temperature range of the experiment.

In most efforts to verify the assumed scenarios, however, the real molecular trajectories of crystallizing chains at the interface were too hard to seize by experiments. The molecular simulation that enables to distinguish individual molecules enables to reveal molecular pathways of crystallizing chains.

Computer simulation of crystal growth in polymers has also begun with a very simple system. Early studies were concentrated on the dynamics of a single chain strongly adsorbed on a flat growth surface and undergoing collapsing and chain-folded crystallization [54] and [55]. These were the first attempts to observe molecular processes of secondary nucleation on the growth front. An initial random coil chain first showed local collapse to form two-dimensional necklace of crystallites, similar to the “baby nucleus” described by Muthukumar in solution crystallization. Then the global reorganization into larger 2D lamellar crystal followed through coalescence of the crystallites. The resulting 2D lamellae were found to be regularly chain-folded and to have larger thickness at higher crystallization temperatures in good agreement with experiments [54-55]. Doye et al. have shown a phase diagram of the crystallizing chain, in which a 3D random coil first transforms into a 2D random coil being adsorbed on the crystal surface, and then it crystallizes by further lowering the temperature [56]. The next step that should be taken was to extend the 2D model to 3D, where both chain diffusion toward and chain adsorption followed by crystallization on the growth front must be considered [57].

Except restrictions on the chain mobility due to larger viscosity or chain entanglements, crystallization from the melt is expected to be faster than that from dilute solutions. However, even in the most favorable case of PE, usual growth rate of lamellae is desperately slow. For example the maximum growth rate is about 10^{-4} nm/ns for PE of $M = 10^5$. Yamamoto et al. adopted a simplified polymer model of PE, where the chains were made of CH_2 united atoms but the equilibrium bond angles were assumed to be 180°. By properly adjusting chain flexibility, however, physical properties of PE relevant to crystallization, such as melting point, heat of fusion, and diffusion coefficient of the chains, were found to be reproduced [58-59]. They made MD simulations for a large system of 1280 chains of relatively short PE C_{100}, and succeeded in observing steady-state growth of chain-folded lamellae from the melt at various T_c (Fig. 11).

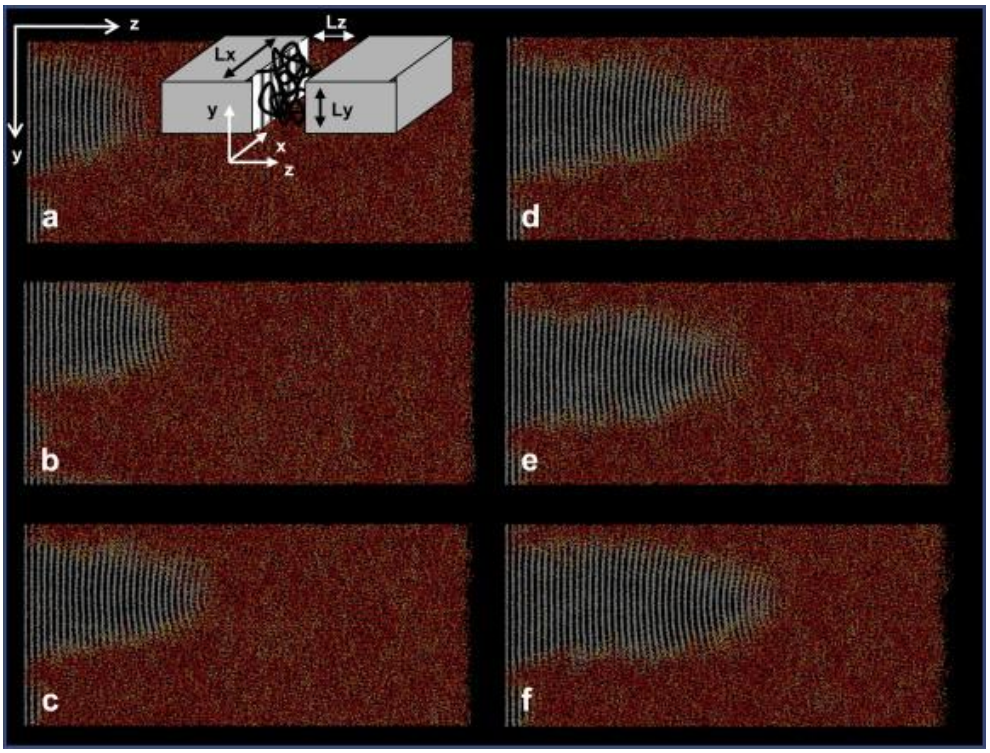

Figure 11: Crystal growth of relatively short PE-like chain in the melt which was placed between two crystal substrates (inset). Pictures show growing lamellae viewed along the x-axis, where the chain axis is along the y-axis; the parallel white lines show crystalline stems; (a) at 28.8 ns, (b) 38.4 ns, (c) 48.0 ns, (d) 57.6 ns, (e) 67.2 ns, and (f) 76.8 ns. The lamellae are making steady-state growth from the left substrate into the melt region (red) and have pronounced taped edge at the growth front [59].

2.1.3 Crystallization from the melt on macroscale

Crystallization from the melt would be most frequently met in polymers. In comparison with crystallization from solutions, melt crystallization does not need long-range diffusion of chains because of sufficient chain supply.

When polymer samples are crystallized from the melt, the most common of the observed structures are the spherulites. They are sphere-shaped crystalline structures that form in the bulk. In this work, high density polyethylene (HDPE) commercial sample and polyethylene prepared by live polymerization have been be used as the matrix. HDPE is relatively simple and well studied, with many parameters available also for the computer simulations. Also polyethylene crystallized from melt in 3-dimmensional space forms spherulites – the sphere centered gradually grown lamellae. For polyethylene, the unit cell structure (the smallest repeated unit in the lamella) was first investigated by Bunn. A number of experiments were reviewed by Natta and Corradinni [60]. The unit cell is orthorhombic,

with cell dimensions of a=7.40 Å, b = 4.93Å and c = 2.534Å. The unit cell contains two mers. The chains are in the extended *zigzag* form; that is, the carbon-carbon bonds are *trans* rather than *gauche*. The *zigzag* form may also be viewed as a twofold screw axis [46].

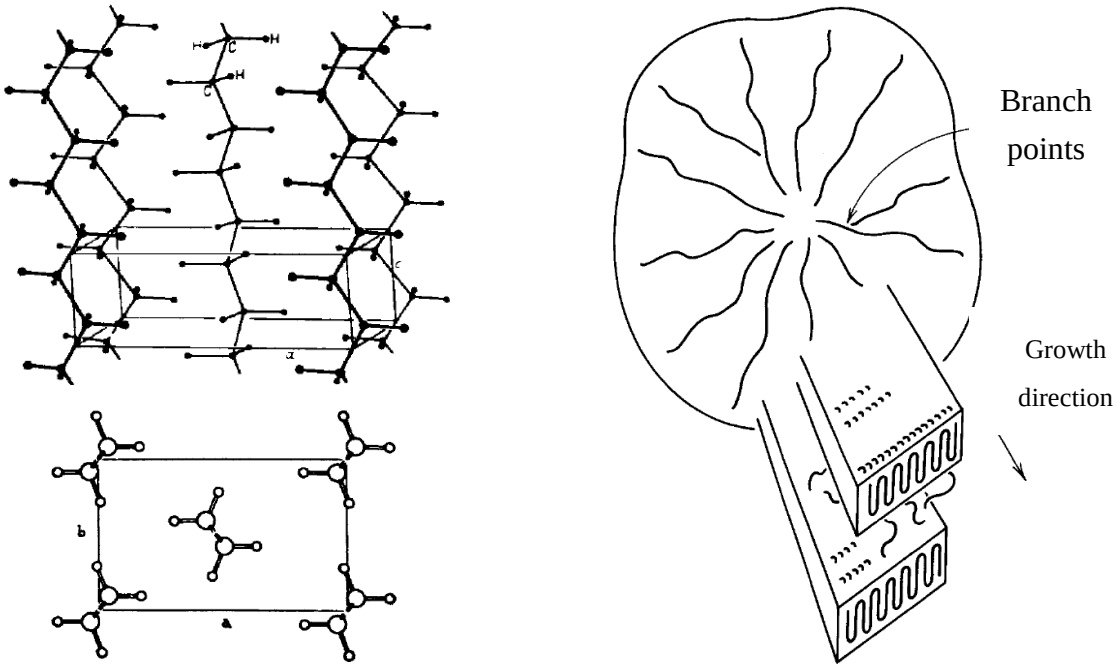

Figure 12: On the left: The schematic illustration of polyethylene single crystal – perspective and along the axis views. On the right: Model of spherulitic structure [46].

The first attempts to describe the conversion of the amorphous material into the crystalline domains were focused on the growth from nuclei randomly distributed in a sample. The most known statistical approaches are those by Kolmogoroff [61] and Evans [62] and the Avrami [63-65] theory based on the concept of so-called "extended volume". The latest describes theoretically on the macroscopic level how sample volume gets covered by growing objects of certain shape. This model can be very well utilized to describe the solid/liquid state transformations. It can be written in the final form [65]

$$\varphi_C = 1 - \exp(-Kt^n) \qquad (3)$$

where φ_c is the crystalline volume fraction developed at time t and constant temperature, K is a rate coefficient and parameter n, that assumes values 2,3 or 4 depending on the type of nucleation and the dimensionality. Although this model can satisfactorily used on the macroscale in it does not consider any molecular detail, where the crystallization in polymers originates.

Computer simulations of the crystallization on the macroscale are quite complicated. Crystalline polymers exhibit multi-scale structures (Fig. 1). As described so far, extensive efforts have been made to reveal molecular mechanisms of polymer crystallization, and MD and MC simulations have now come to reach the scale of several tens of nanometers. For further scale-up of the modeling to macroscopic structures a slightly different approach, besides standard mesoscopic modeling methods of much interest these days[66], would profit where one considers larger units as building blocks of the bulk polymer materials.

Muthukumar et al. have attempted to model macroscopic lamella growth via cluster aggregation process, through which they have shown both kinetic and thermal roughening of the lamella [67]; similar lines of studies taking finer building blocks, the rigid crystalline stems, were already reported to study the surface structures of *n*-alkane and PE [68]. Purely geometrical modeling of spherulites has also been reported recently, where the aggregation of stacked lamellae was investigated by proper space-filling algorithms, and the model spherulites obtained were utilized to study light scattering from and small molecule diffusion through the bulk crystalline polymers [69-71].

2.2 Crystallization in nanocomposites

Crystallization in nano-composites or nanospace is an emerging topic of considerable interest. Several experiments and simulations of PE crystallization in composites with carbon nanotubes [72-74] and of crystallization in microphase separated domains of droplets [20] and [75] or nanorods [19], [76-77] were reported. Also of great scientific and practical interest is the crystallization in very thin films [18] and [78]. It is supposed that the presence of nanoparticles can affect the polymer melt by altering the chain dynamics by the matrix-filler interactions or by introducing a special confinement polymer chains.

2.2.1 Polymer chain dynamics

Since the dynamics of a chain largely governs the crystal growth in the polymeric material and thus is expected to play a key role in nanocomposites as well, the short summary of the two main dynamic concepts - topological and dynamic fragility approach are briefly introduced here.

When approaching the polymer dynamics from the topological viewpoint, two of the most widely used theories reduce the problem to a single chain motion in an effective medium. The Rouse model used for the simple case of un-entangled chains or the short time and length scales [79] and the reptation model used for description of entangled chains or the longer time and length scales [80, 81]. Reptation concept is depicted in Figure 13.

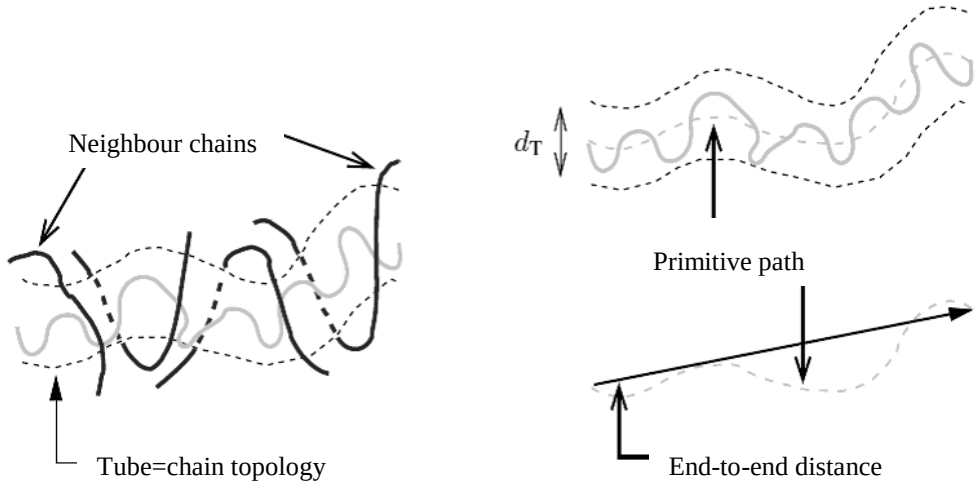

Figure 13: The schematic representation of the topological based idea of the chain dynamics in the melt, reptation [82].

In the Rouse model, a Gaussian chain of beads connected by springs interact with a stochastic medium that mimics the presence of other chains. As a consequence, the chain center of mass is subjected to particle-like diffusion and the self-diffusion coefficient D is expected to reach the asymptotic value

$$D = \frac{k_B T}{\zeta N}, \qquad (4)$$

ς being the effective bead friction coefficient, k_B the Boltzman´s constant and T the temperature.

In the reptation model, the polymer chain is confined inside a "tube" formed by the constraints imposed by entanglements with the other chains. One of the main predictions of this theory is drastic slow down of the chain motion due to the entanglement as revealed by the self-diffusion coefficient:

$$D = \frac{1}{3}\frac{d_T^2}{l^2}\frac{k_B T}{\zeta N^2} \quad , \qquad (5)$$

Where d_T is the tube diameter and l ($l^2 = C_\infty b^2$) the effective bond length. Rouse model is valid for the short chains where the topological constrains play no dominant role, where the longest relaxation time or volume does not exceed a critical entanglement value. The chain has a Rouse relaxation up to the time $\tau_e \approx N_e^2$ where N_e is an entanglement length, in another words, number of chain monomer units necessary to form an entanglement. For polyethylene this value estimation varies from 35-70 monomer units [83-86]. Then, the monomers of the chain move predominantly along their own contour and further relaxation can only occur

along the path of a coarse grained primitive chain consisting of monomers containing about N_e bonds, in another words, one dimensional diffusion along a random walk path, reptation [85].

The change in scaling of D from $D \propto N^{-1}$ according to Rouse model to $D \propto N^{-2}$ as predicted by the reptation model at N_e is schematically represented in Figure 14.

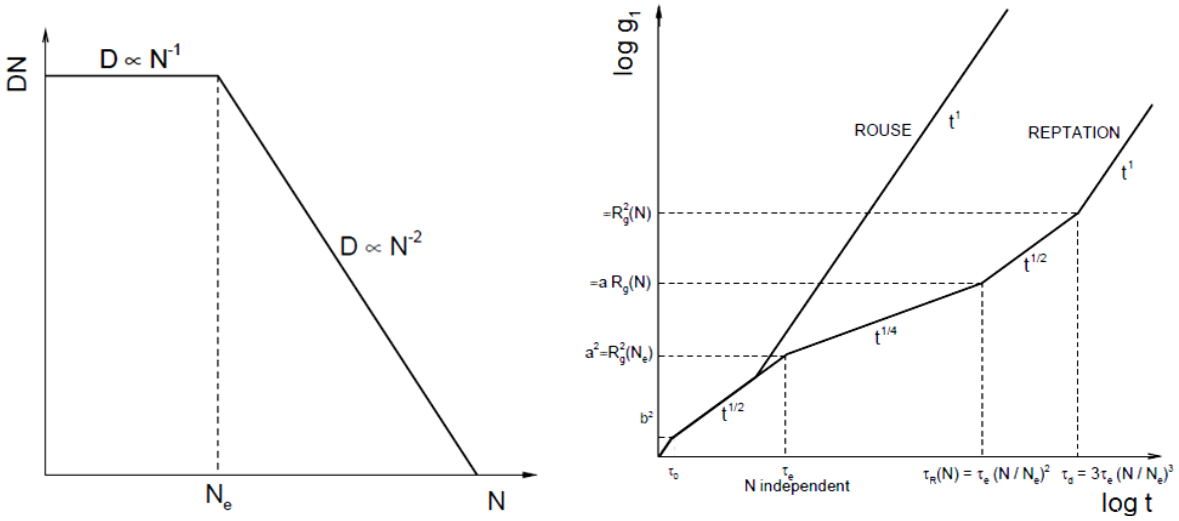

Figure 14: Schematic representation of the chain length dependence of DN. This dependence id predicted theoretically to have a crossover from the Rouse regime to the reptation regime as the chains are long enough to entangle (left) and of the time dependences g_1 conform to the Rouse and reptation models (right)

Picu et al [87] investigated the structure and dynamics of polyethylene melt with homogeneously distributed nanoparticles. The interparticle distance and the particle-monomer interaction were considered as variables. The chain dynamics were monitored by computing the Rouse relaxation modes and mean square displacement (MSD). The dynamics were slowed down by both geometric (confinement of fillers) and energetic (monomer-particle interaction) effects [88]. Starr and Glotzer studied the effect of interaction parameter type to the shift of the glass transition [89]. MC studies of filled polymer have been performed by Vacatello [90] showing the impact of the particle distribution. The polymer chains were reduced in size in comparison with melt to keep the molecular to particle size ratio. It was shown that the polymer units at the interface with the filler particles were arranged in densely packed and ordered shells analogous to the layers found near the flat solid surfaces; the thickness of these shells was approximately twice the transverse diameter of the polymer chains. Even in the absence of specific interactions with the polymer, the filler particles behaved as highly functional physical cross-links, reducing the overall mobility of the polymer chains with respect to the unfilled melt. The conformational distribution of the

polymer is strongly perturbed by the presence of the filler both on the global and on the local scale; in particular, the average dimension of chain segments comprising more than a few units is reduced when compared to the unfilled melt [90].

The dynamic fragility concept refers to deviations from Arrhenius temperature dependence of mass transport or relaxation properties (e.g., relaxation time, viscosity, fluidity) [91-93]. Strong liquids exhibit nearly Arrhenius temperature dependence of these dynamic properties. Fragile liquids by contrast generally display Vogel–Fulcher–Tamman [94-96] or Williams–Landel–Ferry behavior [97].

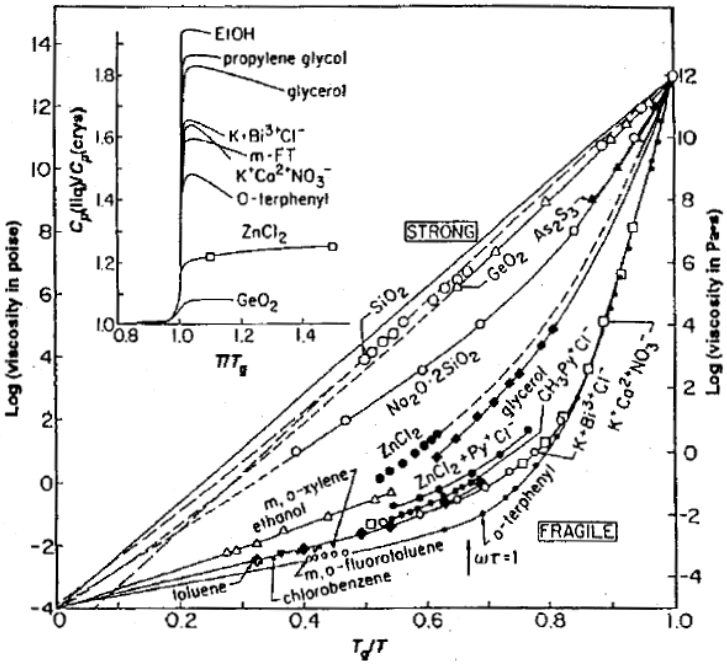

Figure 15: Plot of viscosities of various glass-forming materials against T/T_g (Angell plot). More fragile materials follow the WLF shaped dependencies. The change of the fragility with the changes in the particle-polymers interaction [91].

Douglas [98] interprets this phenomenon from a generalized entropy theory of polymer glass-formation that combines the Adam-Gibbs model for the rate of structural relaxation with the lattice cluster theory (a sort of generalization of the Flory approximation for semiflexible polymer fluids) for polymer melt thermodynamics. The entropy theory of Gibbs and Di Marzio [99] focuses on the conformation entropy of polymers and tries to provide a theoretical explanation for the Kauzmann paradox, considering the canonical partition function of K polymer chain length N in a volume V [98]:

$$Z = \sum_E \Omega(E, K, N, V) \exp(-E/k_B T), \qquad (6)$$

where *E* is the internal energy of the system and *Ω* the microcanonical partition function (i. e. the total number of states). Then, the relative rigidity of the side groups and the chain backbone directly affects the structural relaxation times τ through the Adam-Gibbs relation [98,100]:

$$\tau = \tau_0 exp\{\beta\Delta\mu[s^*/s(T)]\}, \quad (7)$$

where τ_0 is the high-temperature limiting relaxation time in the fluid, $\Delta\mu$ is an (property and system dependent) activation energy at high temperatures (where τ has an Arrhenius temperature dependence, $\tau = \tau_0 exp\{\beta\Delta\mu\}$ and s^* is the postulated high-temperature limit of s as a function of temperature *s(T)*. Equation (7) implies that glass fragility is directly related to the rate of change of *s(t)* as well as to the strength of van der Walls interactions and other microstructure effects through the kinetic parameter $\Delta\mu$. The most convenient measure of the fragility is still being discussed, but one of the most commonly used parameters is fragility index *m*, which is the rate of the change in logarithm of the dynamic property (e.g. viscosity, relaxation time) with the change of temperature:

$$m = d(\ln\tau)/d\left(T_g/T\Big|_{T_g}\right). \quad (8)$$

For strong systems, the rate of change of τ with respect to *T* is smaller that of fragile systems; hence *m* is larger for more fragile glass-forming fluids.

Tremendous amount of work on polymers dynamic fragility has been done by McKenna et al. [101, 102]. Their experimental studies consider the structural characteristics of the polymer chains. It is suggested that polymers with simple backbone and side group structures are the strongest glass formers (e.g polyisobutylene and many polyefines), while flexible chains with bulky, stiff side groups, such as polystyrene, are relatively fragile. Finally, polymers with bulky, stiff backbones (typified by polycarbonate) are highly fragile.

The changes in dynamic fragility with the addition of the nanofillers were focused on by Starr and Douglas [103]. So far, not many experimental studies on the particle effect on the dynamics fragility of the composite materials have been done. However, it is suggested that with the presence of the nanoparticles the fragility or, in another words, the rate of dynamic response to the changing temperature should be changed. According to the obtained results, the fragility of the nanocomposite is altered in following way: increased in case of attractive and decreased in case of non-attractive mutual particle-matrix interactions.

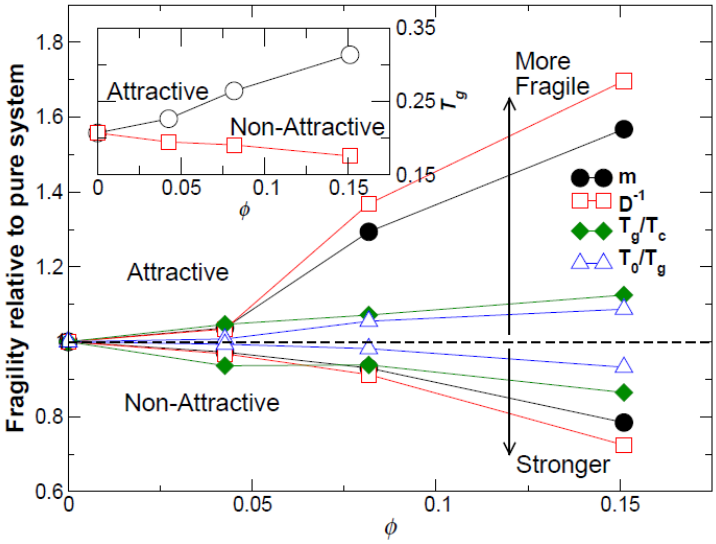

Figure 16: The dynamic fragility changes with the addition of nanoparticles with the various matrix-filler interaction types [103].

In the ergodic system without any strong interactions the materials are viewed as the strong ones within the fragility concepts. Also, the Rouse and reptation-like descriptions of the dynamics are viewed as an unperturbed. With the changes kinetic factors, in mutual interactions in the systems, the adsorption and desorption of the molecules on a surface of e.g. a filler, bridging, e.g. activation energy, friction coefficient or the diffusions are changed, resulting in the changes of activation energy of the process. The same approach is visible also in the fragility based theory combined with a lattice cluster theory, based on the Eyring transitions states [104]. Here, the kinetics factors are included in the activation energy Δμ, which, from the transitions state theory, can be identified with the height of the inter-segmental rotation barriers. Logically, the changes in the inter-segmental rotation barriers will cause the polymer chain to be more active or less opened to the molecular motion, thus will result in the perturbations of the motion on considered scale, reptation.

With the spherical constraints of any kind, speaking in terms of the chain rigidity, packing efficiency or the volume excluded by the fillers, higher densities at the fillers interface caused by the attractive the attractive filler-matrix interactions configuration entropy will be altered. From another point of view, these spherical constraints will be mirrored in the effective entanglement lengths, the length and thickness of the primitive path tube as well as the reduction of the time and length scale for the unperturbed motion of monomer units or the dimensions of the allowed diffusion.

Thus, it suggests approaching the fragile systems as the polymers with perturbed reptation motion and strong ones as the unperturbed ones with a possibility to react quickly to the internal or external impulses and events. Also, primitive path approach can be viewed within Flory approximation for semiflexible chains as it is done in the generalized lattice

cluster theory. However, the crystallization process in comparison with a glass transition region to which the dynamics fragility concepts are strongly related takes place at higher temperatures, where the Arrhenius and the WLF regimes have highly similar courses.

2.2.2 Chain immobilization at the particle surface

Due to the filler-matrix interaction the polymer monomer friction coefficient is effectively changed in the filler interphase. Effectively increased monomer friction coefficient represents the greatest contribution to the lengthening of the reptation time of a chain with given molecular weight partly adsorbed on solid surface. As it has been established by Rubinstein et al. [105], the friction coefficient of a chain adsorbed on solid surface, ζ_c, is composed of two parts and it can be written as follows:

$$\zeta_c = \zeta_0\left(N - N^{1/2}\right) + \zeta_a N^{1/2} \tag{9}$$

The process of the adsorption is not permanent but changes in time, depending also on the filler-matrix interaction strength. Moreover, filler particles should cause an increase in the number of entanglements in the physical systems [106]. Chain entanglements can alter a materials behavior, for example, by affecting the particle diffusivity in a polymer matrix or by causing a strain dependence of dynamic modulus measured simultaneously during stress relaxation in a neat polymer. The process of dynamic adsorption-desorption of the chains at the particle surface can have the same effect as a higher number of effective entanglements.

2.2.3 Spatial confinement

Problems encountered in the description of overall kinetics in fiber-reinforced systems are similar to those for crystallization in a finite volume because the space inhabited by fibers is not accessible for crystallization. The main difference is that fibers are dispersed within a polymer matrix in a more or less random way.

Development of the theory that enables one to account for the spatial confinement effect on the overall crystallization kinetics was initiated by Escleine et al. [107] and Billon et al.[108], who derived the respective dependence for isothermal crystallization in a plate bounded by two parallel planes. In their approach, if the radius of a sphere, *r*, exceeds the distance from the sphere center to the surface of a plate *h*, the volume of a sphere confined within the plate is reduced accordingly.

The computer modeling of crystallization in systems reinforced with long fibers was conducted by Mehl and Rebenfeld [109] and [110] Krause et al. [111] and Piorkowska [112]. In those models, either the instantaneous or spontaneous nucleation in polymer bulk was assumed whereas nucleation on fiber surfaces was treated as instantaneous. Once nucleated,

spherulites grew at a constant rate in all radial directions until impingement with another spherulite or with a fiber. In 2D cases considered by Mehl and Rebenfeld [109] fibers constituted impenetrable obstacles for the spherulite growth and the crystallization proceeded in a similar way as in an assembly of independent finite width strips. In 3D cases, however [110] fibers limited growth of spherulites only partially. Non-overlapping, unidirectional fibers, all of equal thickness distributed randomly [109-110,112] or regularly [111] were considered. In Ref. [112] also, a system with fibers represented by lines with zero thickness was simulated; they were aligned in one direction or in three perpendicular directions.

The results indicated that the fibers depressed the crystallization rate when compared to that of neat polymers or enhanced the crystallization rate by providing nucleation sites.

The effects are enhanced by larger fiber content and also by their smaller thickness. Avrami plots [12-15] might not be in the form of straight lines but curves with varying slope.

For nano-sized fillers, the dimensions are comparable with the gyration radius of polymer chains and thus the lowest size scales are perturbed. The average reptation tube diameter for PE is 50Å and above that it supposed allow proper development of a 3D structure in the neat polymer [113].

2.2.4 Crystal growth rate in nanocomposites

The spherulite growth rates were investigated by Nitta and col. [114]. For polypropylene filled with nano-silica, it has been shown that the crystal growth rate is reduced with the increasing amount of the filler. The observed behavior was subscribed to the geometrical constraints.

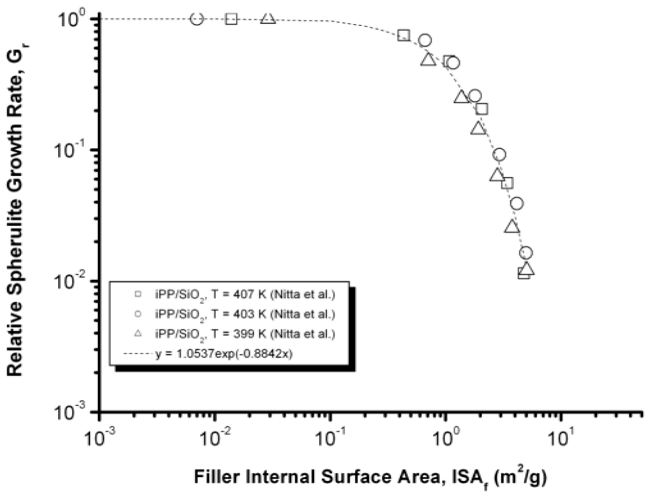

Figure 17: Experimentally measured dependence of spherulite growth rate on internal surface area for iPP-SiO_2 nanocomposite presented by Nitta et al. [114].

Similar trends were observed by Waddon and Petrovic [115] for polyethylene oxide filled with colloidal silica. The focus is given at the behavior at the different crystallization temperatures and Slowing down of the crystal growth with the increasing filler content is interpreted in terms of reduced molecular mobility. However, no direct evidence of this interpretation was given. Recently, the approach to view the crystallization behavior in nanocomposites from the point of the dynamic fragility concept has been presented [116]. It has been shown previously that the chain mobility can be considerably reduced in the presence of nano-sized inclusions near and above the matrix glass transition temperature, T_g [117]. Hence, it could be assumed that the presence of weakly interacting silica nanoparticles could result in an increase of the activation energy of chain diffusion, Q_D^*, in the melt resulting in a considerable change in crystallization kinetics, similarly to the trends observed by Nitta for polypropylene.

3 MAIN GOAL OF THE THESIS

A hypothesis has been proposed that the diffusion controlled rate of crystal growth is reduced due to the immobilization of the chains in the vicinity of the filler particles by either interactions with the surface or by chain confinement between closely packed nanoparticles.

In this PhD thesis, the isothermal crystallization of commercial grade HDPE filled with varying amount of silica nanoparticles has been investigated. Laboratory synthesized monodisperse polyethylene will be used as a model matrix in order to determine the scaling laws of the crystal growth rates with the molecular weight. The polarized optical light microscope equipped with hot stage will be utilized to measure the spherulite growth rate under various crystallization conditions. The nucleation effect of the filler and effect of its spatial distribution will also be explored. In order to verify the proposed hypothesis, experimental results will be compared with the prediction based on the secondary surface nucleation theory of Lauritzen and Hoffman expanded by Miller to include the chain reptation to the crystal surface.

Further, extensive computer modeling employing molecular dynamics (MD) and Monte-Carlo (MC) simulations will be performed to provide further insight into effects of various structural variables on the prediction of crystallization rate and to evaluate the relative contributions from the chain-particle interaction and chain confinement, respectively, to the change in distribution of reptation relaxation times in space and time domains. Results of these simulations will further be compared with experimental data on well defined nanocomposites with monodisperse polymer chains to determine the scaling laws as well as uniform particle distribution to eliminate effects of agglomeration.

4 MATERIALS AND METHODS

4.1 Materials

Fumed silica (Sigma Aldrich, USA) with specific surface area of 390 m^2/g and mean particle diameter d = 8 nm was used as the nano-filler. This type of silica, who has a spherical shape, has been chosen to eliminate the effect of the filler shape.

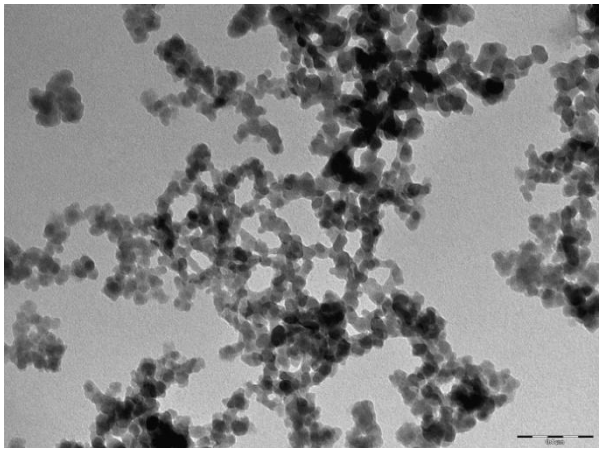

Figure 18: Transmission electron micrograph of the used silica fillers. The tendency of the fumed silica to aggregate is shown.

Commercial high density polyethylene, HDPE, and laboratory synthesized model polyethylene with narrow molecular weight distribution were used as matrices. Homopolymer Liten MB 71 (Chemopetrol, CZ, M_w = 86 000 g/mol (determined by high temperature gel permeation chromatography), M_w/M_n = 5.79) was used as a matrix. Nanocomposites were prepared by adding silica into the xylene solution of HDPE at 130°C under ultrasonic vibrations, intensive mixing and drying at 70°C for 10 hours. Dried nanocomposite powder was compression molded at 170°C using a press (TP 400, Fontijne) into 1 mm thick sheets. The neat PE, used as a reference material, went through the same preparation procedure as the nanocomposites.

Sample	Filler volume content (%)	Specific internal surface of fillers in nanocomposite = filler-matrix contact area (m^2/g of composite)	Specific internal surface of fillers in nanocomposite = filler-matrix contact area (m^2/cm^3 of composite)
Neat HDPE	0	0	0
HDPE 2	2	16	14.1
HDPE 4	4	32	29.1
HDPE 8	8	64	61.8

Table 1: Table of HDPE samples with emphasis on relation of volume filling and the specific internal surface of fillers in nanocomposite.

Model narrow MWD polyethylenes [118] were prepared using phenoxy-imine complex catalyst bis[N-(3-*tert*-butylsalicylidene)-2,3,4,5,6pentafluoroanilinato] titanium(IV)dichloride in combination with methylalumoxane (MAO) as a co-catalyst.

Methods

Average molecular weight (M_n and M_w) and polydispersity index (M_w/M_n) of the synthetized model polyethylenes were determined by high temperature gel-permeation chromatograph (Polymer Laboratories) at 140 °C in decalin using polystyrene standards. Melting temperature (T_m) was determined by DSC upon heating sample to 160 °C at heating rate of 10 °C/min. The polyethylene was dissolved in xylene at 90°C, stabilized with Irganox 1076 [119] and the various contents of silica were added (0,2,4,8 volume percent). The volume content was kept so low to be able to capture the onset of the investigated crystal growth change with the present of the filler. Consequently, the samples were placed in the ultra sound bath for 15 minutes and then casted on a hot microscope slide and heated for 15 minutes at 170°C. Sample properties are listed in Appendix B.

In principal, the method of nanocomposite preparation has the effect on the chain coil statistics and spatial arrangement and as well on the filler distribution. However, the microscopic samples were prior the measurement heated well above their melting temperature to compensate any thermal or mechanical stress and, also, to avoid the melt memory effect. The changes introduced into the spherulite morphology by residual stress in shown in Figures 19 and 20. Thus, it is assumed the sample preparation method should not be affecting the spherulite growth rate investigation.

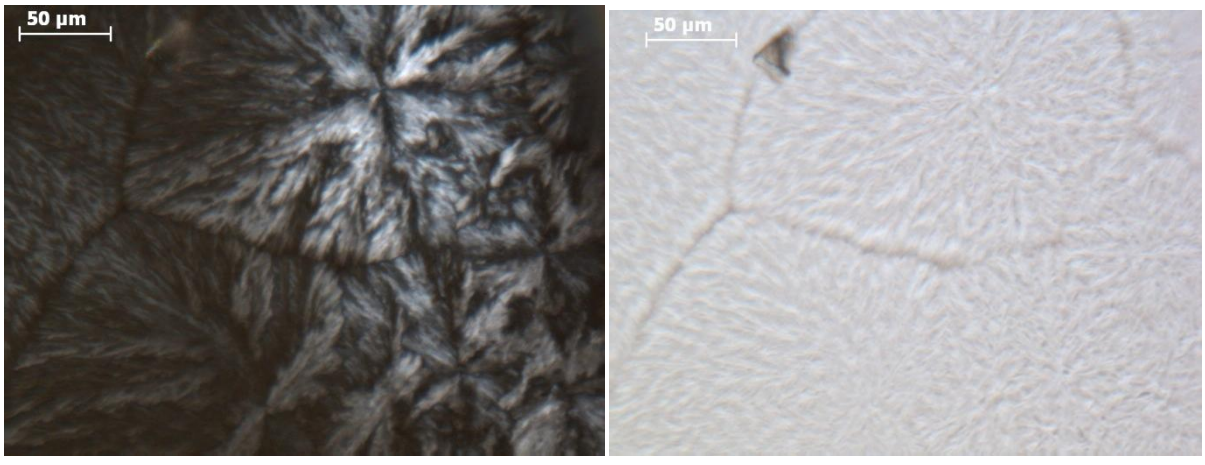

Figure 19: Micrographs of the spherulitic structure. The polarized optical light micrograph is shown on the left and transmission light micrograph on the right. It is possible to see also by naked eye the radial structure in the spherulite.

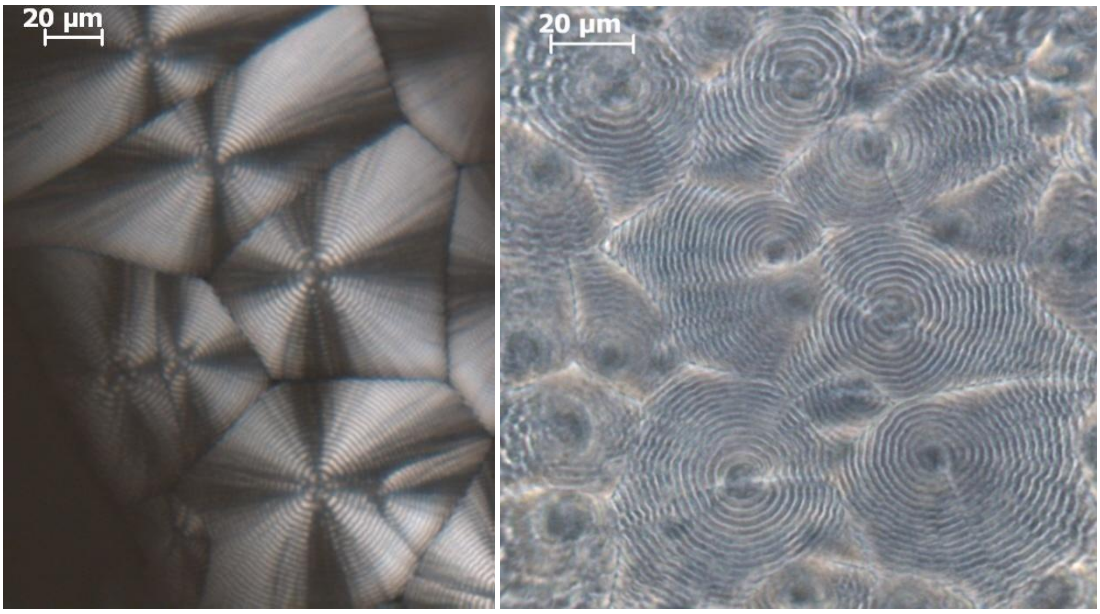

Figure 20: Micrographs of the spherulitic structure. The polarized optical light micrograph is shown on the left and transmission light micrograph on the right. The lamellae are grown from the center in circles. This structure known as a twisted lamellae spherulite in case results from the residual stresses from the sample preparation, in some cases it might be a sign of a branching in the molecule [46].

The spherulite growth rates were investigated using optical microscope (BX50, Olympus) and hot-stage (LTS 350, Linkam) under isothermal conditions at standard pressure

Prepared films of thickness ranging from 5 to 10 μm were used for crystallization kinetics measurements, thin slices cut out from the pressed sheets were placed between two glass slides. Before each measurement of the spherulite radii, the specimen was melted at 170°C. After 5 min at 170^{o}C, the specimen was cooled down below the melting temperature as fast as the hot-stage allowed. The spherulite growth rate was measured isothermally at temperatures 125°C, 126°C, 127°C and 128°C, respectively. These temperatures were chosen to be in the span of crystallization regime II for polyethylene [13]. The samples for the hot stage were prepared using either solution of melting method. The thickness was determined via confocal laser scanning microscopy (CLSM) as the thickness for the spherulite to have a space to fully develop in 3D. To verify the effect of the nucleation of fumed nanosilica in the matrix, the method suggested by Dobreva has been employed [120]. The samples were heated in a differential scanning calorimeter (Pyris 1, Perkin Elmer) up to 170°C at a rate of heating 10°C/min. After 2 minutes at 170°C, cooling down to the room temperature was carried out at rates of cooling 2, 5, 10, 20 and 40°C/min, respectively. Crystallization temperatures were obtained from the DSC peak maxima. SEM and TEM are utilized to study aggregation of the particles.

4.2 Molecular dynamics simulation

The computer simulation stands for the performing an experiments in the computer under predefined conditions. Concerning the matter of interest, they can be run on the various length scales: from sub atomic elementary particle simulation and *Ab initio* quantum simulations at the lowest scale, through molecular and meso-scale levels up to macroscale, where finite element method and its derivations are utilized mainly. One of the greatest challenges in this area is mutual bridging of the given scales.

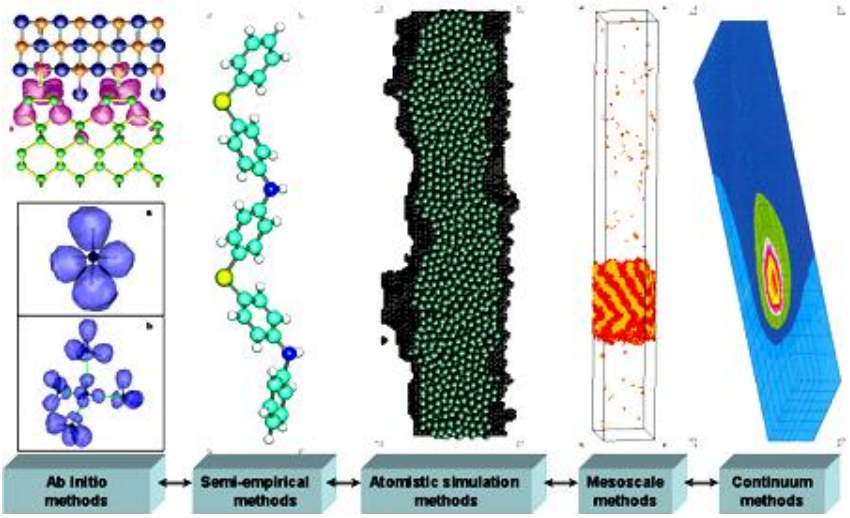

Figure 21: Computer simulations on a various length and time scales

Within this thesis molecular dynamics (MD) and Monte Carlo (MC) methods are employed. Molecular dynamics solves the Newton´s equation of motion with time, the temperature or pressure being kept by coupling to thermostat or barostat, respectively. Monte Carlo method, as suggested by its name, operates on the basics of chance events. The motion is random and mimics the Boltzmann distribution function [121].

A united atom interaction potential was used, in which polymer chains are represented by CH_2 and CH_3 beads that interact via bonding and non-bonding interactions. The importance of using the realistic potential has been shown as crucial for the balance between orienting and crystal packing process. United atom force field for polyethylene melts derived by Paul and coworkers (PYS) [122] has been employed in this thesis.

The PYS force field was configured using experimental data and quantum calculations on short alkanes and has been shown to provide an accurate description of polyethylene melts. The agreement of this model with experimental values is very good for statistic quantities, for dynamic ones it has been found to be 20-30% faster (due to its united atom nature).
The total force field potential consists of several terms [122]:

$$E_{TOT} = E_{BOND} + E_{ANGLE} + E_{TORSION} + E_{NONBOND.} \quad (10)$$

The harmonic bond length potential is expressed by [122]:

$$E_{BOND} = k_b (b - b_0)^2 \ , \tag{11}$$

where k_b = 1470 kJ/mol and b_0 = 1.53Å .

The three body bond angle bending potential is given by [122]:

$$E_{ANGLE} = k_\theta (\theta - \theta_0)^2 \ , \tag{12}$$

where k_θ = 252 kJ/mol.rad^2 and θ_0 = 1.91 rad (109.5°) The torsional potential is in form [Paul 1995]:

$$E_{TORSION} = \tfrac{1}{2} k_1 (1 - \cos(\varphi)) + \tfrac{1}{2} k_2 (1 - \cos(2\varphi)) + \tfrac{1}{2} k_3 (1 - \cos(3\varphi)) \ , \tag{13}$$

where k_1 = 6.804 kJ/mol, k_2 = -3.6414 kJ/mol, and k_3 = 13.608 kJ/mol.These parameters yield a *gauche* energy of 2.1kJ/mol, a *gauche-trans* barrier of 12.6 kJ/mol and *gauche-gauche* barrier of 21kJ/mol. The course of the torsional potential is shown in Figure 22.

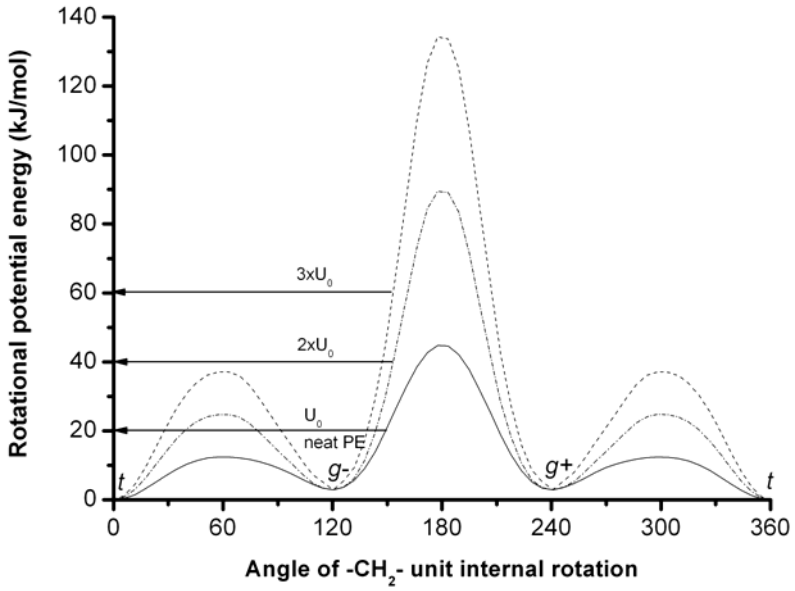

Figure 22: The course of the torsional potential for polymer chain. The U_0 stands for the neat PE, the height of the barriers would increase with increased rigidity or activation energy of the translation motion.

The non-bonded potential for atoms separated by more than three bonds follows the Lennard-Jones (LJ) relation [122]:

$$E_{NONBOND} = 4\varepsilon\left[(\sigma / r)^{12} - (\sigma / r)^{6}\right], \quad (14)$$

where ε = 0.0504 kJ/mol and equilibrium reference distance σ = 4.01Å with a given cut off distance of 12Å. LJ potential is particularly important in the bulk systems.

By variation in LJ particle-matrix interactions the different type of interactions has been set up (Table 2).

	Weakly interacting	Strongly interacting	None	Repulsive
Sigma	4.01Å	4.01Å	4.01Å	4.01Å
Epsilon	0.0504 kJ/mol	0.504 kJ/mol	0 kJ/mol	0.0504 kJ/mol From 0.2 Å : 0 kJ/mol

Table 2: Lennard-Jones potential parameters

Single chain system was created to the test of the physical properties and correctness of the used parameters and methods. The chains of 1000, 2000, 3000 and 5000 units were used as samples. Simulation temperatures were 500K, 400K, 300K, 200K and 100K. The Nose-Hoover temperature coupling was utilized with time constant t = 0.1ps. Velocities at given temperature were generated by the Maxwell distribution. First 5ns of the simulation were taken as equilibration of the system.

The system of 100 chains, each one containing 100 units, was generated by Monte Carlo method respecting the potential field presented. The script was written in C/C++ programming language. The bond lengths and bond angles were kept constant and the torsional angles were distributed according to the Boltzmann distribution at the given temperature. The bulk sample was generated at the reduced density 0.3g/cm^3, because at higher densities the probability to find the acceptable free The Nose-Hoover temperature coupling was utilized with time constant t = 0.1ps. As for the single chain system, velocities at the temperature 500K were generated by the Maxwell distribution and first 5ns of the simulation were taken as equilibration of the system.

The nanoparticles consisted of 46 Lennard-Jones particles bound to form icosahedral shape (Figure 23). It was inserted into the nanocomposite prior the generation of the melt .The diameter of the particle was 2nm. Consequently, the sample was allowed to equilibrate at 500K for 1ns.

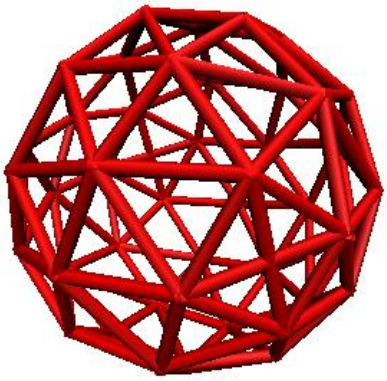

Figure 23: The nanoparticle representation. The Lennard-Jones particles are in the tips of the icosahedral object. The interaction radius of each particle is dependent on the filler-matrix interaction type (Table 2).

According to Yamamoto [123], the crystal surface was defined as the aligned chains in the *xy* plane with the interlayer spacing of 3.78 nm which corresponds to the crystal facet (100). The starting simulation box was 27x80x70A. As we are investigating the crystal growth itself not the nuclei formation or initiation period, this definition of the crystal surface has proven to be in line with the polymer physics.

The standard measure of order used in polymer systems is the global bond orientational parameter at time *t*

$$S(t) = \frac{3\left\langle \left[\nu_i(t) \bullet \nu_j(t) \right] \right\rangle}{2} - \frac{1}{2} \quad , \qquad (15)$$

where $\nu_i(t)$ is the orientation vector of atom *i* at time *t*, defined by the chord from atom *i*-1 to atom *i*+1, and the average is taken over all pairs *i* and *j*. However, in order to calculate the spatial distribution of order within the simulation box a local orientation order must be defined. The method implemented by Waheed [124] based on the convolutions of the local chain orientation vectors with spatial box functions is utilized. The orientation order at a particular *z*-value and time is a function of the distribution of the local order $f_v(z,t)$ as described below,

$$f_z(z,t) = \sum_{i=1}^{n} \nu_i(t)\sigma(z - z_i) \quad , \qquad (16)$$

where z_i is the *z*-component of the position vector of atom *i*. For convolution, the box function $g(u_i)$ is used

$$g(u_i)=\begin{cases}0 & -\infty \le u_i \le \dfrac{-\mu}{2}\\ \dfrac{1}{\mu} & -\dfrac{\mu}{2} \le u_i \le \dfrac{\mu}{2}\\ 0 & \dfrac{\mu}{2} \le u_i \le \infty\end{cases}, \qquad (17)$$

where μ is the convolution width. The script to calculate the local order parameter has been written in Python scripting language. The convolution widths were the magnitude of the defined PE intermolecular distance (4.01A) with the convolution plane determined due to the density profiles created at the primary crystal surface. The growth rates were calculated from the order parameter extrapolation to the completion of the lamellae. The first and second closest lamellae to the crystal surface were taken into account. The original crystal line serves as a reference for the order parameter value. As only the inner parts of a polymer chains undergo a real reptation motion and the beads at the chain ends are free to explore the space out of the tube, the chains ends are not considered in the order parameter or dynamic analysis at this work.

For nanocomposites, the samples were equilibrated for 1ns at the temperature of 500K. The simulation was conducted in the NVT ensemble (constant number of particles (N), volume (V) and temperature (T)) at the temperature of 400K. The molecular simulation package Gromacs 4.0.5 [125] has been used to perform the computer simulation and Visual Molecular Dynamics [126] was utilized for visualization. The computational cost was 25.797 Mnbf/s, simulations were conducted to 100ns. Description of the various model arrangements is shown in Appendix C and Figure 24.

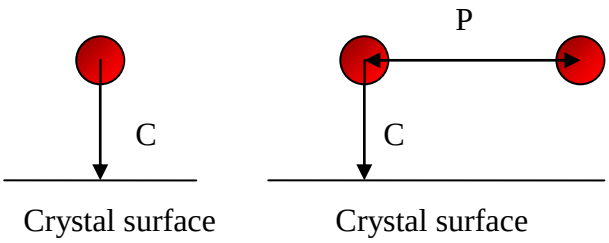

Figure 24: The experiment arrangement for single particle and two particles. The arrows sign the distance from the crystal surface and the inter-particle distance, respectively. C stands for the distance from the crystal surface and P for the distance of particle centers, respectively.

5 RESULTS

5.1 The nucleation effect and aggregation of the fillers

Although this work is primarily focused on the subsequent spherulite growth, it is important to investigate the possible heterogeneous nucleation activity and the aggregation effects of the fillers that could affect the crystallization kinetics and its interpretations, significantly.

5.1.1 The nucleation effect of the fillers

In the first step, the evidence of the nucleation activity of the fillers was investigated visually. According to Liu [42], the homogeneous nucleation starts from the nucleus exceeding a critical size, followed by lamellae formation and further development of the spherulite structure. This type is accompanied by the formation of a typical so-called "pair of eyes" in the spherulite center in contrast to the heterogeneous nucleation [42].

Below, the snapshots of the structure formation in the polyethylene filled with 2%vol of fumed silica are depicted. As indicated by the arrows, the "pair of eyes" formation can be seen, especially in the middle micrograph.

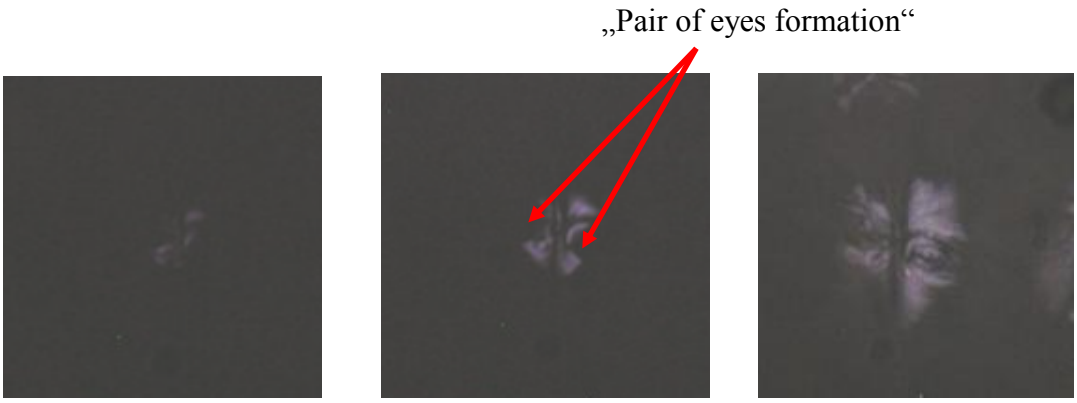

Figure 25: Micrographs of the spherulite formation, HDPE, 2vol % fillers. The creation of the pair of eyes signifying the homogeneous nucleation is shown.

In the case of a nucleation activity of the filler, similar crystallographic plane as the one of the latter structure should be present. Moreover, the seed would remain in the center of the crystallized object. With this in a mind, the HDPE samples were chemically etched and subjected to scanning electron microscopy. No statistically significant presence of the particles in the spherulites centers occurred. The micrographs in Figure 26 are shown as a representative example. Based on these observations, one could assume that there is no significant nucleation effect of the filler on the HDPE used. To support this observation with

more exact experimental data, the method of Dobreva based on the shifts in crystallization temperatures with various DSC cooling rates [120] was used.

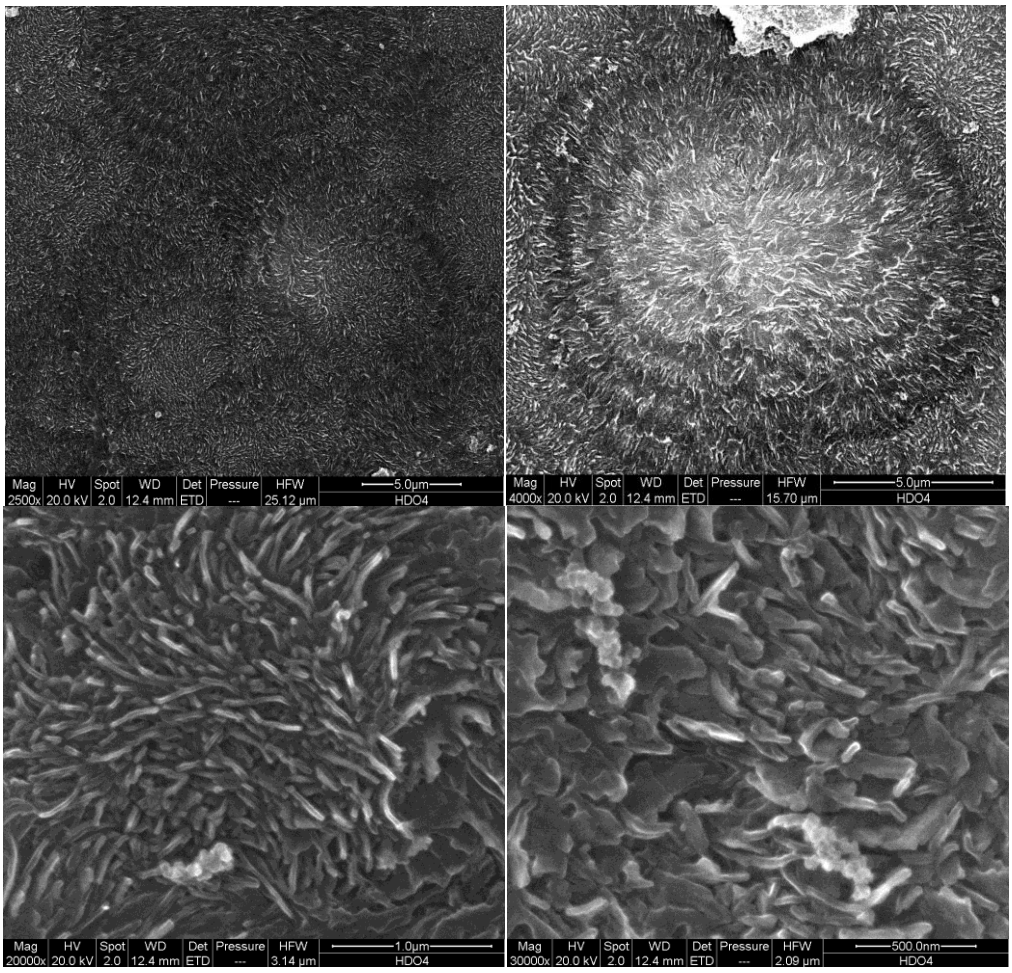

Figure 26: SEM micrograph of chemically etched HDPE containing 8 vol% of silica nano-filler. The silica nano-filers or aggregates are not found in the spherulites center.

According to Dobreva [120], nucleation activity, *v*, is a factor by which the work of nucleation decreases with the addition of a solid substrate. The neat and filled HDPE were cooled down using the Differential Scanning Calorimeter (DSC). For homogeneous nucleation in the melt, the relation between the uniform cooling rate and the undercooling can be expressed as follows:

$$\log r = A - \frac{B}{2.3\Delta T^2}, \tag{18}$$

and for heterogeneous case,

$$\log r = A - \frac{B^*}{2.3\Delta T^2}, \tag{19}$$

where r is the cooling rate, A is a constant and ΔT is the undercooling, $\Delta T = T_m - T_c$; T_c corresponds to the crystallization temperature determined as the peak at the DSC curve and T_m equilibrium melting temperature of ideal crystal. Parameter B can be expressed as:

$$B = \frac{\omega\sigma^3 V_m^2}{3nkT_m\Delta S_m^2}, \tag{20}$$

where ω is the geometrical factor; σ is the specific surface energy, V_m is the molar mass volume of crystallizing substance, n is the Avrami exponent, ΔS_m is the entropy of melting and k is the Boltzmann constant. The nucleation activity ν can be defined using the previous equations as:

$$\nu = \frac{B^*}{B}. \tag{21}$$

Hence, it can be calculated as the ratio of slopes of *log r* versus $1/(\Delta T)^2$ for neat HDPE and filled HDPE system. Its value is in the range from 0 to 1 from extremely active to inert particles.

The final experimental *log r* versus $1/(\Delta T)^2$ dependence is shown in Figure 27. The nucleation factor is unity for all cases within the experimental error suggesting that the silica nano-filler used in our experiments did not exhibit any significant nucleation activity in HDPE matrix under the experimental conditions used.

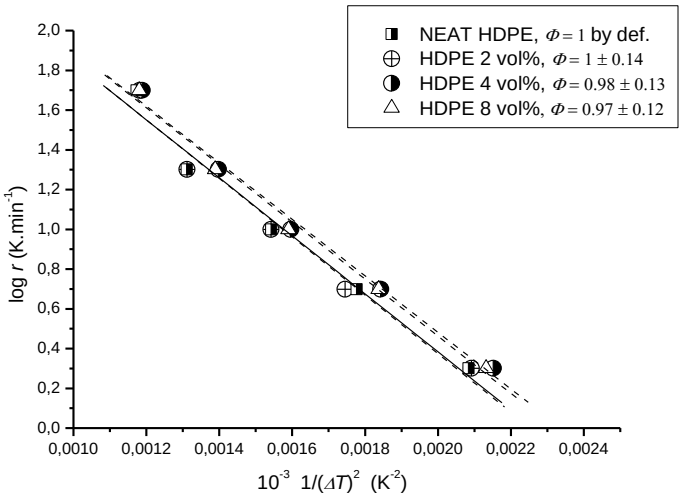

Figure 27: The silica nucleation activity estimation. The nucleation coefficient, ν, is the ratio of the slopes neat/filled HDPE.

5.1.2 Effects of silica aggregation

Results of the measurements can be obscured significantly by a non-uniform spatial particle distribution. Nanometer sized silica particles tend to form more complicated structures, depending on the matrix – filler interaction type and solidification process [127]. In addition to forming particle strings upon synthesis, the fumed silica has a strong tendency to aggregate in polymer matrix similarly to colloids. This results in formation of island like structure of resin rich and particle rich areas (Figure 28). The TEM micrographs have been taken for the HDPE filled with 8 volume % of fumed silica.

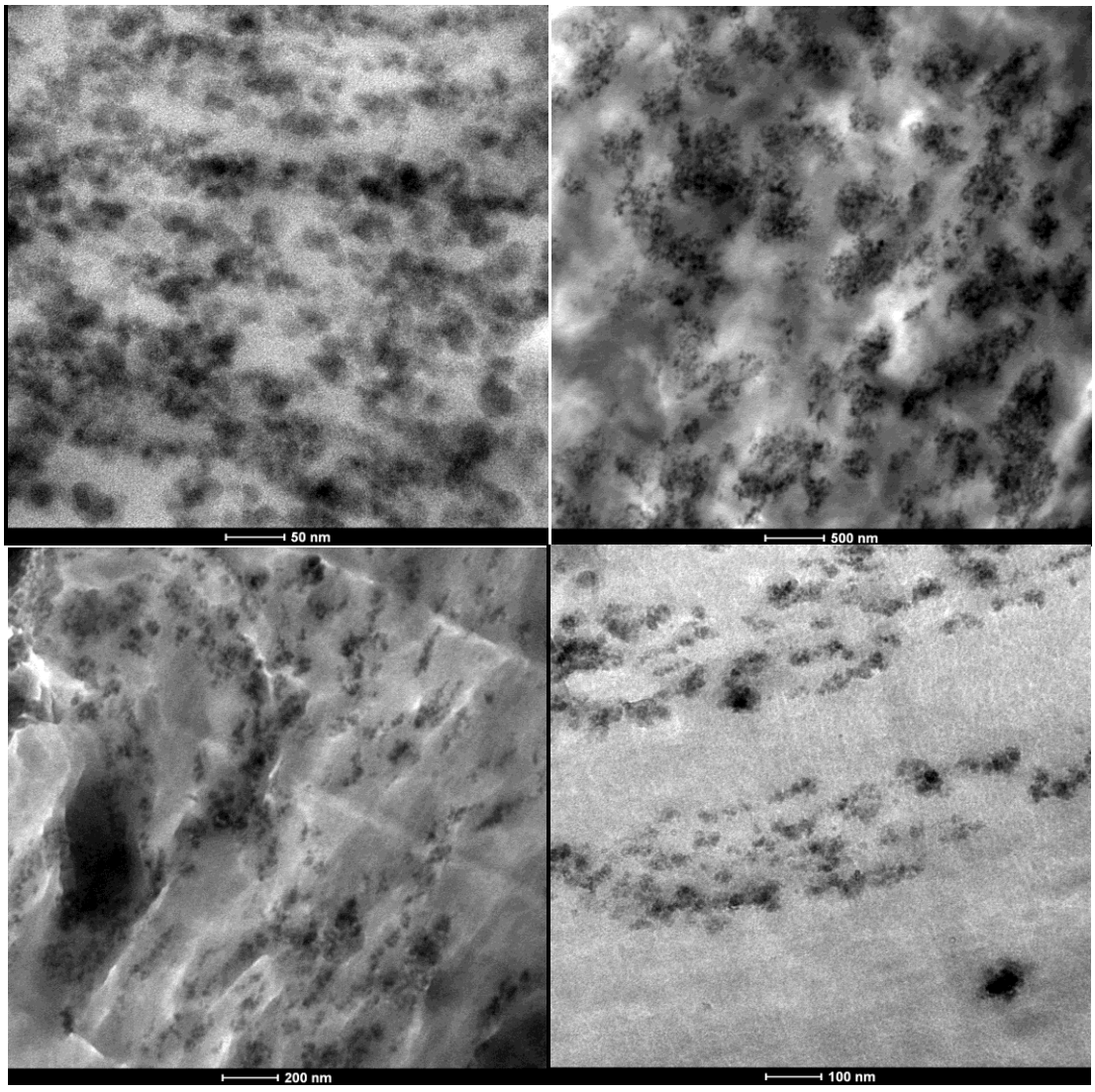

Figure 28: TEM micrograph of HDPE containing 8 volume % of silica nano-filler. The areas with different filler contents are shown. The various scales are shown with the impact on the various scales.

This tendency of nanosilica to aggregate can be explained utilizing the DLVO theory (named after Derjaguin, Landau, Verwey and Overbeek) developed to explain the tendency of colloids to aggregate or remain concrete [128,129]. This approach is based on calculation of electrostatic repulsion and van der Waals attraction forces and the can be successfully used also for the nanosilica particles. Electrostatic repulsion becomes significant when two particles approach each other, van der Waals attraction is actually the result of forces between individual molecules in each particle. By balancing these two opposing forces the most energetically favorable and thus stable mutual distance of the particles can be determined.

These forces can be successfully altered by fillers surface treatment [130]. They grafted polystyrene chains to silica nanoparticles, whose were then impregnated into polystyrene matrixes of different relative molecular mass. It was proved that to control the assembly is crucial to tailor the grafting density of polystyrene and the relative chain length of the grafted and matrix polystyrene.

Within this thesis, surface treatment of the silica nanoparticles would introduce another entity into the matrix-filler interface, changing the dynamics in the investigated area. Thus, to overcome the aggregation issue, the ensemble of the representative samples of the nanocomposite was chosen and the results were averaged.

5.2 The Spherulite Growth Rate

The spherulite growth rate was investigated utilizing polarized optical light microscopy equipped with a hot stage. The thickness of the sample for the experiments was 5-10μm to allow the full development of the three dimensional structure. In confocal laser scanning micrograph (Figure 25), it is possible to see that at the given sample thickness, the spherulites were fully developed and approximately the same size, thus, they were nucleated at the same moment and grew linearly to fill the space. As the spherulites in completely crystallized PE are of the order of tens of micrometers, the polarized optical microscopy can be used to investigate the kinetics of their growth. The growth rates were measured isothermally with the medium level undercooling corresponding to crystallization regime II (see Figure 29) where the effect of particles on the chain reptation is expected to be the most pronounced. For polyethylene, this range corresponds to crystallization temperatures in the range of 120-129 °C [13]. The results of 10 measurements were averaged to determine the average growth rate, G.

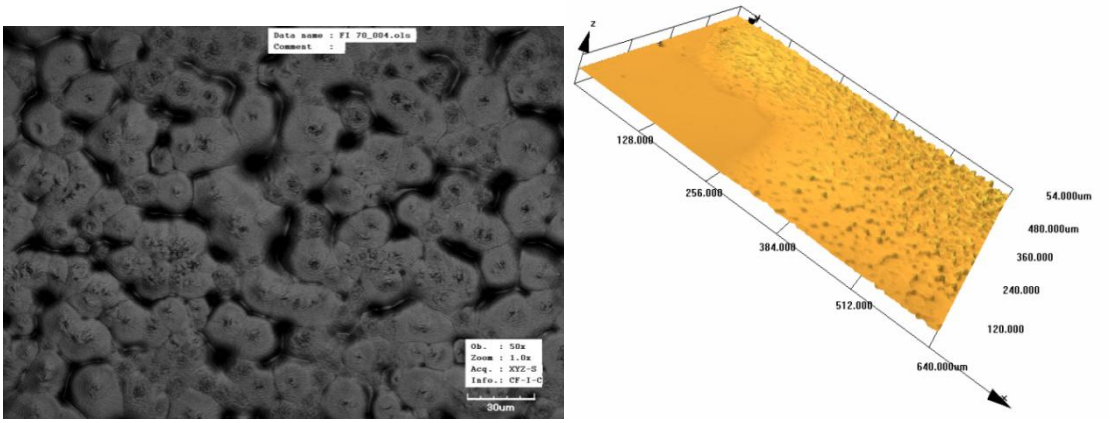

Figure 29: The confocal laser scanning micrograph of the spherulites in HDPE. On the right is shown the example of the sample thickness determination via CLSM as the average distance of the spherulites top from the microscope slide.

The micrographs of the growing spherulites are shown in the Figure 30. They were taken for the neat polyethylene at the temperature 127°C, the interval between the shots was 5 minutes and the last micrograph exhibits the final stage when the crystal growth observable by the polarized microscopy is finished. The black areas correspond to the amorphous parts while the light ones correspond to the crystalline phase. The light objects are crystals of HDPE. In time, the spherulitic structure starts to emerge and grows, until the crystals impinge each other at the boundaries (Final micrograph figure 30).

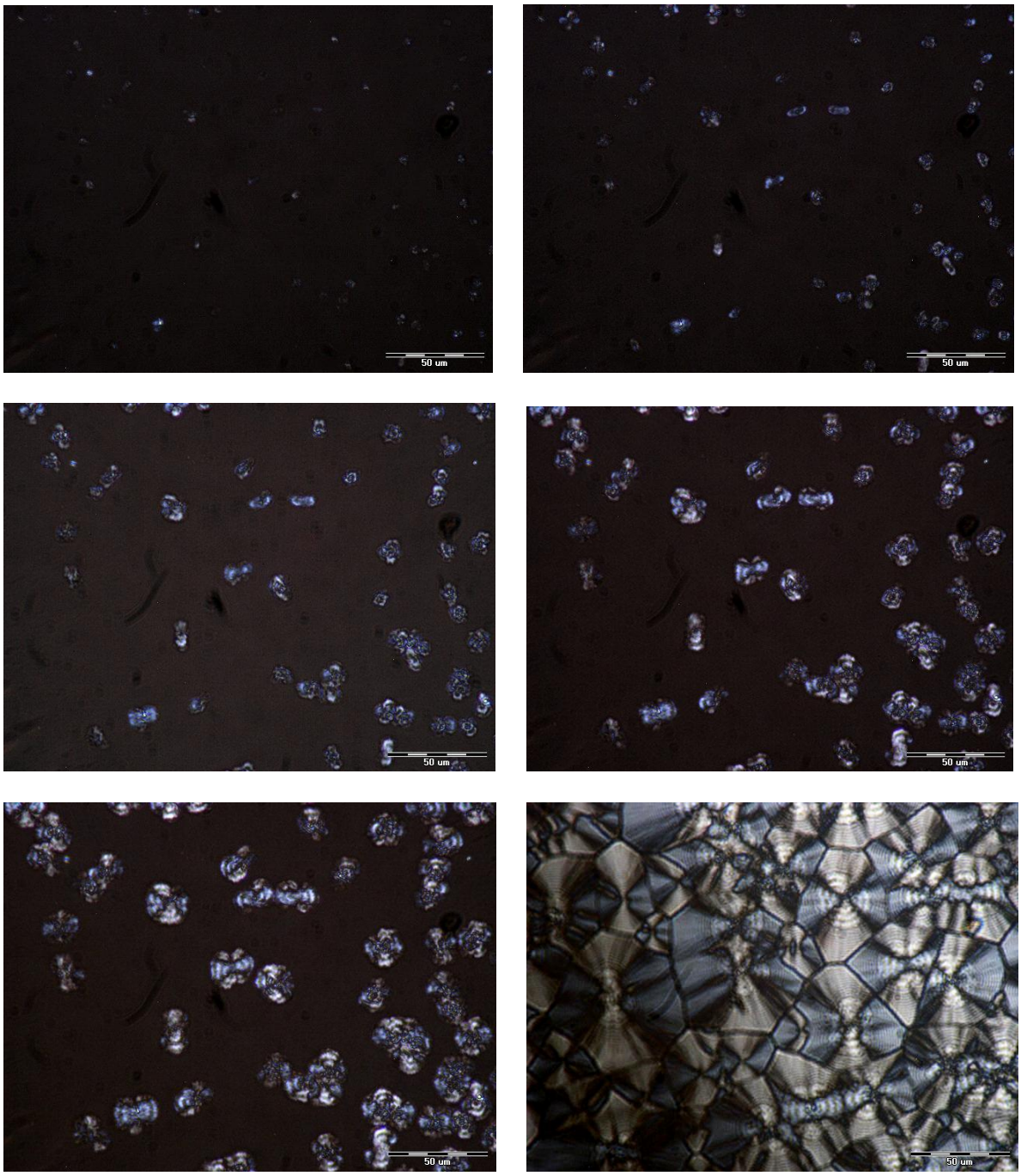

Figure 30: The micrographs of the growing spherulites in the neat HDPE at 127°C. The final micrograph corresponds to the observable final structure.

The crystal growth rate was determined from the polarized optical light micrographs taken automatically at suitable time intervals, as an increase of spherulite radius in time. As expected, the growth of the spherulites was linear in time. Then, the final growth rate G_{II} was given by the slope of time dependence of spherulite radii. It can also be seen that the slope of the linear R vs. t dependence decreased with the increasing filler content (see Figure 31-34).

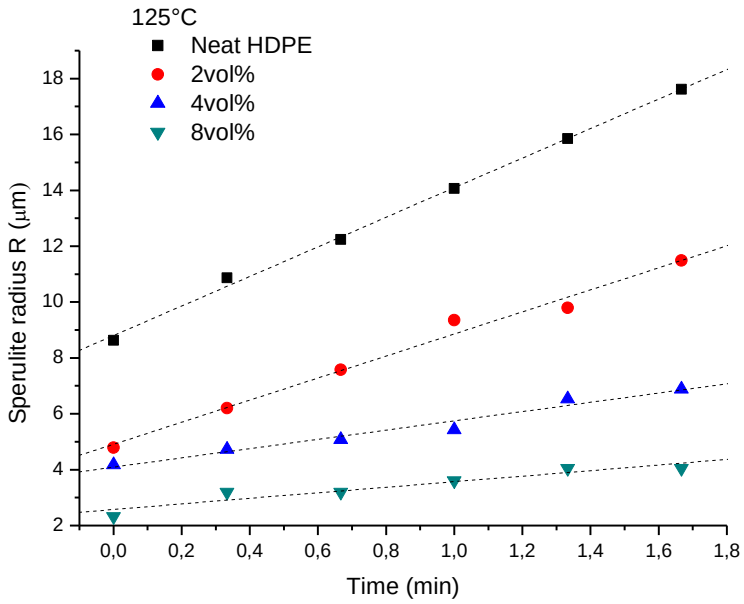

Figure 31: The linear time dependence of spherulite radius R at the temperature 125°C for HDPE/silica nanocomposite with filler content 0, 2, 4 and 8 volume % (specific internal surface 0, 16, 32 and 64 m^2/g of the filler in nanocomposite)

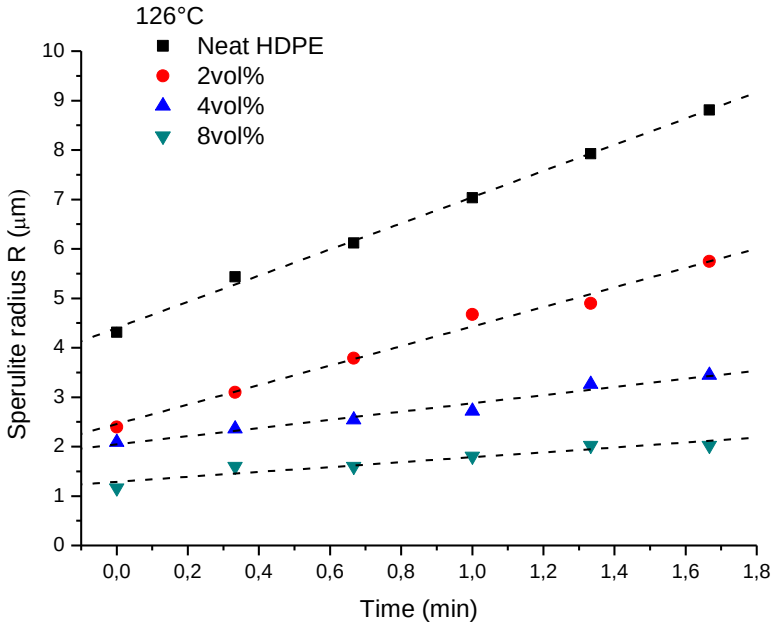

Figure 32: The linear time dependence of spherulite radius R at the temperature 126°C for HDPE/silica nanocomposite with filler content 0, 2, 4 and 8 volume % (specific internal surface 0, 16, 32 and 64 m^2/g of the filler in nanocomposite)

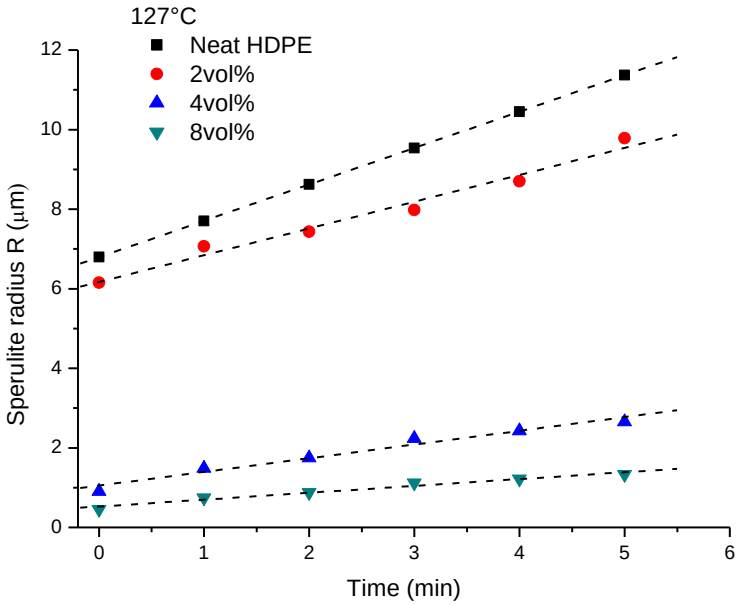

Figure 33: The linear time dependence of spherulite radius R at the temperature 127°C for HDPE/silica nanocomposite with filler content 0, 2, 4 and 8 volume % (specific internal surface 0, 16, 32 and 64 m^2/g of the filler in nanocomposite)

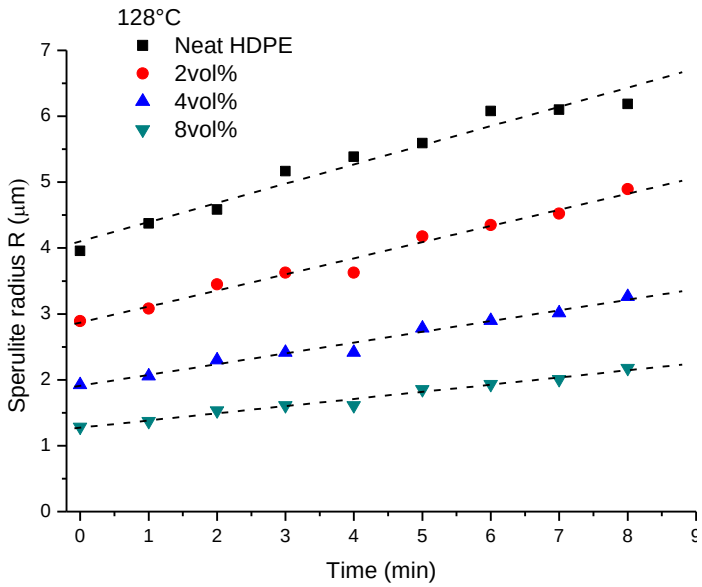

Figure 34: The linear time dependence of spherulite radius R at the temperature 128°C for HDPE/silica nanocomposite with filler content 0, 2, 4 and 8 volume % (specific internal surface 0, 16, 32 and 64 m^2/g of the filler in nanocomposite)

With the increasing area of the matrix-filler interface, for the sample with 8 volume % of silica, the growth rate was reduced to approximately 20%of its value for neat PE. This trend has been observed for the whole range of investigated temperatures in the crystallization regime II. In agreement with the crystallization thermodynamics, the crystallization rates were faster for higher undercooling (Fig. 35, melting temperature T_m = 135°C, temperature of maximum crystallization velocity T_{vmax} = 46°C [3]). However, the trends of the crystal growth dependence on the content of the fillers are very similar in the whole temperature regime (Figure 36). The crystal growth was investigated, thus, the nucleation time was not important in this experiments.

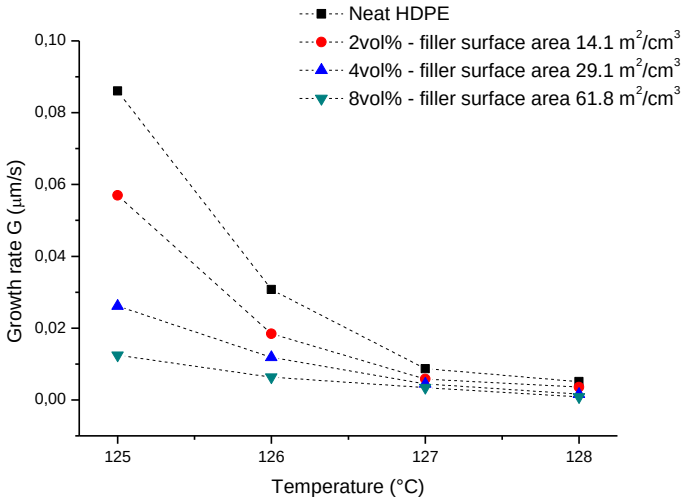

Figure 35: The growth rates dependence on the undercooling for the samples of neat polyethylene and nanocomposite. The diffusion changes are more pronounced at lower temperatures, there are only weak interaction present between the matrix and the filler

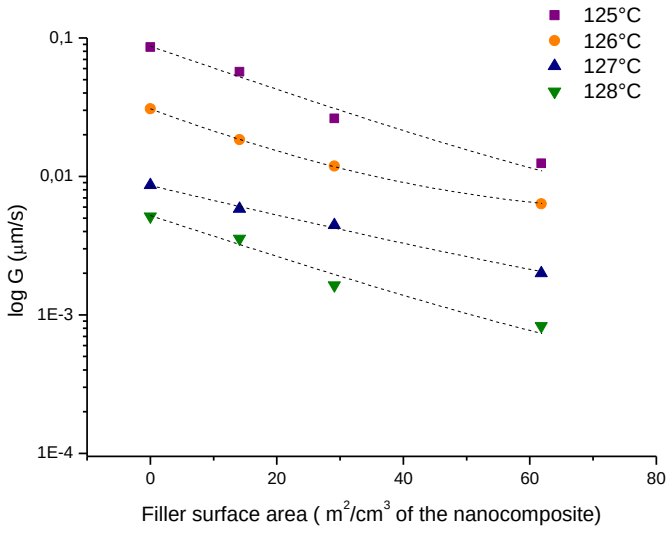

Figure 36: Spherulite growth rate G in dependence on the matrix-filler interface area.

5.2.1 Comparison of experimental results with the L-H theory predictions

To be able to separate various contributions that cause the observed reduction of the crystal growth rate, experimentally measured growth rate data were compared with the predictions based on the Lauritzen Hoffman secondary surface nucleation theory with the incorporated terms for activation energy of the reptation motion.

The main parameters of the kinetic theory proposed by Hoffman and Lauritzen (L-H) [14] to explain the morphology and growth of polymer crystals are the degree of undercooling (ΔT), i.e. the difference between the equilibrium melting temperature (T_m^0) and the crystallization temperature (T_c) and the molecular weight, which would govern the reptation of the macromolecules. According to the Lauritzen-Hoffman model, the spherulite growth rate, *G*, can be expressed for the case of medium undercooling in Regime II as follows [15]:

$$G_{II} = b_0 (2ig)^{1/2}, \tag{22}$$

where b_0 is the thickness of the crystalline layer added to the surface, i is the surface nucleation rate and g is the substrate completion rate. Equation (22) holds for the medium undercooling characteristic of multiple nucleation that is necessary for a chain segment to be attached to the crystal surface The expression for the surface nucleation rate i has been derived by Hoffman and Miller [12] in the form:

$$i = C_0 \frac{\kappa}{2/3n}\left(\frac{kT}{h}\right)\left(\frac{kT(\Delta h_f)(\Delta T)}{4b_0 l_u \sigma^2 T_m}\right)\exp\left(\frac{-Q_D^*}{RT}\right)\times\exp\left(\frac{-4b_0\sigma_e T_m}{\Delta h_f(\Delta T)kT}\right). \tag{23}$$

The substrate completion rate, g, involving chain reptation as the main diffusion mechanism of chains in the melt, can be expressed in the form [12]:

$$g = a_0 \frac{\kappa}{2/3n}\left(\frac{kT}{h}\right)\left(\frac{a_0(\Delta h_f)(\Delta T)}{\sigma T_m}\right)\exp\left(\frac{-Q_D^*}{RT}\right)\times\exp\left(\frac{-q}{kT}\right). \tag{24}$$

For the case of linear PE, the following parameters were utilized in the L-H model [13]: T_m = 418.7 K, ΔT = 15.8-23.8°C (Regime II), heat of fusion Δh_f = 2.810^8 J/m^3, crystalline surface free energy σ_e = 0.093 J/m^2 (93 erg/cm^2), work of chain folding q = 20.48 kJ.mol^{-1}, stem dimensions a_0 = 4.55×10^{-10} m and b_0 = 4.15×10^{-10} m. Parameter κ used in equations (23 and 24) is the result of incorporation of the chain reptation motion into the secondary surface nucleation theory and can be estimated as [12]:

$$\kappa = h \exp\left(\frac{Q_D^*}{RT_m^\infty}\right) \exp\left(\frac{q}{N_A kT}\right) \cdot \frac{1}{\xi_0 l_g^{*2}} \qquad (25)$$

The parameter Q^*_D corresponds to activation energy for reptation motion and the ξ_0 to monomer friction coefficient. Lamella thickness, l_g^*, was calculated according to the relation [12]:

$$l_g^* = \frac{2\sigma_e}{\Delta G} + \frac{kT}{b_0 \sigma} \quad . \qquad (26)$$

At a given crystallization temperature, both the thickness of crystalline layers and the lamellae are nearly independent of molecular weight. The idea of the incorporation of the surface area effect to the filler is illustrated in Figure 37.

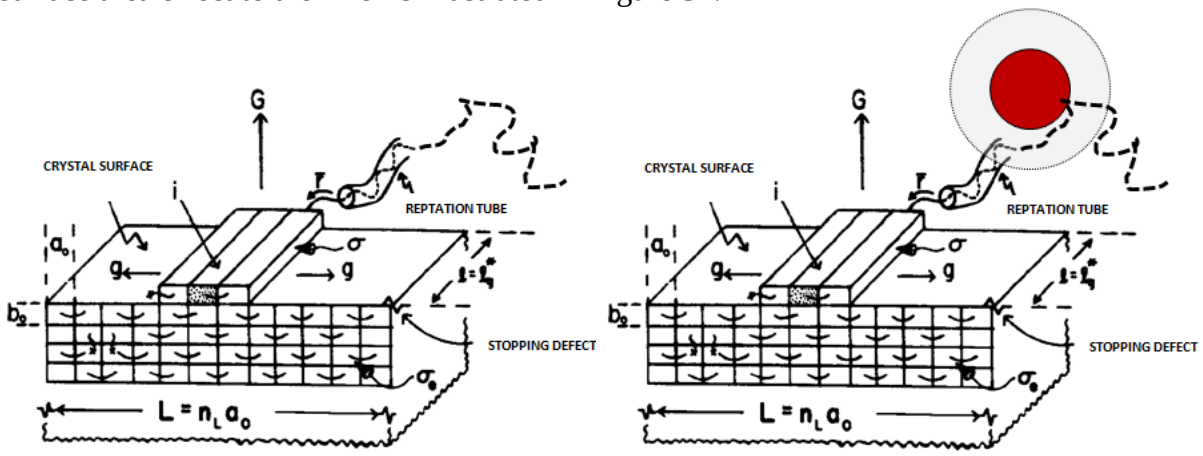

Figure 37: Implementation of the particle presence into the L-H theory. The filler surface area affects the reptation of the chain to reel in at the crystal surface. The abbreviation is used from the L-H theory.

The growth rate observed via polarized light optical microscopy corresponds to the G_{II} in this theory. The activation energy Q^*_D has been taken as a variable parameter to correlate the calculated trends with experimental data. For the neat HDPE, the curve has been fitted to the experimental data and corresponding activation energy value was found to be 24 kJ.mol^{-1} which is in excellent agreement with the activation energy for the reptation motion for PE published in the literature which is in the range from 20 to 25 kJ/mol[131-134]. The comparison of L-H prediction for neat HDPE and the experimentally measured G_{II} for the neat and silica filled HDPE is shown in Figure 38.

Moreover, it was found that with increasing filler-matrix interface area, the Q^*_D calculated from the L-H theory followed the observed trends and increased significantly up to the 108kJ.mol^{-1} for 8vol % of silica. Thus, it can be suggested that in the presence of the weakly interacting surface, the reptation motion was retarded and extend of immobilization

increased with increasing filler-matrix interface area. Assuming interphase layer thickness equal to approximately $1R_g$ (3.74 nm for the HDPE) the diffusion activation energy from the L-H theory can be estimated as $Q_D^{interphase} = 2Q_D^{neat}$. This trend was shown valid over the entire undercooling regime II (Figure 39.)

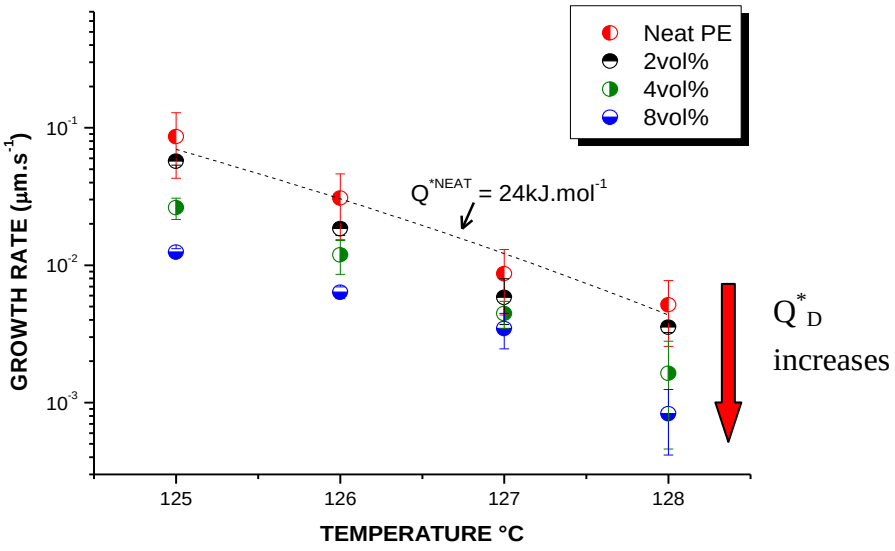

Figure 38: Spherulite growth rate of neat and nano-filled HDPE in dependence on temperature.

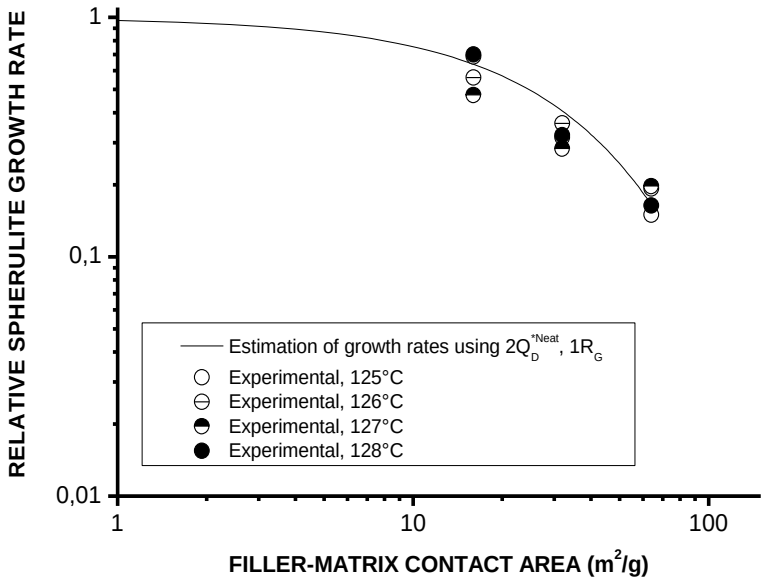

Figure 39: Relative spherulite growth rate of HDPE nanocomposite in dependence on area of the filler-matrix interface with the estimation interface thickness = $1R_g$. The filler-matrix contact area was calculated from known values of filler weight fraction and filler specific surface area.

5.3 Molecular weight scaling of the crystals growth rates

From reptation theory, the diffusion coefficient, D, dependence on molecular weight M is predicted as $D \sim M^{-2}$ [79]. Including two additional effects, constraint release (CR) that happens when a spatially confined chain moves out of the way of a given chain and, thus, opens some space for lateral motion and contour length fluctuations (CLF) when the chain contracts in its tube and after subsequent expansion it loses memory of the initial tube and the D scales as $D \sim M^{-2.30 \pm 0.1}$ up to $M \cong 10^3$ instead of by reptation predicted $D \sim M^{-2}$ [113]. Since the crystal growth rate is measured in relatively thin films in our experiments, the diffusion could be spatially limited to the two dimensions. The geometrical dimensions could also be changed with the chains confinement due to the particle presence.

In this experimental study, the well defined polyethylenes with polydispersity index close to 1 were utilized. For the molecular dynamics considerations, the number molecular weight average, $\overline{M_n}$, was used. The molecular weight was chosen to vary from 64800 to 146800. The micrographs of the PE with $\overline{M_n} = 95400$ filled with different amount of silica are shown in Figure 40.

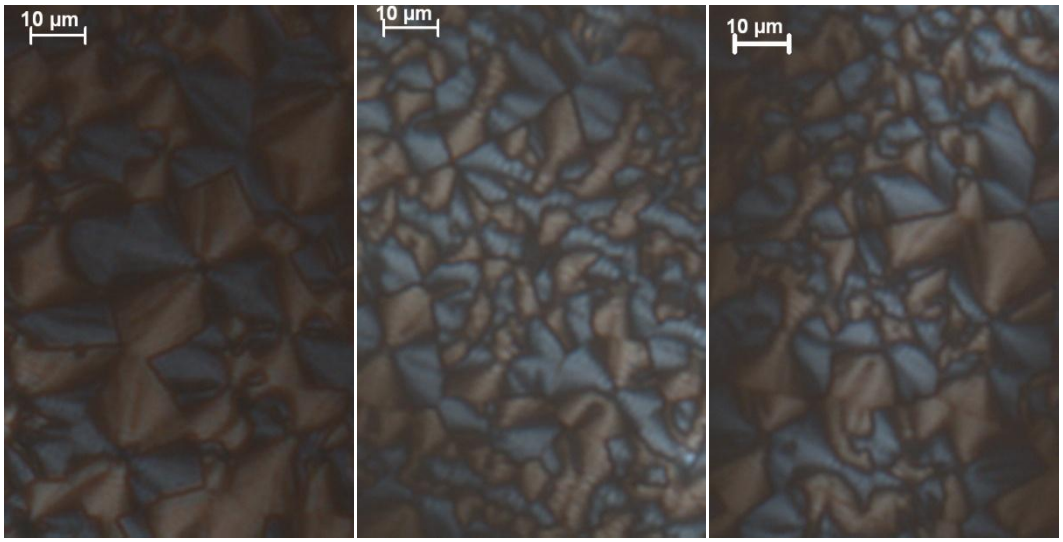

Figure 40: The micrographs taken in the samples of medium molecular weight: neat sample, 2 and 4 volume % of the nano-silica. The spherulitic morphology is not perturbed.

Again, the growth rate of the crystal formation has been determined as a slope of crystal radius time dependences. Similarly to the commercial HDPE, all R vs. t dependences were linear (Figures 41-43). In agreement with the observations in commercial HDPE, the slopes are lower with the increased matrix-filler interface area.

The dependences of G_{II} on the molecular weight of the matrix at all three crystallization temperatures are shown in Figures 44-46 for neat PE and PE filled with 2 and 4 volume % of

fumed silica, respectively. As expected, crystallization temperature exhibited much more pronounced effect for low molecular weight PE. It is important finding that growth rate dependencies on temperature in the crystallization regime II are the similar for the neat system and both nanocomposites that suggests that in the presence of the fillers no additional change in the crystallization mechanism can be expected.

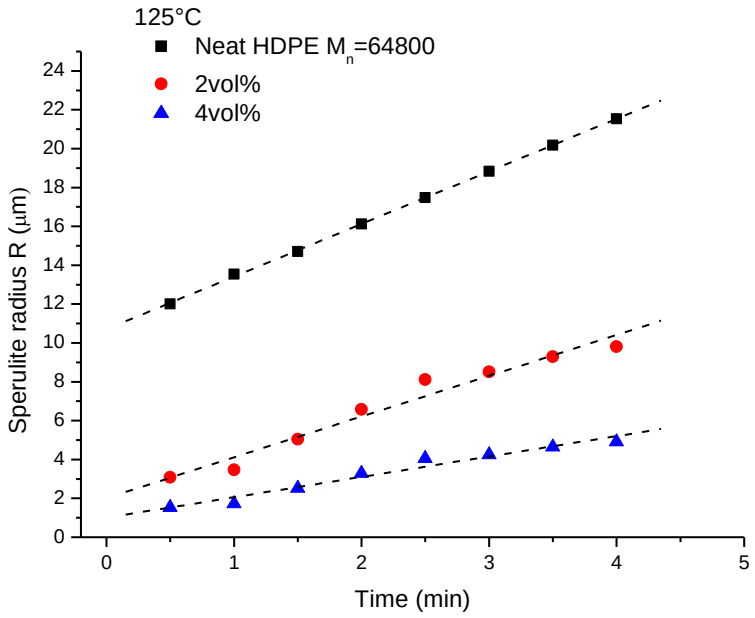

Figure 41: The linear time dependence of spherulite radius R at the temperature 125°C for HDPE/silica nanocomposite with the matrix $\overline{M_n} = 64800$ *and filler volume content 0, 2, 4 % (specific internal surface 0, 16, 32* m^2/g *of the filler in nanocomposite)*

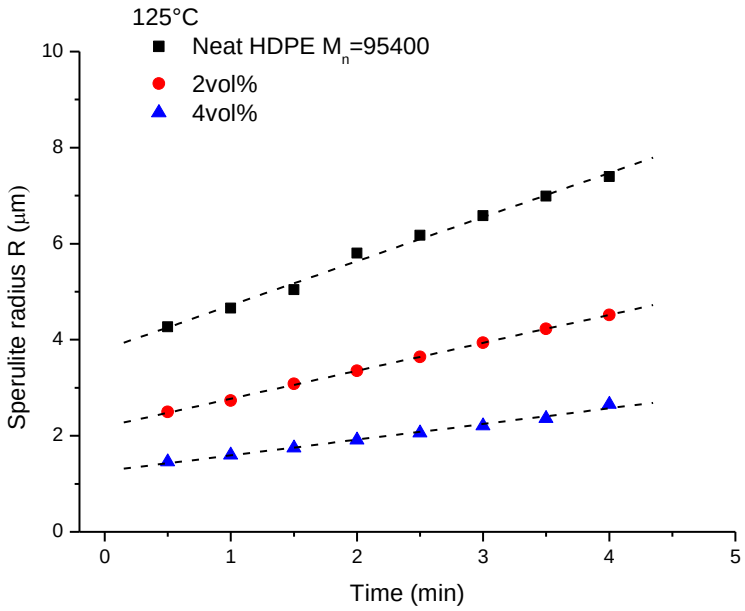

Figure 42: The linear time dependence of spherulite radius R at the temperature 125°C for HDPE/silica nanocomposite with the matrix $\overline{M_n} = 95400$ *and filler volume content 0, 2, 4 % (specific internal surface 0, 16, 32* m^2/g *of the filler in nanocomposite)*

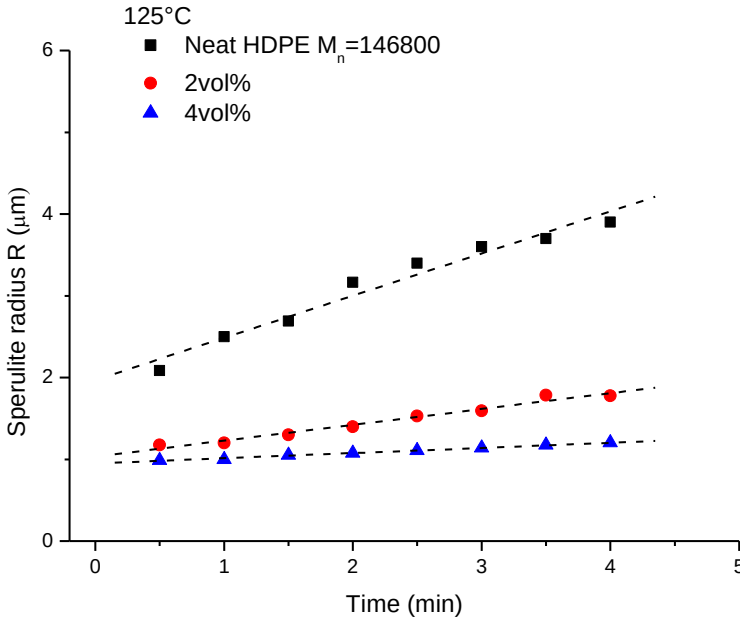

Figure 43: The linear time dependence of spherulite radius R at the temperature 125°C for HDPE/silica nanocomposite with the matrix $\overline{M_n} = 146800$ *and filler volume content 0, 2, 4 % (specific internal surface 0, 16, 32* m^2/g *of the filler in nanocomposite)*

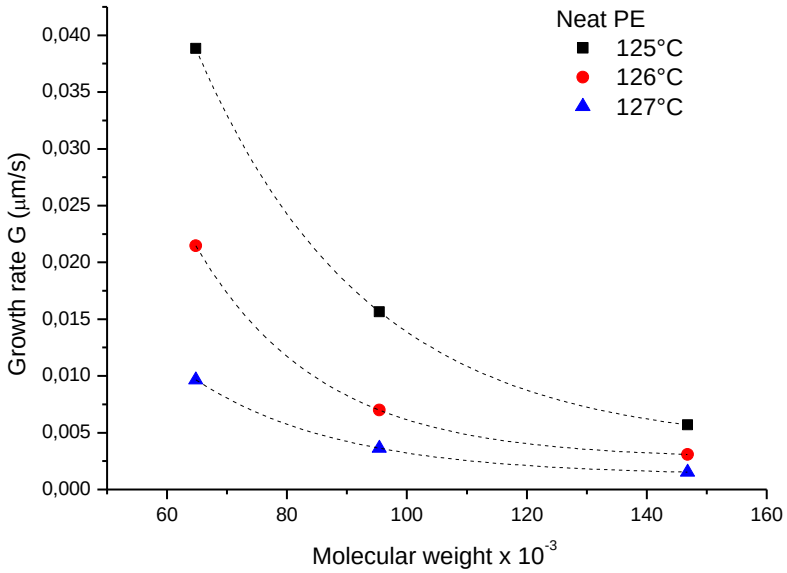

Figure 44: Neat PE; The spherulites growth rates molecular weight dependencies for at various temperatures

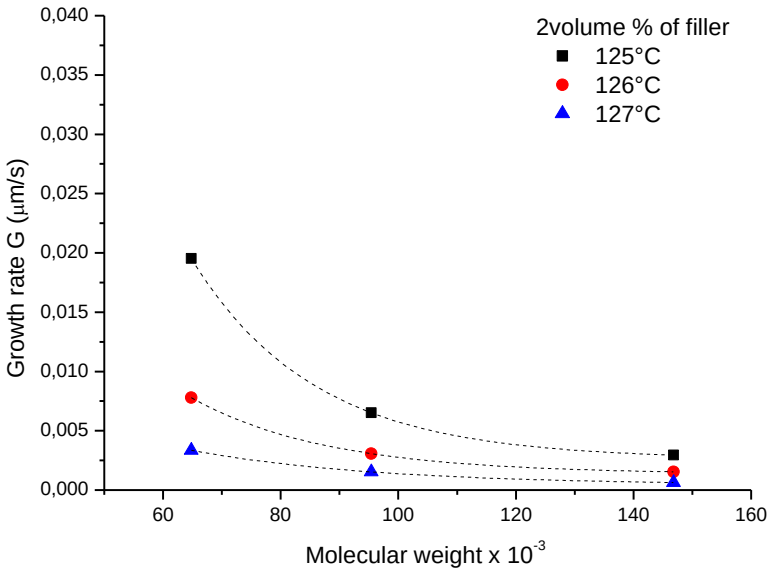

Figure 45: PE filled with 2vol % of fumed silica. The spherulites growth rates molecular weight dependencies for at various temperatures.

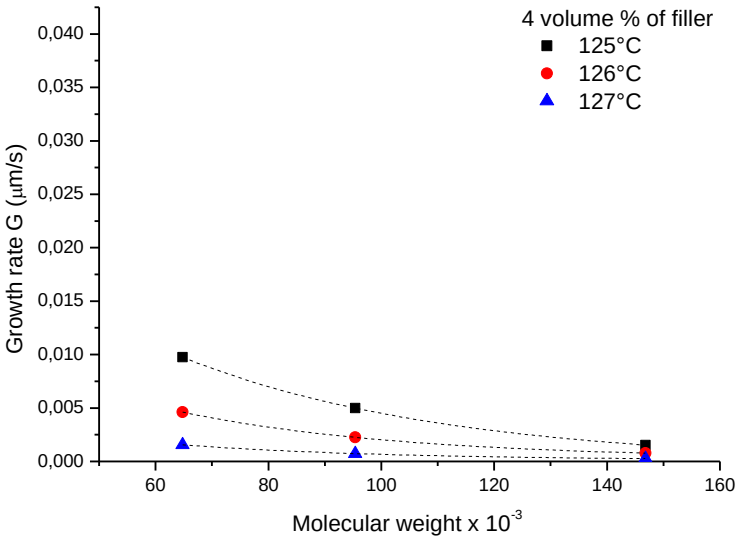

Figure 46: PE filled with 4vol % of fumed silica. The spherulites growth rates molecular weight dependencies for at various temperatures.

Results shown in figures 47-49 suggest that there is no significant change in scaling G_{II} with M_n with adding silica nanoparticles.

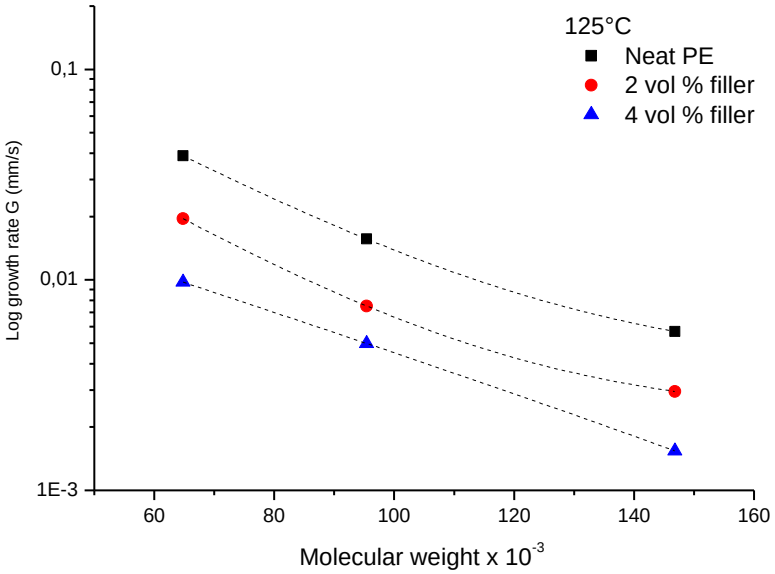

Figure 47: The spherulites growth rates molecular weight dependencies neat and filled PE at 125°C

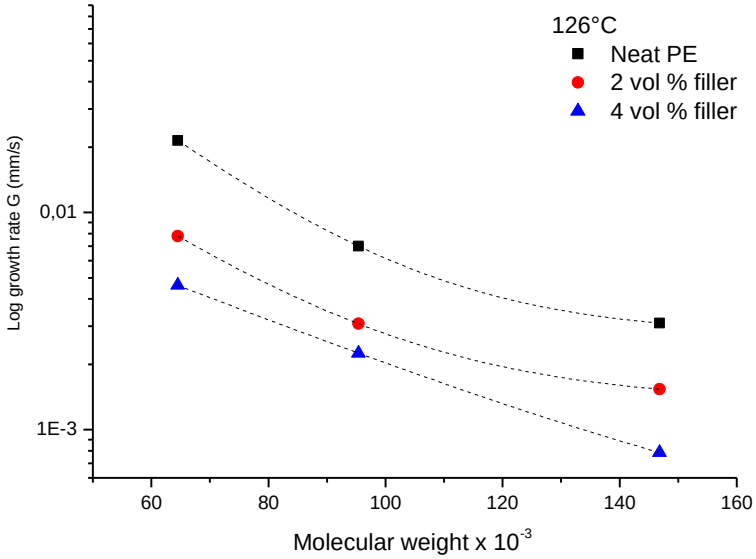

Figure 48: The spherulites growth rates molecular weight dependencies neat and filled PE at 126°C

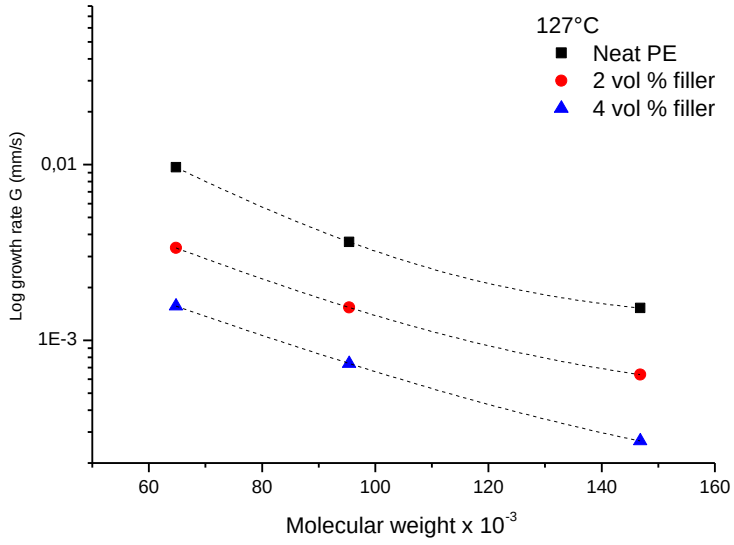

Figure 49: The spherulites growth rates molecular weight dependencies neat and filled PE at 127°C.

The absolute value of G_{II} decreased with increasing amount of silica and increasing molecular weight of PE, however, the scaling exponent remained constant within the experimental error (Table 3). The scaling of crystal growth rate with M_n obeys the reptation plus CLF prediction, $D \sim M^{-2.30 \pm 0.1}$, for both neat and filled PE. This supports the hypothesis that chain reptation remains the main means of mass diffusion to the growing crystal face. With the observed molecular weight scaling of crystals growth rates it is possible to suggest, that the crystal growth rate reduction observable with addition of silica nanoparticles to the PE is of the reptation type and can be contributed to the immobilization effect of the presence of a large internal surface area.

Moreover, the dependence is of the same strength not as it would be expected with changing fragility. Dynamic fragility of the glass forming liquids and fragility index, respectively, reflect the rate of change of the dynamic properties with temperature. From the point of molecular weight, lower molecular weight materials have a higher mobility and thus shorter relaxation times. Thus, the lower fragility is connected with the weaker molecular weight scaling.

Molecular weight dependence	125°C	126°C	127°C
Neat PE	-2.348	-2.348	-2.253
2 vol % filler	*-2.301*	*-1.967*	*-2.034*
4 volume % filler	*-2.267*	*-2.161*	*-2.165*

Table 3: Scaling of the crystal growth rate with molecular weight. The exponential coefficients are listed here.

The increased entanglement density [106] can be one of the mechanisms causing the retardation of chain reptation with adding the nanoparticles into the polymer matrix. In the reptation theory [80], entanglement is viewed as a topological constraint to the chain dynamics. The reduction of the crystal growth rate in the presence of fillers with large specific surface area then can be a result of apparent increase of the effective number of entanglements per chain reducing the reptation tube diameter. Considering the average entanglement length of polyethylene chain in neat PE equal to 35 monomeric units [85], it is possible to ascribe the decreased crystal growth rate (Figure 50) to the increased number of effective entanglements (Figure 51).

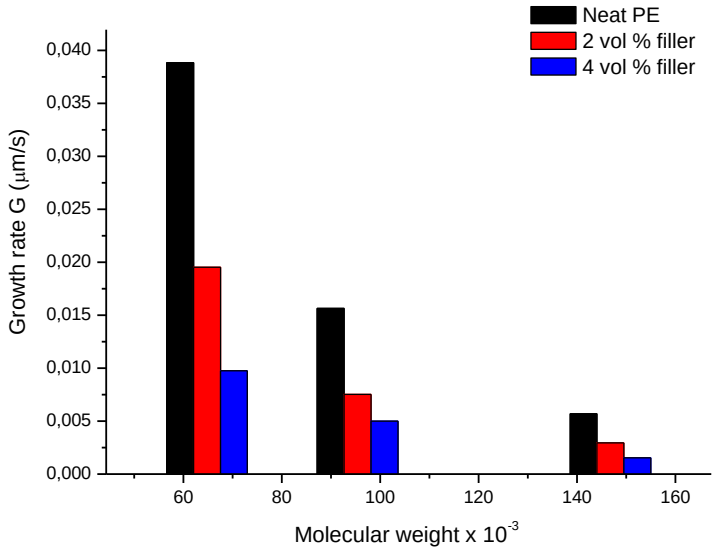

Figure 50: The crystal growth rates at 125°C. The rate decreases with the increasing of the filler content and with increasing molecular weight of the matrix.

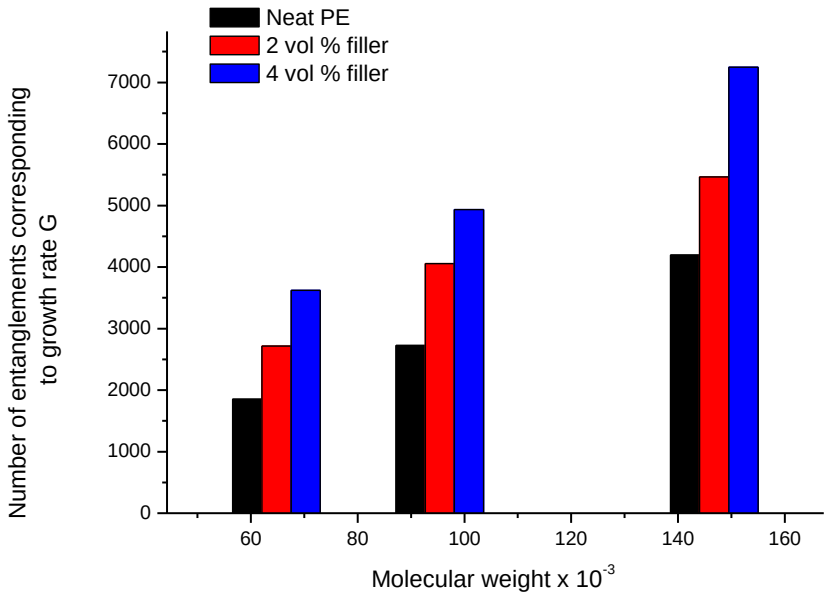

Figure 51: The effective number of entanglements calculated from the crystal growth rates at 125°C.

For PE containing 2 volume % of silica, the number of effective entanglements was increased by factor 1.41 and for PE containing 4vol% of silica by factor of 1.83. The same trend is valid for all temperatures investigated (Figure 53). The trends still follow the reptation expected scaling of the dependence on molecular weight. Based on these results, it can be assumed that the reduction of the crystal growth rate can be interpreted as a result of increased

number of effective entanglements per a polymer chain, in agreement with the theory of the chains immobilization at the particle surface.

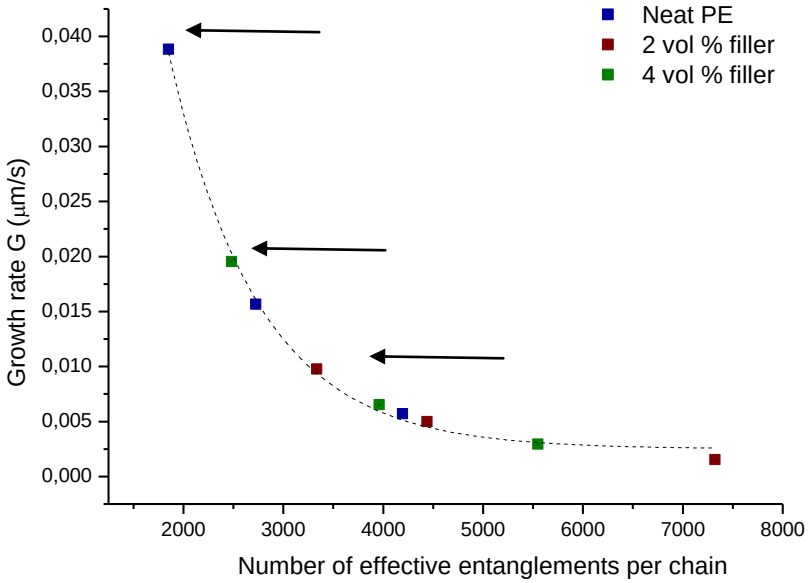

Figure 52: Dependence of the growth rates based on the effective number of entanglements calculated from the crystal growth rates at 125°C. Shift factors are 1 for neat system, 1.41 for nanocomposite containing 2vol% of silica filler and 1.83 for nanocomposite with 4vol% of fillers, respectively. The arrows show the matrices with in reality the same molecular weight.

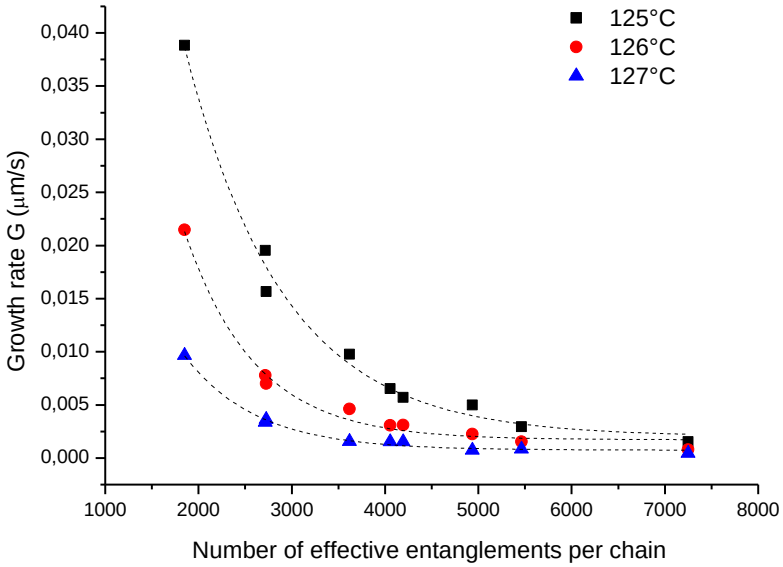

Figure 53: Plot of the growth rates based on the effective number of entanglements calculated from the crystal growth rates at all temperatures, applying the shift factors from the figure.

5.4 Molecular dynamics simulations

The L-H theory provides sound support for the hypothesis that the crystal growth rate reduction is mainly due to the immobilization of the chains at the particle surface and thus, due to the retarded diffusion of chains to the growth front. However, due to its semi-empirical nature, the need for a computer simulation arose. As the observed phenomena take place on the molecular level, the molecular dynamics and Monte Carlo simulations were employed to give further insight into the phenomena investigated. The systems were created step by step to verify the physical basis of the given stage before moving to the higher stage. It is necessary to bear in mind that computer simulation still posses many assumptions and limitations (e.g. much shorter chains, short times, etc.) and, thus, they are used to show the trends rather than to calculate actual values of parameters investigated.

5.4.1 Single chain system

Single chain system can be modeled relatively easily in accordance with polymer physics. The snapshot of the 1000 united atoms chain is depicted in Figure 54. The chain position was captured in a single time frame.

Figure 54: The sample of the 1000 unit chain. Its distribution in space in single time frame is shown.

Two of the most important topological properties of the polymer chains are the chain radius of gyration or the end-to-end distance, respectively, and its characteristic ratio. Both values obtained for simulated chains were compared with calculated theoretical expressions in order to test the physical behavior of the modeled system. For the linear homogeneous chain the mean square end-to-end distance $\langle R^2 \rangle$ for rotational isomeric state model of polymer chain (RIS) can be defined as [45]

$$\langle R^2 \rangle = N \cdot b^2 \cdot \left[\frac{1+cos\theta}{1-cos\theta}\right] \cdot \left[\frac{1+\langle cos\theta \rangle}{1-\langle cos\phi \rangle}\right] = C_N . N \cdot b^2 \quad , \tag{27}$$

where C_N is the characteristic ratio, N is the number of units, b is the bond length, θ is the bending angle and Φ is the dihedral torsional angle.

The radius of gyration measures the average squared distance from each segment to the centre of gravity. It can be calculated using the following equation [45]

$$R_g^2 = \frac{1}{(N+1)} \sum_{i=0}^{N} \langle \left(\overrightarrow{R_i} - \overrightarrow{R_G}\right)^2 \rangle \,. \qquad (28)$$

The dependence of the radius of gyration on the number of chain units is shown in Figure 55. The agreement with the theoretical values calculated by Flory [45] has been found. The increasing difference for the larger chains is subscribed to the necessity for the larger statistical ensemble.

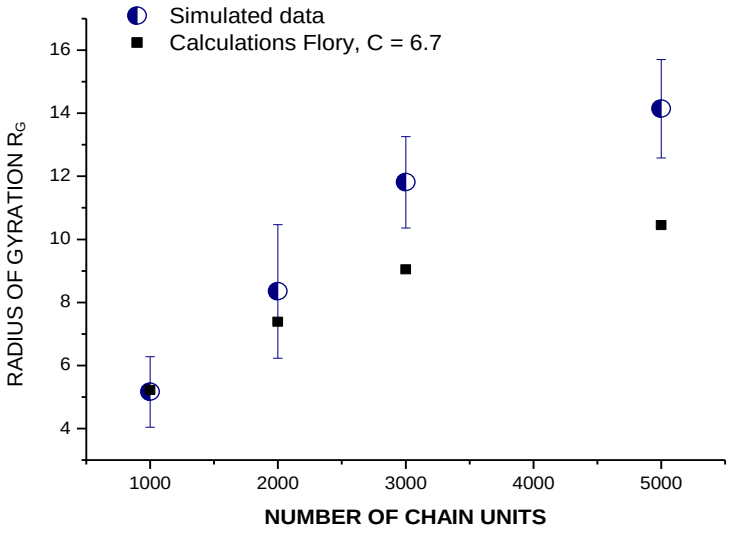

Figure 55: The dependence of radius of gyration on the number of units in the single chain

Characteristic ratio, C_N, corresponds to the bond and torsional angles size and chain rigidity. The characteristic ratio is a specific value for each polymer with value 6.7 has been determined for long chain polyethylene [45]. For its validity, it is crucial that the model predicts the experimentally observed dependence of characteristic ratio on temperature (Figure 56). As possible to see, the simulated characteristic ratio agrees well with the experimental value in the temperature regime of the simulation. The same physical parameters will be verified for the neat bulk PE, prior the insertion of the particle or the crystallization process.

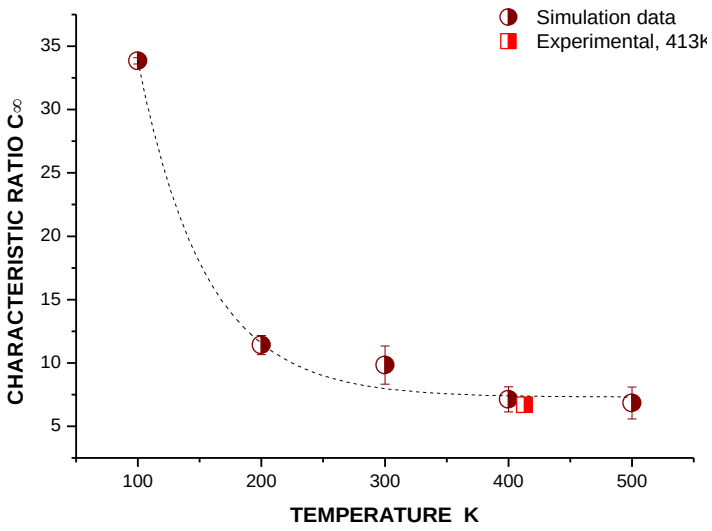

Figure 56: Temperature dependence of the characteristic ratio

5.4.2 Crystallization in neat polymer

Prior inserting the nanoparticle into the system the crystallization of the neat polymer was performed and compared with experimentally available data. Neat PE has been modeled as an ensemble of 100 chains each consisting of 100 segments. The characteristic ratio was found to be 5.7 which is in good agreement with Boyd and Philips giving value of 6 for the chain length of 100 units [134]. The ratio of the chain radius of gyration and end-to-end distance was higher than 6, thus, the systems due to the short chain lengths should not be treated as a Gaussian chain. The R_G calculated based on the theoretical model by Flory (Equation 28) for the chain of 100 was 3.74 nm.

1ns	End to end distance(nm)	Gyration radius (nm)	Persistence length (nm)	Characteristic ratio
Neat System	3.59	1.44	3.90	5.53
Weak Interaction	3.67	1.44	4.40	5.77
Strong Interaction	3.64	1.48	4.14	5.66

Table 4: The static properties of the polymer in bulk and their comparison of the neat polymer system and the samples in the presence of nanoparticle. The strong and weak interaction type describes the mutual filler-matrix interaction (see Table 2).

The crystal development was observed in three layers utilizing the order parameter development, the example of the emerging order is shown in the Figure 43. During the simulation, the additional crystalline order starts to develop on the primarily crystal surface. The first peak on the left side of the graph stands for the primarily crystal surface, the second and further are signifying the crystalline structure ordering. The peaks on the right emerge due to the periodic boundary condition in the simulation settings.

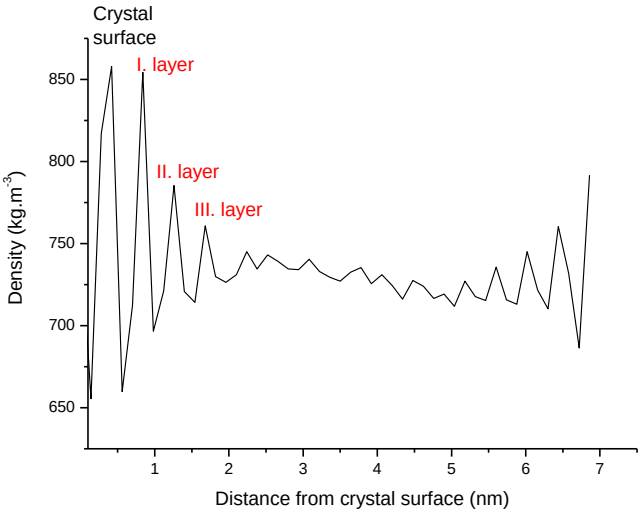

Figure 57: Example of the density profiles utilized to detect the positions of the growing layers. The minima between the peaks were used to set the layer boundaries for each measurement.

The time dependence of the observed order parameters depicted below (Figure 58) is similar to that simulated by Waheed et al. [124] utilizing the Steel type potential field as a crystalline surface. The green line corresponds to the order of the primarily inserted crystalline surface of polyethylene, the black, red and blue show the order development in time for the newly created crystalline layers. The growth rate or the composite was determined for each sample by the completion of the ordering in the crystallization plane averaged over the first two crystalline layers emerging during the simulation at the primary surface of polyethylene crystal.

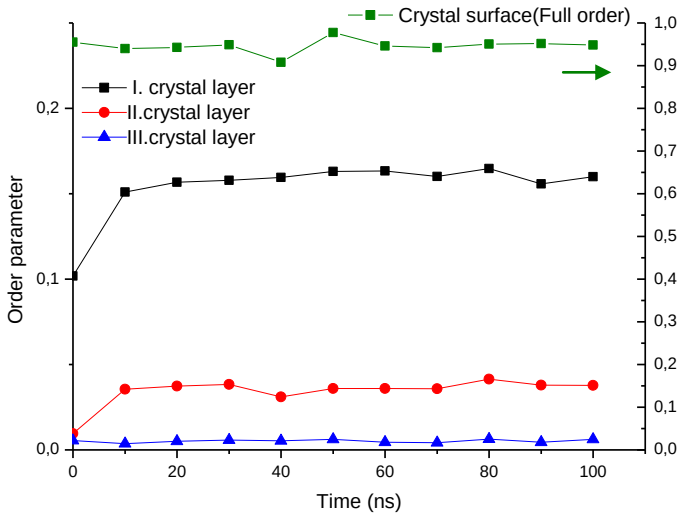

Figure 58: Example of the order parameter used to calculate the growth rate or the crystalline order formation, respectively. The points are the times when the order was analyzed. The simulation of each system was up to 100ns. For each simulation of this type was analyzed.

The simulated crystal growth rate for the neat polymer was found to be 4.10^{-4} nm.ns^{-1}. This value fits the theoretical predictions of van Krevelen and Strobl and is in agreement with the simulations data of Waheed [135, 53, 124]. The maximal experimentally obtained value for the crystal growth rate was of the order of 1.10^{-5} nm.ns$^{-1.}$ The difference between experimental and theoretical value could be ascribed to the higher molecular weight of the experimentally measured samples and, thus, higher entanglement density. Also, simulation techniques operate on molecular scale and experimental techniques probe the problem starting on a macroscale, thus, the direct comparison can face a certain difficulties.

5.4.3 The crystallization in the presence of a nano-filler

In Figure 59, the snapshots of the polymer chains order being created near the crystal surface are shown. The dashed arrow shows the original inserted crystal surface at which the crystallization order occurs. The full ones are showing the simulated development of the structure with time. Red icosahedral in the middle of the figure is the nanoparticle. It is expected that the nano-filler should significantly change the development of the crystalline layers in the simulated system. The matrix-filler mutual interactions were altered in order to separate the various contributions to the crystal growth. The diameter of the particle was 2nm.

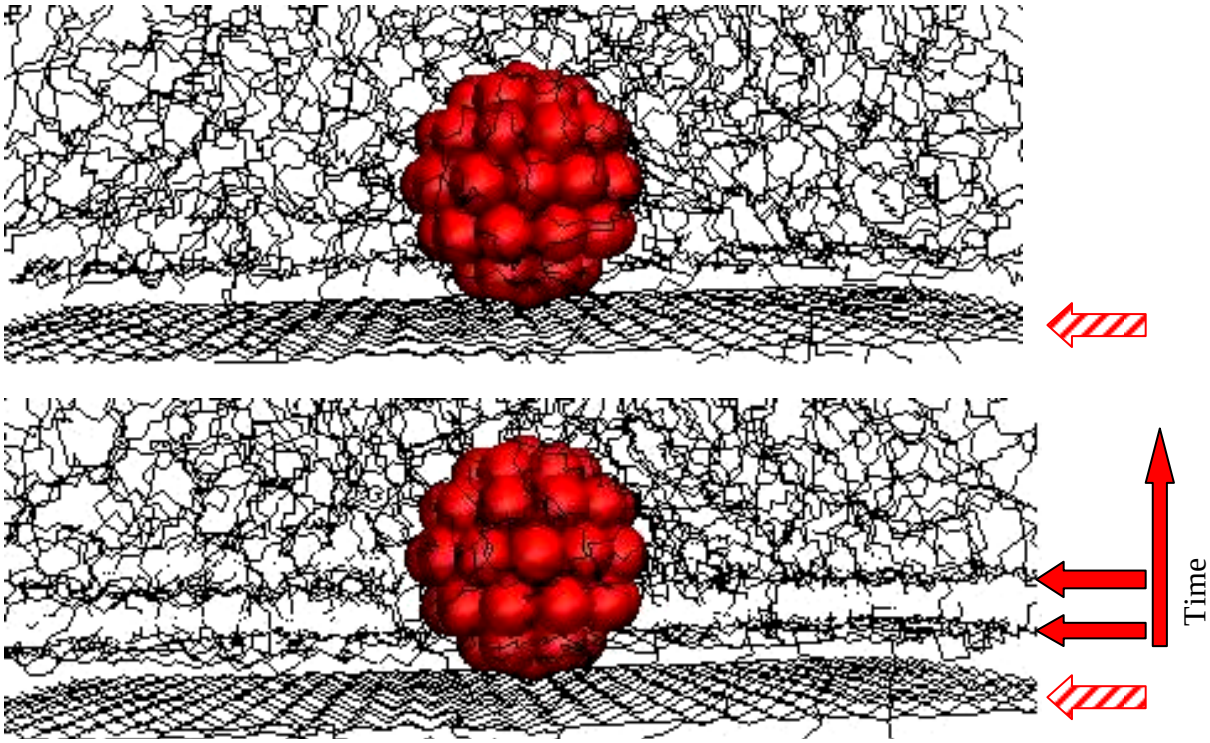

Figure 59: The snapshots of the crystal growth at the simulation start and after 30ns.The textured arrows stand for the primary crystal surface while the red full arrows signify formation of the new lamellae in time of the computer simulation.

In Figure 60, one can compare that order development rates in the case of strongly or weakly interacting particle is lower than in neat polymer. For the repulsive or non interacting particle, no significant perturbation of the order development is observable, when the crystal surface is in a distance from the particle (here 2.4 nm) where the entanglements can transfer the immobilization effect to the distance more far from the actual immobilization site at the particle surface. These trends are reproduced also when moving the particle closer to the crystalline surface. When the primary crystal surface is close to a particle, the geometrical constraints are becoming more pronounced.

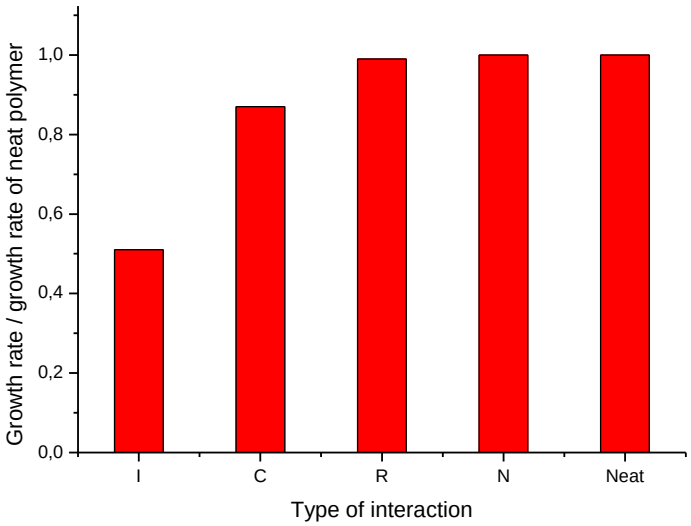

Figure 60: The ordered structure development for the simulated HDPE nanocomposite with silica content 1.81vol %, comparison of the various interaction types. The values are taken relatively to the neat system.

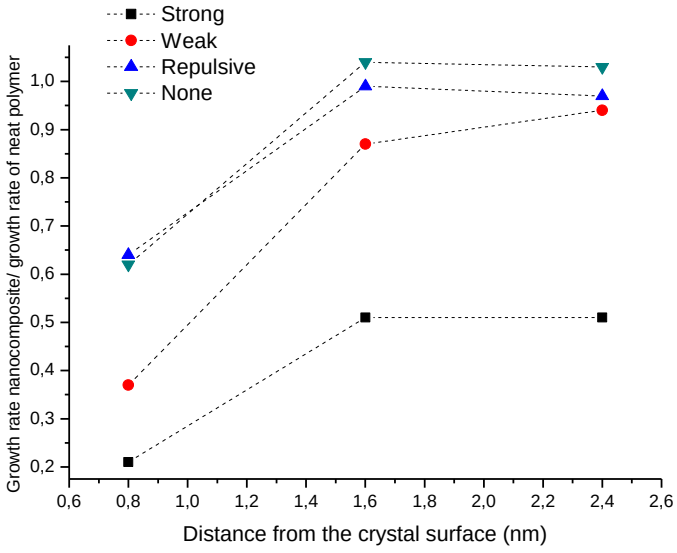

Figure 61: The relative crystal growth rate for the various particle-chain interactions in dependence on the particle distance from the crystal surface. Silica content 1.81vol %.

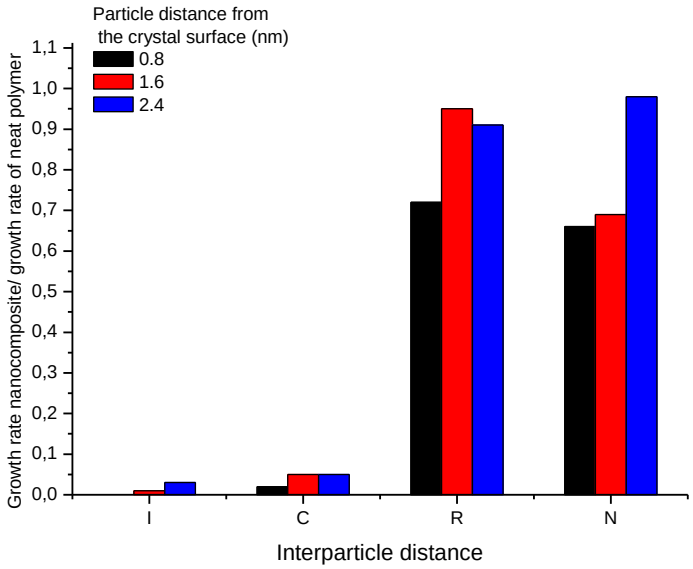

Figure 62: The relative crystal growth rate for the various particle-matrix interactions (from left to right): neat PE, weak (relative particle/CH2 unit interaction = 1) and strong (relative particle/CH2 unit interaction = 10), repulsive and none. An x-axe gives the type of the interactions.

The emphasis has been given to the comparison of the crystal growth rates with different type of interactions. As shown in Figures 61 and 62, the experimentally observed retardation is dominant only in attractive system and increased with the attractive interaction strength. The geometrical effects are supposed to happen due the constraints imposed on the chains in the inter-particle spaces and distance of the particle from the crystallizing surface. No increase in the growth rate for repulsive particle-matrix interaction in comparison with the final growth rate in polymer suggested that the dynamic fragility concept cannot be used. For the attractive filler-matrix potential, the chain packing at the surface is more perturbed in comparison with a neat melt. This can result in a higher structural frustration in a nanocomposite material.

Even more insight into the phenomenon was given by simulating the effect of two particles on G_{II}. From the comparison with the previous results, it can clearly be seen that adding second particle makes the simulation more realistic resulting in further decrease in the crystalline order development rate depending on the particles-matrix interaction, mutual position of the particles and the distance from the crystal surface.

For strong attraction, the crystal growth is significantly retarded at all distances from the surface investigated (Figure 63). This, in lesser extent, was valid also for the weakly interacting systems (Figure 64). In contrast, the repulsive and non-interacting systems tend to slow down the order formation only in the very close vicinity of the crystal surface. Very

importantly, for non-attractive systems, no significant difference was obtained between the tendencies of system with one and two particles for the same distance from the crystal surface.

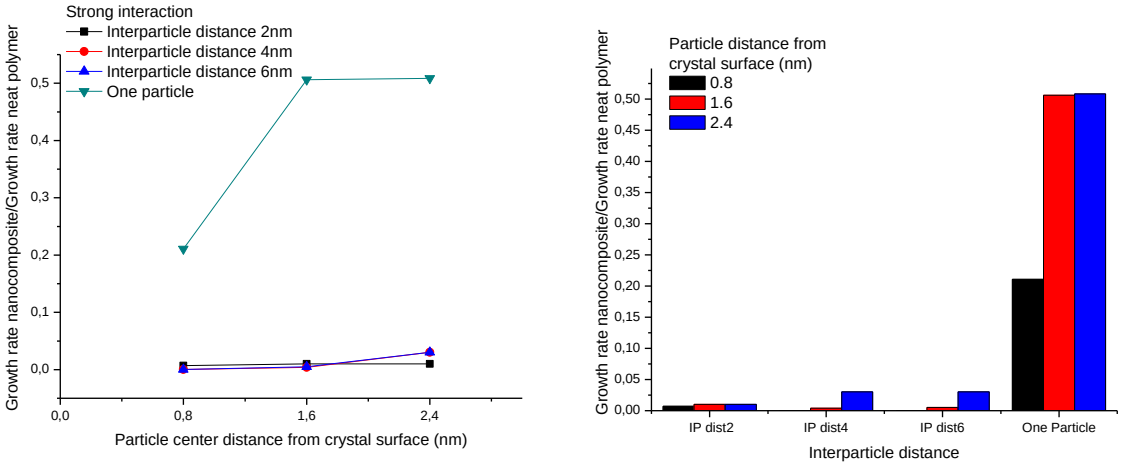

Figure 63: Comparison of the crystal growth rates single particle- double particle for the strong mutual interaction. The distance of the filler(s) from the crystal surface (left) and the effect of the inter-particle distance, thus, vertical confinement (right).

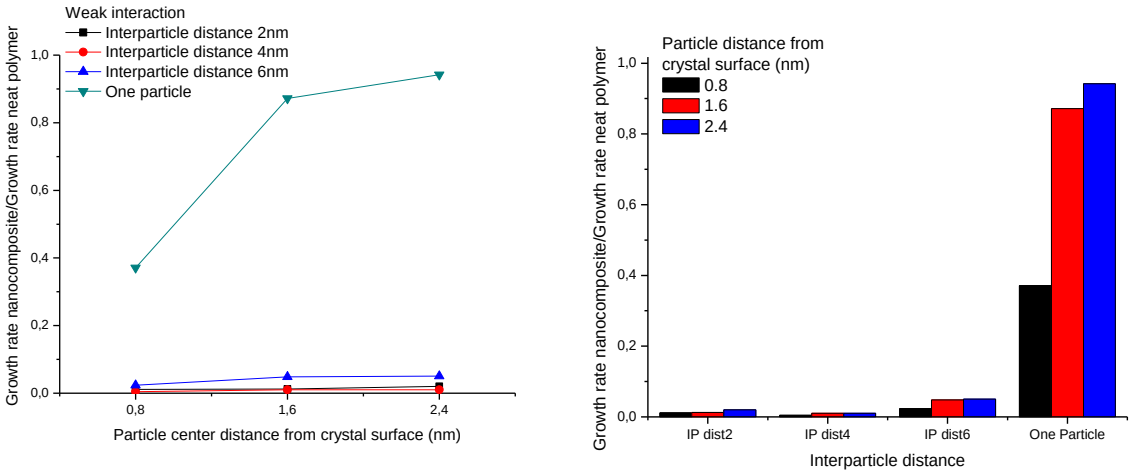

Figure 64: Comparison of the crystal growth rates single particle- double particle for the weak mutual interaction. On the left, distance of the filler(s) from the crystal surface and on the right the effect of the inter-particle distance, thus, vertical confinement.

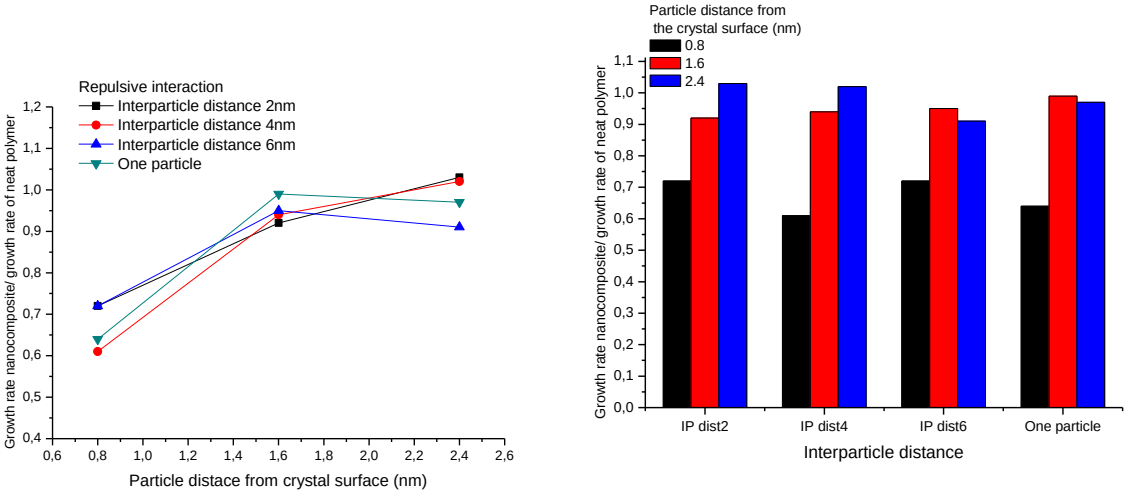

Figure 65: Comparison of the crystal growth rates single particle- double particle for the repulsive mutual interaction. On the left, distance of the filler(s) from the crystal surface and on the right the effect of the inter-particle distance, thus, vertical confinement.

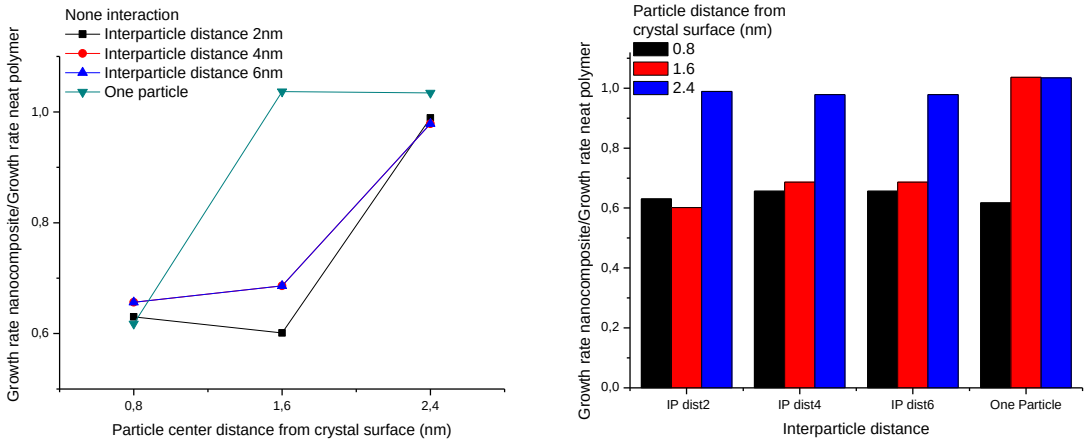

Figure 66: Comparison of the crystal growth rates single particle- double particle for the no mutual interaction. On the left, distance of the filler(s) from the crystal surface and on the right the effect of the inter-particle distance, thus, vertical confinement.

It is possible to see that the chain dynamics retardation in the vicinity of the particle surface is controlled by the chain-particle interaction strength, (Figures 67-69). The restrictions observable also for the non-interacting and repulsive types it never reach such a scale as in the case of interacting filler. What is important here is that with moving of the particle closer to the crystal surface the growth rate decreases. This trend is true for all the particle centers distances. It can be interpreted as the larger amount of the immobilized chain units present in both the crystallizing surface and the particle interfacial area.

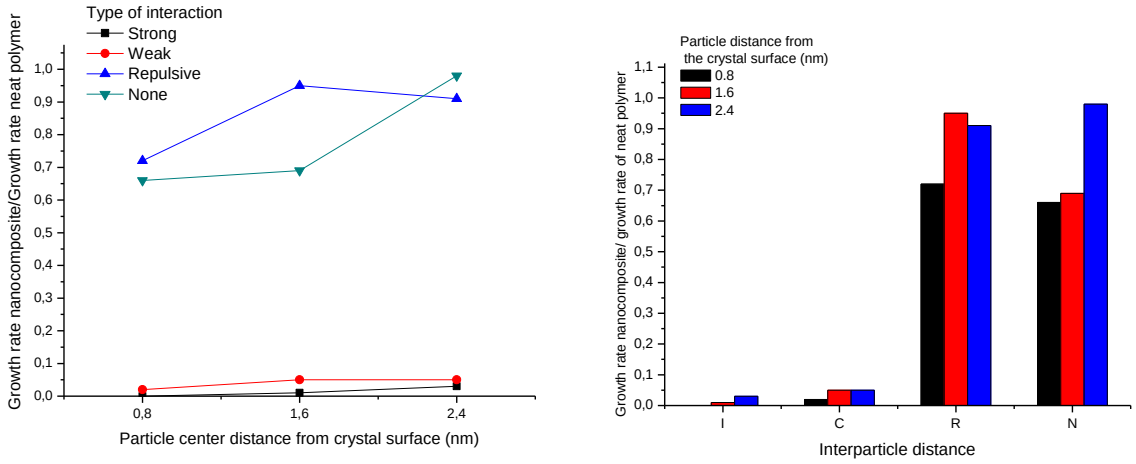

Figure 67: The order development rates in dependence on the distance of the particles from crystal surface and for various interaction types (left). The distance of particle centers is constant (6nm). I stands for strong interaction, C-weak interaction, R-repulsive, N-non-interactive system, respectively.

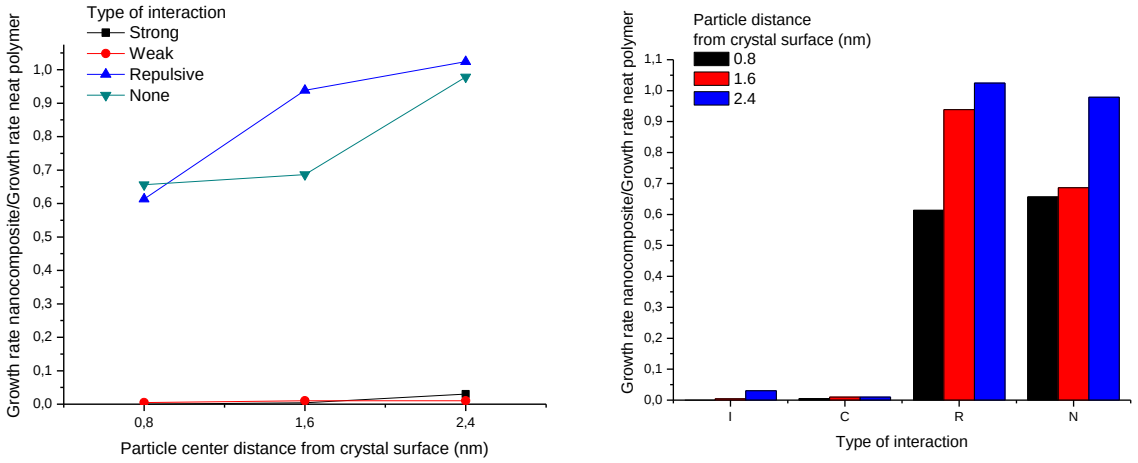

Figure 68: The order development rates in dependence on the distance of the particles from crystal surface and for various interaction types (left). The distance of particle centers is constant (4nm). I stands for strong interaction, C-weak interaction, R-repulsive, N-non-interactive system, respectively.

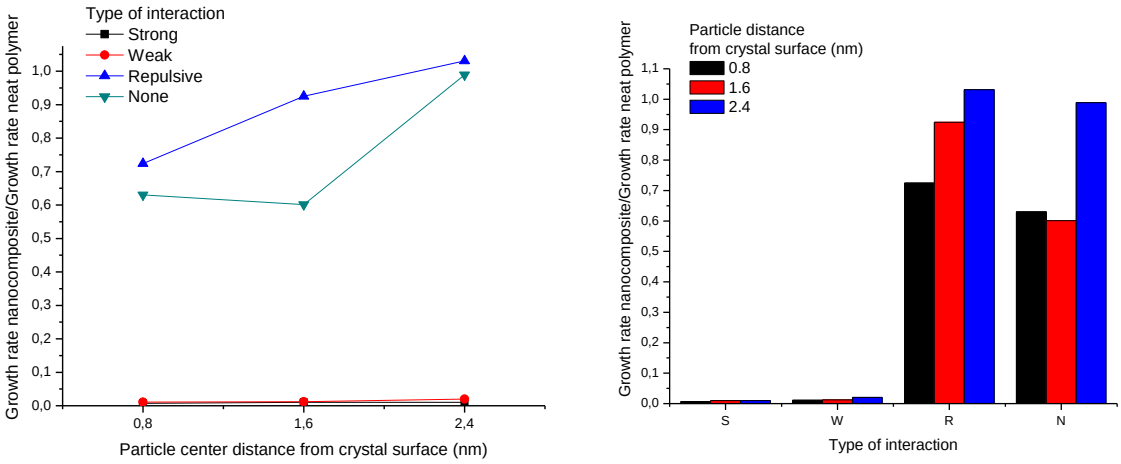

Figure 69: The order development rates in dependence on the distance of the particles from crystal surface and for various interaction types (left). The distance of particle centers is constant (2nm). I stands for strong interaction, C-weak interaction, R-repulsive, N-non-interactive system, respectively.

When moving particles closer to each other while keeping their distance from the crystal surface constant, the vertical confinement enhanced the possibilities to create a simple particle-polymer network via bridges or loops. The following figures (70-72) show, that with the decreasing inter-particle distance, the crystal growth rate remains unaffected within the experimental error. These data suggest that the vertical confinement of the chains is playing an important role in the chains immobilization. It implies, the bridging effects had no significant effect on the crystal growth rate in the model PE/silica nanocomposites.

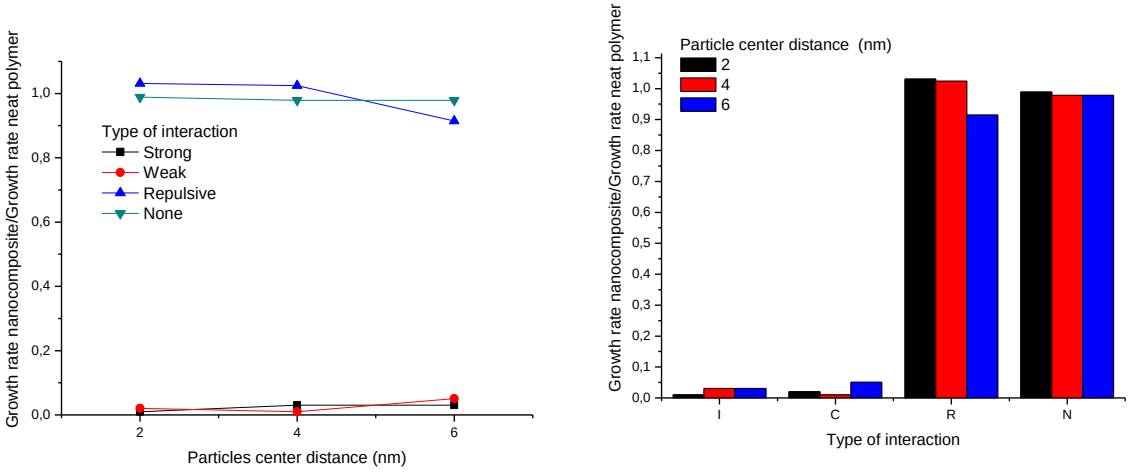

Figure 70: The order development rates in dependence on the distance of the particles centers and for various interaction types (left). The distance from the crystal surface is constant (2.4nm.. I stands for strong interaction, C-weak interaction, R-repulsive, N-non-interactive.

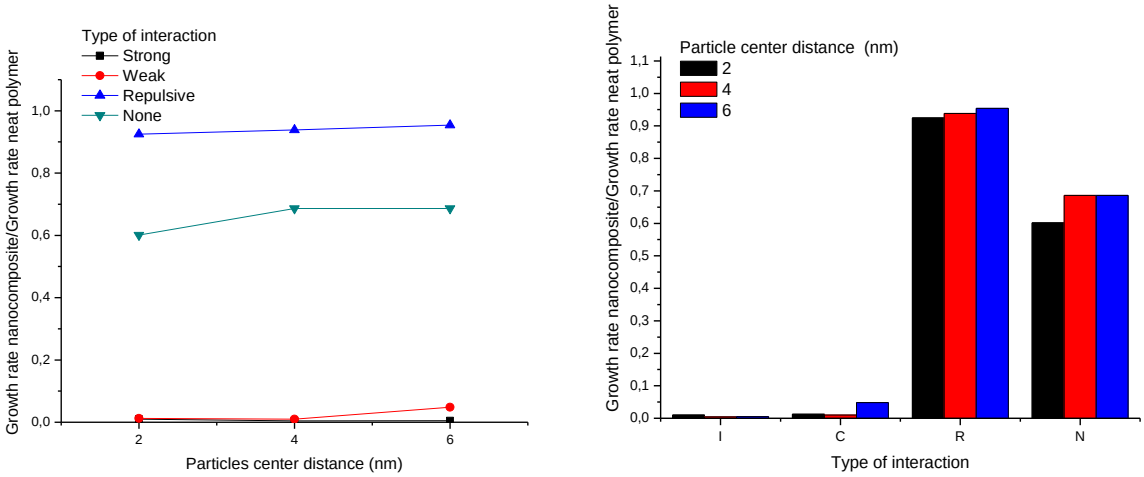

Figure 71: Comparison of the order development rates in dependence on the distance of the particles centers for various interaction types. The distance from the crystal surface is constant (1.6nm). I stands for strong interaction, C-weak interaction, R-repulsive, N-non-interactive system, respectively.

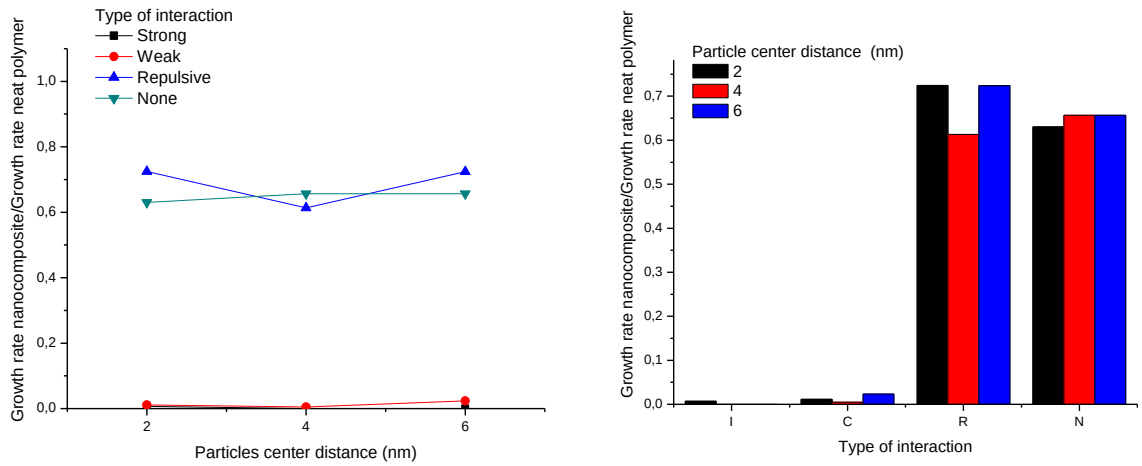

Figure 72: The order development rates in dependence on the distance of the particles centers and for various interaction types (left). The distance from the crystal surface is constant (0.8nm). I stands for strong interaction, C-weak interaction, R-repulsive, N-non-interactive system, respectively.

5.4.4 Summary

The isothermal crystallization of HDPE was investigated using the polarized light microscopy. Neat HDPE and nanocomposites containing 2, 4 and 8 volume % of silica nano-filler were analyzed. The spherulite radii were measured as a function of time. The crystal growth rate was significantly reduced with increasing matrix-filler interface. The silica fillers used does not act as a nucleating agent in the high density polyethylene. The nucleation was homogeneous and uniform within the sample volume, particle aggregation issue was taken into account. The experimentally obtained data were correlated with the Lauritzen-Hofmann surface nucleation theory, where the chain diffusion motion via the reptation mechanism was included. The limit value of diffusion motion activation energy was calculated from L-H equation equals to 24kJ.mol-1 for neat HDPE and with increasing filler volume content considerably higher activation energy of diffusion motion is required. In other words, larger portion of chains is immobilized at the filler surface and their motion is restricted, proportionally to the surface area and interaction strength. Thus, the hypothesis that retarded reptation is the principal mechanisms causing changes in crystallization kinetics and morphology of filled polymers has been verified.

The molecular weight scaling of the crystal growth rate were investigated in both neat and filled model PE. It was found that the growth rate follows the reptation predicted scaling with implemented contour length fluctuation for both neat and filled polyethylene. Based on the results, there appears to be no linear dependency of the growth rates on the molecular weight. Also, the effective number of entanglements has been calculated and the growth rates for filled systems successfully shifted at all temperatures. Based on this observation assumption has been made that the main factor responsible for the crystal growth reduction does not lie within the geometrical concepts or the theory of dynamic fragility, but as suggested in the reduced reptation motion that can be seen as an increased number of effective entanglements in the matrix chains.

The performed MD simulations suggested that the rate of the order development in the nanocomposite system is closely connected with the particle-matrix interaction strength. The growth rate for repulsive interaction type never exceeds the value for the neat system and the geometrical factors start to play very important role in the vicinity of the surface, thus, it is assumed that there is some critical filling limit where the spatial constraints will become the main mechanism controlling the crystal growth rate.

The growth rates in the presence of one particle follow the trends observed in the hot stage experiments: With decrease of the distance from the crystal surface, the crystal growth rate rapidly decreases. Also, this is most significant for the strongly interacting systems. For the non-interacting systems at a certain distance, the particle doesn’t seem to affect the crystal growth rate. This is not valid in the case of interacting systems, as the immobilization effect

transported via entanglements plays mayor role. In the presence of the two particles the results show that the growth rates are highly reduced in the presence of the interacting systems. The non-attractive samples show only the conformational reduction in the near vicinity of the growing surfaces. Moreover, the repulsive interactions show the slight increase in the growth rate with the increase of the surface area, however, it is suggested that is due to the increased mobility. But still, it is lower than the growth rate in the neat system.

In the systems with two particles, the distance from the crystal seems to play major role and changes in the growth rates with the varying inter- particle distance seems to have a minor effect.

In a chain, each monomer unit may be considered a Brownian particle executing thermally activated motion. During the crystallization, the direction of the motion is added also by crystallization driving force. However, as the monomer units are connected through the bond interaction giving high dissociation energy, the internal bond rotation is virtually the only way for a monomer unit to make a movement, the chain reptation motion is a consequence of the successive internal bond rotations of all the monomer units resulting in the chain translation primarily in the lengthwise direction. Based on the results of these simulations it may be suggested that the main additional restriction to this movement is due to the particle-filler interaction strength.

6 CONCLUSIONS

The significance of the obtained results is twofold. First, knowledge of the fundamental processes affecting the chain dynamics in the presence of particles with size of the order of the radius of gyration of the chains was gained. Second, quantification of the relationships between structural variables, crystallization kinetics, crystalline structure and deformation response in polyolefin nanocomposites can provide a base for developing new advanced high volume polymer materials for a wide range of applications. The computer model will help to understand and predict properties of semicrystalline nanocomposites by allowing optimizing of the composition and processing conditions. Results of this research can also contribute significantly to the basic understanding of the effects of chain immobilization on various aspects of behavior of nanostructured polymeric systems in both molten and solid state.

Within frame of this PhD work the isothermal crystallization of neat HDPE has been investigated using the polarized light optical microscope and hot stage. The results clearly showed that the rate of spherulite growth was substantially decreased by the addition of silica nanoparticles. In order to explain the observed crystallization behavior interpretation based on the assumption that the segmental diffusion is considerably reduced in presence of nanoparticles has been suggested. To verify the proposed hypothesis, the experimental data were correlated with Lauritzen- Hoffman secondary surface nucleation theory. The role of the fillers nucleation and aggregation was included. The nanocomposite nucleates homogeneously and uniformly within the sample. Further on, the molecular dynamics simulations on molecular level were performed.

Within this PhD thesis, the following evidence supporting the immobilization theory has been observed:

The correlation of the experimentally measured decrease in crystal growth rates with the Lauritzen-Hoffman secondary surface nucleation theory clearly showed the increase of the activation energy of the reptation motion with the increased internal surface area of the filler. The molecular weight scaling was following the reptation prediction with the contour length fluctuation included. The results clearly showed that the reduction of the crystal growth rates can be interpreted via immobilization theory as the increased number of effective entanglements.

From the molecular dynamics simulation as the primary mechanism affecting the morphology development was identified the mutual particle-matrix interaction type and thus the immobilization of the chains at the filler surfaces.

Based on these results, the crystal growth and thus the morphology formation in the filled systems should be up to the certain threshold tailored by altering the mutual interactions.

7 FURTHER RESEARCH

The crystallization kinetics in semicrystalline nanocomposites is a wide area with still wide amount of the application potential.

In the next future, the rigid amorphous phase detection should be determined, either by DSC or dielectric measurements. Also, the aggregation issue should be better explored and answered seeking to understand what effect would random distribution exhibit. For this purpose, it is suggested to focus on either colloidal particles or in situ precipitation of the silica in the polymer reactor. Also, a proper surface treatment should be tested, where the distribution should vary significantly with changes in the mutual interactions between the particle and the matrix. The interaction strength should be tested on strongly interacting systems for example the polyamide filled with silica particles. All the observed trends should be confirmed by measurements on the other polymers, for example polypropylene. This experiments may actually reveal another points and rise more questions, for example the growth rate reduction dependence on the filler surface area strength and the interpretation of the observed weaker or stronger tendency for a various polymers. Also, the nucleation rate in the nanocomposites could be focused on.

Concerning the computational model, it should be varied to be able to capture the order development for a various matrices as well. Also, it would be desirable to be able to obtain prediction of the expected behavior and trends, minimum on the molecular scale. Further on, the connection of the various length scales should be the aim.

For the future, the filled polymer blends will bring another improvements and interesting compromises between permeability, impact properties and cost of the materials. Here, silica particles should preferentially choose the phase to occupy and in this case, the way they effect the crystallization kinetics in given phase will be even of more importance.

APPENDICES

Appendix A

Materials:

Sample	M_n	Polydispersity index
Commercial	14.9	5.79

Sample commercial	Filler volume content (%)	Specific internal surface of fillers in nanocomposite = filler-matrix contact area (m^2/g of composite)
Neat HDPE	0	0
HDPE 2	2	16
HDPE 4	4	32
HDPE 8	8	64

Appendix B

Materials:

Sample	Mn	Polydispersity index
JM178	64.8	1.09
JM176	95.4	1.13
JM177	146.8	1.20

Sample JM1178	Filler volume content (%)	Specific internal surface of fillers in nanocomposite = filler-matrix contact area (m^2/g of composite)	Specific internal surface of fillers in nanocomposite = filler-matrix contact area (m^2/cm^3 of composite)
Neat	0	0	0
HDPE 2	2	16	14.1
HDPE 4	4	32	29.1

Sample JM176	Filler volume content (%)	Specific internal surface of fillers in nanocomposite = filler-matrix contact area (m^2/g of composite)	Specific internal surface of fillers in nanocomposite = filler-matrix contact area (m^2/cm^3 of composite)
Neat	0	0	0
HDPE 2	2	16	14.1
HDPE 4	4	32	29.1

Sample JM177	Filler volume content (%)	Specific internal surface of fillers in nanocomposite = filler-matrix contact area (m^2/g of composite)	Specific internal surface of fillers in nanocomposite = filler-matrix contact area (m^2/cm^3 of composite)
Neat	0	0	0
HDPE 2	2	16	14.1
HDPE 4	4	32	29.1

Appendix C

Sample	Particle 1 (p,c)(nm,nm)		Particle 2 (p,c)(nm,nm)		Types of interactions	Growth rate	G/G neat
						nm/ns	%
1	8	0,8	14	0,8	Weak	9.39E-06	0.023
2	8	1,6	14	1,6	Weak	1.92E-05	0.048
3	8	2,4	14	2,4	Weak	2.03E-05	0.051
4	9	0,8	13	0,8	Weak	1.89E-06	0.005
5	9	1,6	13	1,6	Weak	4.05E-06	0.010
6	9	2,4	13	2,4	Weak	4.05E-06	0.010
7	10	0,8	12	0,8	Weak	4.55E-06	0.011
8	10	1,6	12	1,6	Weak	4.94E-06	0.012
9	10	2,4	12	2,4	Weak	8.10E-06	0.020
10	11	0,8	-	-	Weak	1.48E-04	0.371
11	11	1,6	-	-	Weak	3.49E-04	0.872
12	11	2,4	-	-	Weak	3.77E-04	0.942
13	8	0,8	14	0,8	Strong	4.05E-08	0.000
14	8	1,6	14	1,6	Strong	2.03E-06	0.005
15	8	2,4	14	2,4	Strong	1.22E-05	0.030
16	9	0,8	13	0,8	Strong	4.05E-08	0.000

17	9	1,6	13	1,6	Strong	1.62E-06	0.004
18	9	2,4	13	2,4	Strong	1.22E-05	0.030
19	10	0,8	12	0,8	Strong	2.84E-06	0.007
20	10	1,6	12	1,6	Strong	4.05E-06	0.010
21	10	2,4	12	2,4	Strong	4.05E-05	0.010
22	11	0,8	-	-	Strong	8.43E-05	0.211
23	11	1,6	-	-	Strong	2.03E-04	0.506
24	11	2,4	-	-	Strong	2.03E-04	0.508
25	8	0,8	14	0,8	None	2.63E-04	0.656
26	8	1,6	14	1,6	None	2.75E-04	0.686
27	8	2,4	14	2,4	None	3.91E-04	0.979
28	9	0,8	13	0,8	None	2.63E-04	0.656
29	9	1,6	13	1,6	None	2.75E-04	0.686
30	9	2,4	13	2,4	None	3.91E-04	0.979
31	10	0,8	12	0,8	None	2.52E-04	0.630
32	10	1,6	12	1,6	None	2.41E-04	0.601
33	10	2,4	12	2,4	None	3.96E-04	0.989
34	11	0,8	-	-	None	2.47E-04	0.618
35	11	1,6	-	-	None	4.15E-04	1.036
36	11	2,4	-	-	None	4.14E-04	1.034
37	8	0,8	14	0,8	Repulsive	2.90E-04	0.724
38	8	1,6	14	1,6	Repulsive	3.82E-04	0.954
39	8	2,4	14	2,4	Repulsive	3.66E-04	0.915
40	9	0,8	13	0,8	Repulsive	2.45E-04	0.613
41	9	1,6	13	1,6	Repulsive	2.95E-04	0.938
42	9	2,4	13	2,4	Repulsive	4.10E-04	1.024
43	10	0,8	12	0,8	Repulsive	2.90E-04	0.724
44	10	1,6	12	1,6	Repulsive	3.70E-04	0.925
45	10	2,4	12	2,4	Repulsive	4.24E-04	1.031
46	11	0,8	-	-	Repulsive	2.58E-04	0.645
47	11	1,6	-	-	Repulsive	3.96E-04	0.991
48	11	2,4	-	-	Repulsive	3.87E-04	0.968

REFERENCES

[1] B.Wunderlich, Macromolecular physics vols. 1–3, Academic, New York (1976).

[2] Woodward, A.E., Atlas of polymer morphology. **1988**, Munich, Hanser publishers, 25,47.

[3] van Krevelen, D.W., Properties of Polymers, Elsevier, Amsterdam, **1997**.

[4] Strobl G., The physics of polymers, Springer, 2006.

[5] H. Tadokoro, Structure of crystalline polymers, John Wiley and Sons (1979).

[6] E.A. Colboun and J. Kendrick, Computer simulation of polymers, Longman Scientific & Technical (1994).

[7] G. Rutledge In: M. Kotelyanskii and D.N. Theodorou, Editors, Simulation methods for polymers, Marcel Dekker, New York (2004).

[8] Interphases and mesophases in polymer crystallization. In: G. Allegra, Editor, Adv. Polym. Sci. vols. 180, 181, 191, Springer, Berlin (2005).

[9] L. Mandelkern, Crystallization of polymers vols. 1–2, Cambridge University Press, Edinburgh (2002).

[10] D.C. Bassett, Principles of polymer morphology, Cambridge University Press (1981).

[11] Yamamoto T., Orimi N., Urakami N., Sawada K. ,Faraday Discuss., **2005**, 128, 75-86.

[12] J.D. Hoffman and R.L. Miller, Polymer 38 (1997), p. 3151.

[13] K. Armistead and G. Goldbeck-Wood, Adv Polym Sci 100 (1992), p. 219.

[14] Hoffman, J. D.; Lauritzen, J. I. Jr.; J Res Natl Bur Stand - A **1961**, 65, 297.

[15] Hoffman, J. D., Frolen, L.J. Ross, G.S., Lauritzen, J. I. Journal of Research of the National Bureau of Standards Sectiona-Physics and Chemistry **1975**,79(6),671-699.

[16] K. Kaji, K. Nishida, T. Kanaya, G. Matsuba, T. Konishi and M. Imai, Adv Polym Sci 191 (2005), p. 187.

[17] K. Kaji, K. Nishida, T. Kanaya, G. Matsuba, T. Konishi and M. Imai, Adv Polym Sci 191 (2005), p. 187.

[18] G. Reiter and J.U. Sommer, J Chem Phys 112 (2000), p. 4376.

[19] P. Huang, L. Zhu, S.Z.D. Chen, Q. Ge, R.P. Quirk and E. Thomas et al., Macromolecules 34 (2001), p. 6649.

[20] Y. Loo, R.A. Register and A.J. Ryan, Phys Rev Lett 84 (2000), p. 4120

[21] Mandelkern, L., Crystallization if polymers, McGraw-Hill, NewYork, **1964**.

[22] Woodward A. E., Understanding polymer morphology, Hanser, New York, **1995**.

[23] Liu Y, Chan C, Li J, Ng K, Wang Y, Jiang Y, et al. The birth of an embryo and development Macromolecules 2002, 35: 6751-3.

[24] D. Rigby and R.J. Roe, J Chem Phys 89 (1988), p. 5280.

[25] K. Esselink, P.A. Hilbers and B.W.H. van Beest, J Chem Phys 101 (1994), p. 9033.

[26] H. Takeuchi, J Chem Phys 109 (1998), p. 5614.

[27] N. Waheed, M.S. Lavine and G. Rutledge, J Chem Phys 116 (2002), p. 2301.

[28] T.K. Xia and U. Landman, J Chem Phys 101 (1994), p. 2498.

[29] H. Li and T. Yamamoto, J Chem Phys 114 (2001), p. 5774.
[30] T.A. Kavassalis and P.R. Sundararajan, Macromolecules 26 (1993), p. 4144
[31] T.A. Kavassalis and P.R. Sundararajan, J Chem Soc Faraday Trans 91 (1995), p. 2541.
[32] T. Miura, R. Kishi, M. Mikami and Y. Tanabe, Phys Rev E 63 (2001), p. 061807.
[33] M.S. Lavine, N. Waheed and G.C. Rutledge, Polymer 44 (2003), p. 1771.
[34] S. Fujiwara and T. Sato, J Chem Phys 107 (1997), p. 613.
[35] H. Meyer and F.J. Mueller-Plathe, J Chem Phys 115 (2001), p. 7807.
[36] H. Meyer and F.J. Mueller-Plathe, Macromolecules 35 (2002), p. 1241.
[37] B.J. Alder and T.E. Wainwright, J Chem Phys 27 (1957), p. 1208.
[38] T. Yamamoto, J Chem Phys 129 (2008), p. 184903.
[39] R.H. Gee and L.E. Fried, J Chem Phys 118 (2003), p. 3827.
[40] R.H. Gee, N. Lacevic and L.E. Fried, Nat Mater 5 (2006), p. 39.
[41] M. Muthukumar and P. Welch, Polymer 41 (2000), p. 8833.
[42] Liu Y, Chan C, Wang Y, Ng K, Jiang Y, Li L, Polymer 2003, 44, 4673-9.
[43] Keller, A., Journal of Polymer Science **1955**, 17, 351-364.
[44] A Keller (1968) Rep. Prog. Phys. **31** 623.
[45] Flory P.J., (1988) Munich: Hanser publishers.
[46] Sperling, L.H., 2001, Wiley, New York.
[47] J.J. Point, Macromolecules 12 (1979), p. 770.
[48] A. Keller, M. Hikosaka, S. Rastogi, A. Toda, P.J. Barham and G. Goldbeck-Wood, J Mater Sci 29 (1994), p. 2579.
[49] M. Hikosaka, Polymer 31 (1990), p. 458.
[50] D.M. Sadler and G.M. Gilmer, Polymer 25 (1984), p. 1446.
[51] G. Allegra and S.V. Meille, Adv Polym Sci 191 (2005), p. 87.
[52] G. Strobl, Eur Phys J E 3 (2000), p. 165.
[53] Strobl G., , Prog. Polym. Sci, 31, 2006, 398-442.
[54] T. Yamamoto, *J Chem Phys* **107** (1997), p. 2653.
[55] L. Toma, S. Toma and J. Subirana, Macromolecules 31 (1998), p. 2328.
[56] J.P. Doye and D. Frenkel, J Chem Phys 109 (1998), p. 10033.
[57] T. Yamamoto, J Chem Phys 109 (1998), p. 4638.T.
[58] Yamamoto, J Chem Phys 115 (2001), p. 8675.
[59] T. Yamamoto, Polymer 45 (2004), p. 1357.
[60] Natta, G., Corradini, P., Rubber Chem Tech., 1960, 33, 703.
[61] Kolmogoroff AN. Izvestia Akad Nauk SSR Math 1937 1, 355-9.
[62] Evans, U.R, Trans Faraday Soc 1945;41,365-75.
[63] Avrami, M Kinetics of Phase Change. I. General Theory. Journal of Chemical Physics 7 (12): 1103–1112, 1939

[64] Avrami, M ,Kinetics of Phase Change. II. Transformation-Time Relations for Random Distribution of Nuclei". Journal of Chemical Physics 8 (2): 212–224,1940.

[65] Avrami, M "Kinetics of Phase Change. III. Granulation, Phase Change, and Microstructure". Journal of Chemical Physics 9 (2): 177–184, 1941.

[66] In: M. Karttunen, I. Vattulainen and A. Lukkarinen, Editors, Novel methods in soft matter simulations, Springer (2004).

[67] J. Zhang and M. Muthukumar, J Chem Phys 126 (2007), p. 234904.

[68] J. Zhang and M. Muthukumar, J Chem Phys 126 (2007), p. 234904.

[69] T. Yamamoto, J Chem Soc Faraday Trans 91 (1995), p. 2559. D.

[70] Tahara and Y. Miyamoto, Polymer 49 (2008), p. 317.

[71] A. Mattozzi, M. Minelli, M.S. Hedenqvist and U.W. Gedde, Polymer 48 (2007), p. 2453.

[72] D. Raabe, Acta Mater 52 (2004), p. 2653.

[73] L. Li, C.Y. Li and C. Ni, J Am Chem Soc 128 (2006), p. 1692.

[74] H. Yang, Y. Chen, Y. Liu, W.S. Cai and Z.S. Li, J Chem Phys 127 (2007), p. 094902.

[75] T. Miura and M. Mikami, Phys Rev E 75 (2007), p. 031804.

[76] M. Steinhart, P. Goering, H. Dernaika, M. Prabhukaran, U. Goesele and E. Hempel et al., Phys Rev Lett 97 (2006), p. 027801.

[77] M. Wang, W. Hu, Y. Ma and Y. Ma, J Chem Phys 124 (2006), p. 244901.

[78] J.U. Sommer and G. Reiter, J Chem Phys 112 (2000), p. 4384

[79] Rouse, Jr., P.E., , J. Chem. Phys, **1935**, 21(7),1272-1280.

[80] de Gennes, P.G., Cornell University press, Ithaca, **1979**, NY.

[81] Doi, M., and Edwards,S.F., , **1989**, Claredon Press, Oxford.

[82] Baschnagel, J., Wittmer, J.P., Meyer H., Computational Soft Matter, Lecture Notes, Vol. 23, 83-140,**2004**.

[83] Shaffer, J.S., Effects of chain topology on polymer dynamics: bulk melts.J. Chem Phys. 101(5) 4205-4213. **1994**.

[84] Paul, W., Binde, K., Heermann, D.W and Kremer, K.:,. J. Phys II (France) 1. **1991.**

[85] Kremer, K. and Grest, G.S., , J. Chem. Phys. **1990**, 92(8),5057-5086.

[86] Pütz, M. Kremer, K., grest, G.S., Europhys. Lett. 49, 735-741, **2000**.

[87] Picu R., C., Sarvestani A.S., Polymer, Volume 45, Issue 22, 13 October 2004, Pages 7779-7790.

[88] Dionne P.J., Ozisik R., Picu C.R.,. Macromolecules 2005, 38, 9351-9358.

[89] Starr, F.W., Schrøder, T. B. and Glotzer, S. C.:.Macromolecules, **2002**. 35, 4481-4492.

[90] Vacatello M. Macromolecules, **2001**, 34, 1946-1952.

[91] Angell**,** C.A., J. Non-Cryst. Solids 73,**1985**, p. 1.

[92] Angell CA. Entropy and fragility in supercooling liquids. J Res natl Inst Stand Technol 1997; 102.

[93] Angell C A, Science 267, 1995, 1924.
[94] Vogel, H. Phys. Z. 22, 1921, p. 645.
[95] Fulcher, G.S. ,J. Am. Ceram. Soc. 8 1923, p. 339.
[96] Tamman G.,and W. Hesse, W., Z. Anorg. Allg. Chem. 1926; 156, p. 245.
[97] Williams, M.L. Landel R.F. and Ferry, J.D. J. Am. Chem. Soc 1955; 77, p. 3701.
[98] Dudowitz, J., Freed, K. F., Douglas, J.F.,. J. Phys. Chem. B 2005,109,21350-21356.
[99] J. H. Gibbs and E. A. DiMarzio, J. Chem. Phys., 28, 373, 807. (1958)
[100] G. Adams and J. H. Gibbs, J. Chem. Phys. 43, 139 (1965)
[101] McKenna, G., Computational materials Science 4, 1995, 349-360.
[102] Qin Q., McKenna G.,B :. Journal of Non-Crystalline Solids, 352, 2977-2985, 2006.
[103] Starr, F., W., Douglas, J., F., Influence of the Nanoparticle Additives on the Fragility of Polymer Glass Formation and the Buchenau Relation. Submitted 2009.
[104] Eyring, H. (1935). J. Chem. Phys. 3: 107. doi:10.1063/1.1749604.
[105] Rubinstein, M, Colby, R.H, Polymer Physics, Oxford, 2003.
[106] Bueche, F., In reinforcement of elastomers, Interscience: New York, 1965.
[107] J.M. Escleine, B. Monasse, E. Wey and J.M. Haudin, Influence of specimen thickness on isothermal crystallization kinetics. A theoretical analysis, Colloid Polym Sci 262 (1984), pp. 366–373.
[108] N. Billon, J.M. Escleine and J.M. Haudin, Isothermal crystallization kinetics in a limited volume. A geometrical approach based on Evans' theory, Colloid Polym Sci 267 (1989), pp. 668–680.
[109] N.A. Mehl and L. Rebenfeld, Computer simulation of crystallization kinetics and morphology in fiber-reinforced thermoplastic composites. I. Two-dimensional case, J Polym Sci Part B: Polym Phys 31 (1993), pp. 1677–1686.
[110] N.A. Mehl and L. Rebenfeld, Computer simulation of crystallization kinetics and morphology in fiber-reinforced thermoplastic composites. II. Three-dimensional case, J Polym Sci Part B: Polym Phys 31 (1993), pp. 187–193.
[111] T.H. Krause, G. Kalinka, C. Auer and G. Hinrichsen, Computer simulation of crystallization kinetics in fiber-reinforced composites, J Appl Polym Sci 51 (1994), pp.
[112] E. Piorkowska, Modeling of crystallization kinetics in fiber reinforced composites, Macromol Symp 169 (2001), pp. 143–148
[113] Ewen B., Richter D., Neutron Spin Echo Investigations on segmental dynamics of polymers in melts, network and solutions. Vol 134, pp 1-130.2005.
[114] Nitta, K.; Asuka, B.; Liu, M.; Terano; Polymer 2006, 47, 6457.
[115] Waddon, A.J, Petrovic, Z.S.: Polymer Journal, 2002, 34, 876.
[116] Douglas, J., Kumar, S.: discussion within the workshop "Late night show on polymer nanocomposites II, Brno, CR, 2009.
[117] Kalfus, J.; Jancar, J.; J Polym Sci: Part B: Polym Phys 2007, 45, 1380.

[118] Merna, J.: Koordinační polymerace alkenů katalytickými systémy na bázi přechodových kovů. PhD thesis, FCH VUT Brno, 2005.

[119] Sheet: http://www.tri-iso.com/SiteAdmin/Portals/0/12_238_Irganox%201076.pdf

[120] Dobreva A, Gutzov I, J Non-Cryst Solids 1993; 162:1.

[121] Frenkel, D. and Smit, B. Understanding molecular simulations from algorithm to applications, 2 edn, 2002, Academic press, San Diego.

[122] Paul, W. , Yoon D.Y. ,and Smith, G.D. Journal of Chemical Physics 103 1995, p. 1702.

[123] Yamamoto T., Orimi N., Urakami N., Sawada K., M, Faraday Discuss., 2005, 128, 75-86.

[124] Waheed, N., Ko, M.J.m Rutledge, G,C., , Polymer 2005, 46,8689-8702.

[125] Hess, et al., J. Chem. Theory Comput. 4: 435-447, 2008.

[126] The images were made with VMD software support. VMD is developed with NIH support by the Theoretical and Computational Biophysics group at the Beckman Institute, University of Illinois at Urbana-Champaign.

[127] Kumar SK, NanoLett,2008.

[128] Derjaguin, L Landau, , Acta Physico chemica URSS 14:633, (1941)

[129] Verwey EJW, Overbeek JThG, , Elsevier, Amsterdam (1948)

[130] Kumar S, Late Night Show on Nanocomposites II, Brno, presentation,2009

[131] Gutzov I, Schmelzer J. The vitreous state. Thermodynamics, structure, rheology and crystallization. Berlin, Springer, 1995.

[132] Jackle J., Models of the glass transition, Rep Prog Phys 1986; 49, 171-231.

[133] Zarzycki J, editor. Glasses and amorphous materials. Materials science and technology, vol 9.

[134] Boyd, R.H, Philips, P.J., , Cambridge University Press.

[135] van Krevelen, D.W., Crystallinity of polymers and the means to influence the crystallization process. Chimia 1978, 32(8),279-294.

AUTHOR´S ACKNOWLEDGEMENTS

I would love to thank for help, support and motivation, when needed, for a useful discussions and hints, personal example in both science and life. Meeting some of them has changed my life in a significant way.

If I may name a few of many my acknowledgements go for, they would definitely be Josef Jancar, Jaroslav Kučera, Lukáš Recman, Jirka Sadílek and Martin Moos.

Manželovi a rodině
To my dearest husband and family

Our deepest fear is not that we are inadequate. Our deepest fear is that we are powerful beyond measure. We ask ourselves, who am I to be brilliant, gorgeous, talented, and fabulous? Actually, who are you not to be? We are born to make manifest the glory of God that is within us. And as we let our own light shine, we unconsciously give other people permission to do the same.

[Marianne Williamson]